Title
The Role of Epidermal Growth Factor Receptor Signaling in Hematopoietic Stem Cell Regeneration

Author
Fang, Tiancheng

Publication Date
2020

Peer reviewed|Thesis/dissertation

UNIVERSITY OF CALIFORNIA

Los Angeles

The Role of Epidermal Growth Factor Receptor Signaling in Hematopoietic Stem Cell Regeneration

A dissertation submitted in partial satisfaction of the requirements

for the degree Doctor of Philosophy

in Molecular and Medical Pharmacology

by

Tiancheng Fang

2020

ABSTRACT OF THE DISSERTATION

The Role of Epidermal Growth Factor Receptor Signaling

in Hematopoietic Stem Cell Regeneration

by

Tiancheng Fang

Doctor of Philosophy in Molecular and Medical Pharmacology

University of California, Los Angeles, 2020

Professor Harley I. Kornblum, Co-Chair

Professor John P. Chute, Co-Chair

Hematopoietic stem cells (HSCs) are capable of self-renewing to maintain the stem cell pool as well as differentiating into different mature blood cells to replenish the blood system. Genotoxic stress, such as chemotherapy and radiation, could induce DNA damage in the HSCs, increasing the risk of malignant transformation and decrease the normal function of HSCs. Therapies to promote DNA repair in HSCs after exposure to genotoxic stress remains not well developed. This dissertation reports that the epidermal growth factor receptor (EGFR) signaling promotes DNA repair in HSCs through activation of the non-homologous end-joining (NHEJ) pathway and regulates HSCs regeneration. Data in this dissertation demonstrates that epidermal growth factor (EGF) treatment reduces DNA damage in HSCs after radiation and chemotherapy. EGFR signaling

preferentially enhances the activity of the NHEJ pathway, as indicated by NHEJ specific molecules such as DNA-dependent protein kinase, catalytic subunit (DNA-PKcs), Artemis, and Ku70. Mechanistically, EGF binds and activates EGFR, which subsequently activates Akt, further leading to the activation of DNA-PKcs. Pharmacological inhibition of Akt and DNA-PKcs confirmed the EGFR/Akt/DNA-PKcs pathway for DNA repair in HSCs in vivo. Systemic administration of EGF accelerated the hematopoietic recovery of irradiated or chemotherapy-treated mice without affecting the relapse of acute myeloid leukemia. Conditional suppression of EGFR in the hematopoietic stem and progenitor cells (HSPCs) impaired DNA repair and functional recovery, underlining the necessity of EGFR signaling in DNA repair in HSCs. Moreover, EGF treatment accelerated the recovery of irradiated human bone marrow HSCs shown by immunophenotyping in vitro and multilineage reconstitution in vivo. EGF treated human HSPCs also presented enhanced DNA repair. Whole-genome sequencing of HSPCs from irradiated EGF-treated mice revealed no significant difference in the coding regions in terms of mutation rate compared to irradiated control mice, despite increased intergenic copy number variant mutations. RNA sequencing of HSPCs from irradiated EGF-treated mice displayed no significant alterations of the transcription of leukemogenesis related genes. This thesis project uncovered the EGFR/Akt/DNA-PKcs pathway for NHEJ DNA repair in HSCs and explored the therapeutic potential of EGF to promote human HSCs regeneration.

The dissertation of Tiancheng Fang is approved.

Donald B. Kohn

Gay M. Crooks

Harley I. Kornblum, Committee Co-Chair

John P. Chute, Committee Co-Chair

University of California, Los Angeles

2020

Table of Contents

List of Figures

Acknowledgment

First, I would like to express my appreciation towards my Ph.D. mentor Dr. John Chute for his support throughout my graduate school. During my years in the lab, I have learned about critical thinking, gained knowledge of clinical applications of translational research, and much more. As a mentor, Dr. Chute has not only taught me how to conduct experiments, compose manuscripts but also helped me advance to the next step of my career.

I also want to thank the rest of my thesis committees: Dr. Donald Kohn, Dr. Gay Crooks, and Dr. Harley Kornblum, for they have always been supportive to me. They have provided me with many insightful suggestions along the way to help me shape the thesis project. They are also very encouraging when I get frustrated in the process. For these reasons, I'm very grateful to them.

My gratitude also goes to my dear colleagues who have all taught me about research and contributed to my co-author publications during my graduate school. Dr. Heather Himburg, Dr. Mamle Quarmyne, and Dr. Xiao Yan trained my technical skills. Dr. Martina Roos, Dr. Christina Termini, and Dr. Vivian Chang helped me improve on academic writing and presentation skills. Dr. Yurun Zhang, Lia Signaevskaia, Amara Pang, Paulin Lin, Jenny Kan, Anna Javier, and Liman Zhao have provided help with labor-intensive experiments and mouse colony management. They have also been great friends who brought much joy to my lab life.

I'm grateful for the graduate division of the University of California, Los Angeles, for awarding me the dissertation year fellowship. This fellowship provided me with financial and time support during my dissertation year. Research conducted in this dissertation was funded by the National Institutes of Health, National Institute of Allergy and Infectious Diseases grants AI107333 and AI067769, and California Institute for Regenerative Medicine Leadership Award (LA1-08014) with my mentor Dr. John Chute being the awardee.

Finally, I would like to thank my friends and family. Studying abroad hasn't been the easiest decision I've made, so I'm grateful for my parents' understanding and support. I'm thankful for my friends always being there for me through the happy and tough time. Among them, I want to thank my boyfriend Hongxiang Gu the most, for being such a patient and cheerful partner.

The past six years have been such a blessing in retrospect. It has not been smooth and easy, but because of that, it's more precious and memorable. I want to sincerely thank everyone who has supported me during my graduate life, for without them, I won't be where I am and who I am.

Chapter 2 and Chapter 3.3 together is a version of [Tiancheng Fang, Yurun Zhang, Vivian Y. Chang, Martina Roos, Christina M. Termini, Lia Signaevskaia, Mamle Quarmyne, Paulina K. Lin, Amara Pang, Jenny Kan, Xiao Yan, Anna Javier, Katherine Pohl, Liman Zhao, Peter Scott, Heather A. Himburg, John P. Chute. Epidermal growth factor receptor-dependent DNA repair promotes murine and human hematopoietic regeneration. *Blood* (2020) 136 (4): 441–454. DOI:10.1182/blood.2020005895].

Biographical sketch

TIANCHENG FANG

EDUCATION

Nankai University Tianjin, CHINA

B.S. Biological Science Sept. 2010 – Jun. 2014

PUBLICATIONS

1. **Tiancheng Fang**, Yurun Zhang, Vivian Y. Chang, Martina Roos, Christina M. Termini, Lia Signaevskaia, Mamle Quarmyne, Paulina Lin, Amara Pang, Jenny Kan, Xiao Yan, Anna Javier, Katherine A. Pohl, Liman Zhao, Peter Scott, Heather A. Himburg, John P. Chute. Epidermal Growth Factor Receptor–dependent DNA Repair Regulates Hematopoietic Stem Cell Regeneration. Blood. 136, pp. 441–454 (2020).
2. Heather A. Himburg, **Tiancheng Fang**, Martina Roos, Amara Pang, Yurun Zhang, Lia Signaevskaia, Orel Tabibi, Paulina K. Lin, Joshua Sasine, Christina M. Termini, John P. Chute. Semaphorin 3A Signaling Controls Vascular and Hematopoietic Regeneration Following Myelosuppression. (In preparation) (2020).
3. Heather A. Himburg, Martina Roos, **Tiancheng Fang**, Yurun Zhang, Christina M. Termini, Lauren Schlussel, Mindy M. Kim, Amara Pang, Jenny Kan, Liman Zhao, Hyung Suh, Joshua P. Sasine, Schiller Gary, John P. Chute. Chronic Myelogenous Leukemia Stem Cells Require Cell-autonomous Pleiotrophin Signaling. The Journal of Clinical Investigation. 130, pp. 315–328, (2020).
4. Christina M. Termini, Amara Pang, Michelle Li, **Tiancheng Fang**, Vivian Y. Chang and John P. Chute. Syndecan-2 expression identifies hematopoietic stem cells with enhanced repopulating capacity. (In preparation) (2020).
5. Yurun Zhang, Martina Roos, Heather A. Himburg, Christina M. Termini, Mamle Quarmyne, Michelle Li, Liman Zhao, Jenny Kan, **Tiancheng Fang**, Xiao Yan, Katherine Pohl,

Emelyne Diers, Hyo Jin Gim, Robert Damoiseaux, Julian Whitelegge, William McBride, Michael E. Jung, John P. Chute. PTPσ Inhibitors Promote Hematopoietic Stem Cell Regeneration. Nature Communications. 10, p. 3667, (2019).

6. Wanxing Chai-Ho, Martina M Roos, Michelle Li, Pang Amara, Yurun Zhang, **Tiancheng Fang**, Christina Termini, John P Chute. Grb10 Is a Tumor Suppressor in Human Acute Myeloid Leukemia. Blood. 132, pp. 1344–1344, (2018).
7. Vivian Y. Chang, **Tiancheng Fang**, Katherine A. Pohl, Evelyn Tran, Heather A. Himburg, John P. Chute. Blood. 2018 132:1284, (2018).
8. Heather A. Himburg, Christina M. Termini, Lauren Schlussel, Jenny Kan, Michelle Li, Liman Zhao, **Tiancheng Fang**, Joshua P Sasine, Vivian Y. Chang, John P. Chute. Dichotomous regulation of hematopoietic stem cell maintenance and regeneration by bone marrow stromal cells and endothelial cells. Cell Stem Cell. 23, pp. 370–381, (2018).
9. Xiao Yan, Heather A Himburg, Katherine Pohl, Mamle Quarmyne, Evelyn Tran, Yurun Zhang, **Tiancheng Fang**, Jenny Kan, Nelson J Chao, Liman Zhao, Phoung L. Doan, John P. Chute. Deletion of the Imprinted Gene Grb10 Promotes Hematopoietic Stem Cell Self-Renewal and Regeneration. Cell Rep. 17, pp. 1584–1594, (2016).
10. Fan Wu, Yasunori Watanabe, Xiang-Yang Guo, Xin Qi, Peng Wang, Hong-Yu Zhao, Zheng Wang, Yuko Fujioka, Hui Zhang, Jin-Qi Ren, **Tiancheng Fang**, Yu-Xian Shen, Wei Feng, Jun-Jie Hu, Nobuo N Noda, Hong Zhang. Structural Basis of the Differential Function of the Two C. elegans Atg8 Homologs, LGG-1 and LGG-2, in Autophagy. Molecular Cell. 60, pp. 914–929, (2015)

1. Introduction

1.1. Hematopoietic stem cells

Hematopoietic stem cells (HSCs) are defined by their capacity to repopulate the entire blood system and self-renewal [1]. Bone marrow is the primary organ where HSCs reside, whereas the spleen, thymus, and liver can serve as extramedullary hematopoietic organs [2, 3]. HSC is a rare population, consisting of less than 0.005% of the bone marrow (BM) mononuclear cells (MNCs) in mice [4] and less than 0.05% of BM MNCs in adult human [5]. Under steady-state, adult HSCs remain mostly quiescent which is considered necessary for the maintenance of their "stemness" [6]. Experimental proof of the existence of HSCs dates back to 1961 when Till and McCulloch demonstrated that transplantation of mouse bone marrow cells could rescue irradiated hosts, as well as form colonies in the spleen [7, 8]. Ever since then, the field of HSC research has seen tremendous breakthroughs such as Elucidation of the ontogeny of the hematopoietic system; Refinement of immunophenotyping of HSCs allowing the purification of HSCs; Single-cell profiling for better understanding of the heterogeneity in HSCs; Extensive investigation of the interaction between HSCs and their microenvironment. These findings are advancing both scientific exploration and clinical application of hematology.

1.1.1. Development of hematopoietic stem cell

It remains a challenge for hematologists to identify the origin of HSCs due to different surface markers and function displayed by HSCs at early ontogeny versus adulthood. Embryonic hematopoiesis in the murine system has been characterized in most detail. Thus, a murine ontogeny timeline will be used to describe the development of HSCs.

Hematopoiesis appears in multiple anatomic sites during embryogenesis in many species, including fish, rodents, and human [9]. Murray first coined “hemangioblast” to describe the pool of cells at the thickened area of mesoderm that gives rise to blood and endothelium of the blood islands [10]. However, hemangioblast as the origin of HSCs is still arguable. Blood cells become identifiable at E7.5 in the murine yolk sac blood islands, together with endothelium [11]. The emergence of blood cells at this time point is referred to as primitive hematopoiesis. Red blood cells (RBCs) are the primary blood cells produced at this stage to meet the oxygen demand of the actively developing embryo. Definitive hematopoiesis takes place in the (AGM) region starting at E10. HSCs isolated from AGM at E10 can successfully repopulate lethally irradiated adult recipients.

In contrast, HSCs collected from yolk sac and liver that possess repopulating capacity appear later [12]. By E12, the fetal liver emerges as the predominant hematopoietic organ where HSCs expand and differentiate [13]. HSCs in the fetal liver later migrate to bone marrow and persist throughout adulthood. The placenta has also been reported as a source of hematopoiesis [14].

Among the embryonic and extraembryonic hematopoietic organs, which generate the HSCs that later contribute to adult hematopoiesis stays controversial. HSCs in the fetal liver were arguably not de novo. Moore and Owen hypothesized that the yolk sac is the origin of HSCs, and these HSCs later migrate to the fetal liver through blood circulation [15]. Despite the support of some experiments [16], other data refute this hypothesis [17]. However, owing to the variations in the experiment design, it is still of debate whether this hypothesis is bona fide. Nonetheless, scientists are continually making efforts to sort out the origin of HSCs with newer tools such as lineage tracing.

1.1.2. Hierarchy of the hematopoietic system

The hematopoietic system comprises HSCs, progenitors, and mature blood cells. These cells form a hierarchy stemming from the HSCs to progenitors and eventually to mature cells of different lineages. Conventionally, the paradigm is that long-term HSCs (LT-HSCs) can generate short-term HSCs (ST-HSCs) which have limited self-renewal ability but can repopulate more rapidly as compared to LT-HSCs [18, 19]. ST-HSCs further give rise to multipotent progenitors (MPPs). MPPs lost the self-renewal ability but can still produce lineage-committed progenitors [20]. The lineage-committed progenitors are divided into two groups: common myeloid progenitors (CMP) and common lymphoid progenitors (CLP). CLPs generate pro-B, pro-T, and pro-NK cells which yield mature B cells, T cells, NK cells, and dendritic cells, respectively. On the other hand, CMPs can commit to megakaryocyte erythrocyte precursors (MEP) or granulocyte macrophage precursors (GMP). GMPs can differentiate into dendritic cells (DC), granulocytes, and macrophages, whereas MEPs produce megakaryocytes and erythrocytes [21].

Over the last decade, the conventional roadmap of the hematopoietic hierarchy has been challenged. The previously defined ST-HSCs were shown to sustain rather long-term multilineage engraftment up to 387 days in a transplant experiment [22]. There is also no sharply-defined difference between ST-HSCs and MPPs despite attempts of marker refinement and function discrimination [23]. These data could suggest a continuous change of the stem cells during lineage commitment and heterogeneity within a phenotypically distinct population. The former is revealed by single-cell RNA-sequencing of hematopoietic cells [24, 25], and the latter is proven by single-cell transplant demonstrating the existence of a myeloid-biased progenitor population in the HSC compartment [26].

Regardless of the ambiguity in the definition of early progenitors, the presence of progenitors with limited self-renewal ability but with multi-lineage plasticity is of no doubt. The intrinsic and extrinsic signals that govern the fate decision of HSCs remains an actively pursued research field.

1.2. Immunophenotype of hematopoietic stem cells

Investigation of HSCs relies heavily on purifying them with proper cell surface markers. Human and murine HSCs exhibit different surface markers. Human LT-HSCs display a combination of Lineage negative (Lin^-)$CD34^+CD38^-CD90^+CD45RA^-$ [27]. Lineage markers are a cocktail of CD3, CD14, CD16, CD19, CD20, and CD56. These markers label mature blood cells such as T cells, B cells, NK cells, monocytes, and neutrophils. Thus, the Lin^- population represents a mixture of progenitors and HSCs. $CD34^+$ $CD38^-$ cells are enriched in the primitive hematopoietic progenitors, comprise less than 0.05% +/- 0.08% of the mononuclear cells in the cord blood [28, 29]. Furthermore, Majeti et al. demonstrate that as few as 10 $Lin^-CD34^+CD38^-CD90^+CD45RA^-$ cells can reconstitute long-term multi-lineage hematopoiesis in vivo [30], confirming that this combination of markers enriches for LT-HSCs.

Murine LT-HSCs are phenotyped by $CD150^+CD48^-CD41^-$c-Kit^+Sca-1^+Lin^- ($SLAM^+KSL$). c-Kit^+Sca-1^+Lin^- (KSL) cells mark the hematopoietic stem and progenitor cells (HSPCs). KSL cells consist of 0.08% of bone marrow mononuclear cells. One hundred KSL cells can rescue lethally irradiated recipients and reconstitute hematopoiesis [31]. A stringent transplant experiment where a single cell was injected into irradiated mice identifies $CD150^+CD48^-CD41^-$ KSL cells as the LT-HSCs. One out of

every 2.2 bone marrow $CD150^{+}CD48^{-}CD41^{-}$ KSL cells can produce long-term multi-lineage hematopoiesis [32].

It is worth mentioning that CD34 expression in human versus murine HSCs exhibit a different pattern. As mentioned above, human $CD34^{+}$ enriches the LT-HSCs population. However, in mice, only the $CD34^{-/low}$ fraction of the KSL cells were able to achieve long-term hematopoietic reconstitution in a previous study [33]. Also, murine HSCs isolated from different developmental stages displayed a decrease in CD34 expression, from being present in fetal and neonatal HSCs to being absent in adult LT-HSCs [34].

1.3. Hematopoietic stem cell assays

1.3.1. Colony-forming cell assay

Before the development of in vivo methods for measuring HSC function, colony-forming cell (CFC) assay was the primary method for assessing HSPCs since the introduction by Till and McCulloch. Precisely speaking, the CFC assay identifies progenitors rather than HSCs. When cultured in semi-solid culture media (such as methylcellulose) supplied with proper cytokines, progenitors can differentiate into mature blood cells that form cell clusters that can be visualized under the light microscope. Different types of colonies are characterized by their morphology. They indicate the lineage restriction of the progenitors. Burst-forming unit-erythroid (BFU-E), Colony-forming unit-granulocyte, macrophage (CFU-GM), and Colony-forming unit-granulocyte, erythroid, macrophage, megakaryocyte (CFU-GEMM) are the colonies commonly seen on a CFC plate. Among them, CFU-GEMM represents the most primitive progenitor due to its ability to generate cells of both erythroid and myeloid lineages. CFC assay is still widely used as a way of assessing hematopoietic progenitor [35].

1.3.2. Long-term culture-initiating cell

Long-term culture-initiating cell (LTC-IC) serves as a surrogate for in vivo transplantation assay to measure the primitive HSPCs. Different from CFC assay, LTC-IC requires supporting cells, irradiated marrow feeder or stromal cell line, in the culture system [35]. Samples containing HSPCs would be co-cultured with supporting cells for 3-5 weeks and replated on CFC dishes [36]. Cells cultured in the wells can be plated in secondary LTC-IC [37], and only the primitive cells can be maintained through the culture period and able to generate colonies in the CFC dishes. However, the in vitro assays mentioned here are still not able to distinguish early precursor cells versus HSCs.

1.3.3. Competitive repopulating unit assay

Upon the first proposal by DE Harrison in 1980 [38], the competitive repopulating unit (CRU) assay has been widely used to measure the function of hematopoietic stem cells. The competitive repopulating assay is set up by transplanting the mixture of donor cells and competitor BM cells into lethally irradiated recipients. HSCs to be tested are within the donor population, and the “fitness” of donor HSCs is challenged by competitor BM cells. Therefore, a higher percentage of donor cells in the recipients’ hematopoietic cells correlates with higher activity of HSCs. Secondary and tertiary CRUs can also be set up to measure the long-term repopulating potential of the HSCs. The percentage of donor cells can be estimated by the equation below:

$$\%\ \text{Donor cells} = \text{Donor cells} \div (\text{Donor cells} + \text{Competitor cells})$$

Donor cell percentage in the blood of the recipient is measured by flow cytometry every four weeks for 4 – 6 months due to the contribution of mature blood cells by the

progenitors up to 3 months after transplantation [39, 40, 41]. Stable long-term hematopoiesis after four months reflects the function of donor HSCs. Donor percentage is usually measured in total hematopoietic cells (CD45) and three mature hematopoietic populations: myeloid, B cell, and T cell [42, 43, 44].

Lethal irradiation allows suppression of hematopoietic cells from the recipients to create space for donor and competitor cells lodging. Competitor cells are non-irradiated BM cells that serve both as a supporter of recipient survival and as a standard for comparison with the donors in their repopulating capacity. Donor cells can be bone marrow cells, KSL cells or $SLAM^+$ KSL cells, etc. However, donor cells should be distinguishable from competitor cells. C57BL/6J and B6.SJL-$Ptprc^a$ $Pepc^b$/BoyJ is a commonly used donor – competitor pair for competitive repopulating assay. They are congenic strains with a single allele difference in a pan leukocyte marker: C57BL/6J mice express $Ptprc^b$ (CD45.2 or Ly5.2) whereas B6.SJL-$Ptprc^a$ $Pepc^b$/BoyJ mice express $Ptprc^a$ (CD45.1). Another way of characterizing the donor cells is to utilize fluorescent labeling. Transgenic approaches can be taken to introduce fluorescent proteins such as DsRed or green fluorescent protein (GFP) to the donor cells. As a result, donor cells and competitor cells can be distinguished by flow cytometry.

The competitive repopulating assay provides a more accurate way of measuring the quantity and quality of HSCs compare to in vitro assays, albeit taking longer.

1.4. Hematopoietic stem cell microenvironment

1.4.1. Vasculature

HSCs have been tightly regulated by endothelial cells since in fetal development. The emergence of definitive HSCs begins at hemogenic endothelium [11, 45]. In the past

two decades, more researches uncovered the role of endothelial cells in the generation and maintenance of HSCs. The co-culture of endothelial cells with HSCs in vitro demonstrated the expansion of adult LT-HSCs [46]. Notch signaling between endothelial cells and HSCs have been reported to be essential for the development of HSCs in the embryo[47] and preservation of HSCs in adulthood [46]. Under stress setting, anti-apoptotic or activated endothelial cells promote the regeneration of HSCs [48,49]. Infusion of endothelial progenitor cells also promoted the reconstitution of HSCs after radiation injury [50].

Genetic models and imaging were utilized to dissect the role of different types of endothelial cells in the regulation of HSCs. Imaging of the bone marrow identifies hypoxic sinusoidal niche as the leading site for quiescent HSCs to reside [51], and that reconstitution of HSCs after genotoxic injury depends on the regeneration of bone marrow sinusoidal endothelial cells [52]. However, stem cell factor (SCF), a known factor for HSC survival, was reported to be selectively expressed by arteriolar endothelial cells [53]. Both arteriolar and sinusoidal endothelial cells likely contribute to the regulation of HSCs despite more evidence suggesting that sinusoid is the preferred site of residence for HSCs.

1.4.2. Stromal cells

Arguably, bone marrow stromal cells were also reported as a critical component in the niche environment for HSCs maintenance and self-renewal. In vitro co-culture of mesenchymal stem cells (MSCs) with HSCs demonstrates the expansion of HSCs [54]. Deep imaging shows HSCs mainly reside in perisinusoidal niche contacting stromal cells [55]. Chemokines and cytokines secreted by the bone marrow cells were considered

mediators of how bone marrow stromal cells regulate HSCs. For example, secretion of stromal cell-derived factor 1 (SDF1), also known as CXC chemokine ligand (CXCL) 12, by the human MSCs supports hematopoiesis of human CD34+ HSPCs [56]. In the murine system, CXCL12-abundant reticular (CAR) cells, a type of primitive mesenchymal cells, was shown to be essential for the maintenance of HSCs pool after myelotoxic injury through CXCL12-CXCR4 Chemokine Signaling [57]. Stroma mediated Wnt/β-Catenin signaling was shown to promote HSC self-renewal [58].

Bone marrow stromal cells are heterogeneous and characterized by different markers such as Leptin receptor (LepR), nerve/glial antigen 2 (NG2), nestin, and the aforementioned CXCL12. Further investigations were made to examine the relationship of each cell type with HSCs. Deep imaging discovers that HSCs mostly reside with $Lepr^{+}Cxcl12^{high}$ cells [55]. However, genetic modeling reveals that different populations of the stromal cells may specialize in the secretion of distinct cytokines to support HSCs: Nestin+ secrete a significant amount of CXCL12 and SCF, NG2+ cells primarily secrete CXCL12, and LepR+ cells preferentially secrete SCF [59].

1.4.3. Other niche cells

Apart from bone marrow endothelial cells and stromal cells, there are numerous studies suggesting megakaryocyte, osteoblast, sympathetic nerves, and Schwann cells also contribute to HSCs maintenance and regeneration [60]. Two studies independently reported that megakaryocytes maintain HSCs quiescence, though one focuses on CXCL4 [61], and the other focuses on TGF-β–SMAD signaling [62]. Bone-lining osteoblast was considered a key regulator of HSCs before more recent studies revealing the role of endothelial cells and stromal cells. Evidence suggested that osteoblasts regulate HSCs

through Notch signaling after activation by parathyroid hormone (PTH) [63, 64]. Thrombopoietin (TPO) secreted by osteoblast was also demonstrated to maintain HSC quiescence [65]. As for sympathetic nerves, it is involved in the emergence of HSCs in the embryo [66], migration of the adult HSCs [67, 68], regeneration of HSCs after stress [69], and aging of HSCs [70]. Nonmyelinating Schwann cells were also reported to facilitate maintenance of HSC quiescence [71].

Therefore, different cell types in the bone marrow niche could all regulate the development, maintenance, regeneration, and aging of HSCs. It is plausibly context-dependent when looking at which cell type plays a crucial role in HSC regulation.

1.5. Epidermal growth factor and EGFR

1.5.1. Structure of epidermal growth factor and receptor

The epidermal growth factor receptor is a 170kD transmembrane receptor. It is a member of the ErbB receptor family, so it is also known as ErbB1. EGFR consists of the extracellular domain, transmembrane domain, and intracellular domain (Figure 1).

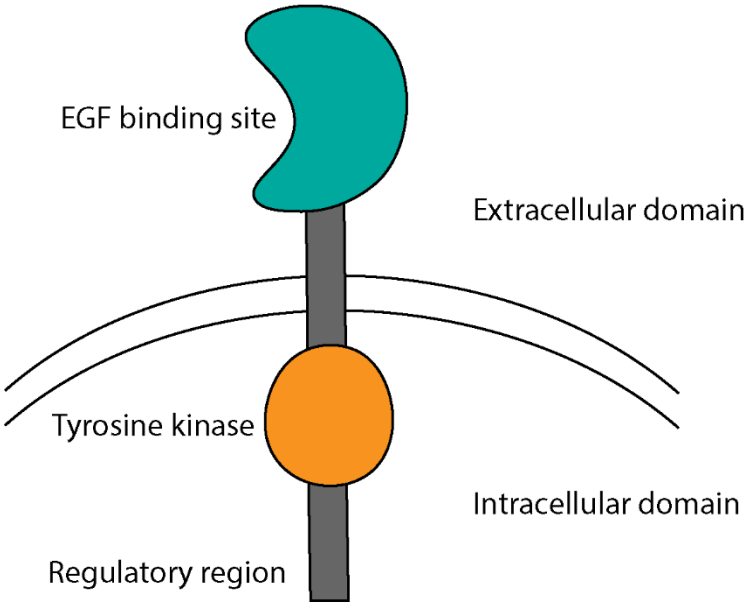

Figure 1. Schematic of EGFR structure.

In the extracellular domain, there are ligand binding sites where the receptor binds with specific ligands. Ligand binding at the ligand-binding sites of the extracellular domain triggers the dimerization of EGFR monomer and confers conformational change [72]. EGFR could also form heterodimers with other ErbB family members [73,74]. The transmembrane domain spans through the cell membrane lipid bilayer and also goes under dimerization upon ligand binding [75]. The tyrosine kinase domain and C-terminal regulatory region are in the intracellular domain. In the active state, the tyrosine kinase domain could autophosphorylate at several tyrosine residues at the C-terminal, including Y992, Y1045, Y1068, Y1148, and Y1173 [76], which activates downstream molecules. The C-terminal regulatory region was suggested to regulate EGFR activity negatively [77, 78,79].

There are seven reported EGFR ligands: Epidermal growth factor (EGF), Transforming growth factor-alpha (TGF-α), Amphiregulin (AREG), Epiregulin (EREG), Betacellulin (BTC), Heparin-binding epidermal growth factor-like growth factor (HB-EGF),

and Epigen (EPGN) [80]. Notably, these ligands have different specificity and affinity towards EGFR binding. EGF, TGFA, AREG, and EPGN interact solely through EGFR, whereas EREG, HBEGF, and BTC could also bind and activate ErbB4. As a canonical ligand of EGFR, EGF is prevalently expressed in many tissues in the human body.

1.5.2. The function of EGFR under normal and disease setting

EGFR activation has been shown to promote cell proliferation, differentiation, and survival [81]. Due to the critical functions, EGFR is expressed in many human organs among which the highest expression appears in the placenta (data from the Human Protein Atlas). EGFR is also highly expressed in skin cells according to the Genotype-Tissue Expression (GTEx) project. Administration of EGFR inhibitor leads to adverse effects on skin [82,83]. EGFR is also displayed to be indispensable for mammary ductal growth and branching [84].

Overexpression or mutations rendering overactivation of EGFR have been reported in many types of cancer such as non-small cell lung cancer (NSCLC), glioblastoma, breast cancer, head and neck cancer, ovarian, cervical, bladder, and oesophageal cancers. In some cancers, EGFR expression is a robust prognostic indicator but not in others [85]. For this reason, numerous chemical EGFR inhibitor and antibodies were developed in an attempt to treat cancers by suppressing EGFR activity [81].

On the other hand, deficiency of EGFR could also lead to diseases in the skin, kidney, brain, and gastrointestinal tract. EGFR knockout mice could only live up to 8 days after birth due to severely impaired epithelial development in multiple organs [86]. Mice

lacking EGFR also display impaired astrocyte development and neuronal death [87,88]. Missense mutation of EGFR in the murine model developed cardiovascular disease [89].

1.5.3. Epidermal growth factor receptor signaling

The two most studied signaling cascades downstream of ligand-activated EGFR are phosphoinositide 3-kinase–pyruvate dehydrogenase kinase–AKT (PI3K – PDK – AKT) pathway and RAF–mitogen-activated protein kinase kinase–extracellular signal-regulated kinase (RAF–MEK–ERK) pathway [90,91]. Effector proteins include c-Myc, Cyclin D, Cyclin E, CDK4/6, etc. which regulate the cell cycle and p53 as well as Bad which regulates apoptosis.

1.5.4. EGF/EGFR in hematopoietic stem cells

Despite the prevalent expression of EGFR in tissues of epithelial origin, it remains unknown whether EGFR was expressed on HSCs until a study by Dr. Phoung Doan et al. [43]. Thus, the role of EGF and EGFR signaling in HSCs remains poorly understood.

1.6. DNA damage and repair

1.6.1. Types of DNA damage

Deamination of DNA could be mediated by DNA deaminase [92] or by chemicals such as bisulfite [93]. Spontaneous deamination of DNA could lead to single nucleotide mutation. Deamination of cytosine converts it to uracil, deamination of 5-methylcytosine produces thymine, deamination of guanine forms xanthine, and deamination of adenine converts it to hypoxanthine. Among them, the conversion of adenine to hypoxanthine substitutes A – T base pair to C – G base pair.

Alkylation of guanine or other bases causes error in base pairing leading to DNA breakage, making cells actively cycling more susceptible [94]. A common type of alkylation in DNA is methylation. Production of 6-O-Methylguanine could occur naturally or be induced by N-nitroso compounds (NOC). Alkylation of DNA could be detrimental to cells and is thus utilized as a cancer treatment. However, since the alkylation of DNA leads to a mispaired nucleotide, it could also be carcinogenic. Hence, balancing the role of alkylating agents between cancer treatment and carcinogenesis is critical [95].

Depurination in DNA leads to DNA structure change. It occurs naturally at an estimated rate of about 5,000 times per human cell [96].

Oxidation of DNA happens at the nucleotide of guanine, adenine, cytosine, and thymine. Among these, 8-oxo-2'-deoxyguanosine (8-oxo-dG) is the most common oxidative lesion observed [97].

Pyrimidine dimers form upon Ultraviolet (UV) - light exposure. It could alter the structure of DNA as well as base-pairing.

Hydrolysis of DNA is extremely rare, at a half-life of 30 million years when tested at 25ºC [98]. The phosphodiester bond is stable, but could still be hydrolyzed by deoxyribozymes at sequence-specifical manner [99], leading to breakage of the DNA strand.

Single-stranded break (SSB) and double-stranded break (DSB) could be induced by various endogenous and exogenous stresses such as reactive oxygen species (ROS) [100], ionizing radiation [101], or certain chemotherapies [102].

1.6.2. Types of DNA repair

There are six main types of DNA repair corresponding to different types of DNA damage: Base excision repair (BER), nucleotide excision repair (NER), Non-Homologous End Joining (NHEJ), Homologous recombination (HR), Mismatch repair (MMR), and direct reversal (DR).

Base excision repair (BER) removes damaged nucleotide by a multi-step process starting from damage-specific glycosylation, removal of nucleotide, to replacement with the corrected nucleotide through DNA synthesis and ligation [103,104]. The removal of nucleotide is either single or several nucleotides in length.

NER can remove genome-wide lesions induced by UV – light and bulky chemical adducts [105]. There are two types of NER: repair of lesions over the entire genome, named as global genome NER (GG-NER), and repair of transcription-blocking lesions present in transcribed DNA strands, called transcription-coupled NER (TC–NER) [106]. The length of the removed lesion is typically 24-32 nucleotides.

NHEJ and HR repair DNA double-stranded breaks. NHEJ is different from HR in that it does not require a homologous template for repair, involves different molecules, and is not cell cycle-dependent [107]. As a result, NHEJ mediated DNA repair is more prevalent, faster but error-prone, whereas HR mediated DNA repair preserves genome fidelity.

DNA mismatch repair (MMR) pathway is responsible for correcting base substitution mismatches and insertion-deletion mismatches (IDLs) generated during DNA replication [108].

DR targets DNA alkylation damage by direct removal of the alkyl group from the damaged site. One example is transferring the methyl group of 6-O-methylguanine to other sites such as cysteine [109].

1.6.3. DNA repair machinery

Different types of DNA repair mentioned above have distinct molecular types of machinery together with some shared enzymes.

At least eleven different types of glycosylases were reported in BER, such as uracil DNA glycosylases (UNG) [103]. AP endonuclease removes the damaged nucleotide, DNA Polymerase-β matches the correct nucleotide and DNA ligase 3 ligates the phosphodiester linkage [104].

In NER, Xeroderma pigmentosum, complementation group C (XPC) acts as a DNA-damage sensor and repair-recruitment factor. Transcription factor II Human (TFIIH) mediates strain separation. Replication protein A (RPA) stabilizes the opened DNA strand. DNA excision repair protein ERCC1-XPF endonucleases are responsible for DNA incision [105,106,110].

Molecules specific in NHEJ are Ku70, Ku80, DNA-dependent protein kinase (DNA-PKcs), and Artemis [111,107]. Ku70 and Ku80 forms complex to recognize and bind to the DNA break site. This complex subsequently recruits and activates DNA-PKcs, which in turn recruits and phosphorylate Artemis [112]. In the end, DNA ligase IV and X-Ray Repair Cross Complementing 4 (XRCC4) are responsible for final ligation [107]. Earlier this year, a study revealed that DNA-PKcs, specifically the phosphorylation at T2609 site, is critical for hematopoiesis in murine model [113].

HR consists of a series of steps. The meiotic recombination 11 homolog A (MRE11A) – Nijmegen breakage syndrome 1 (NBS1) – RAD50 (MRN) complex detects and binds the broken ends leading to the recruitment of ataxia telangiectasia mutated (ATM). Breast cancer type 1 (BRCA1)-dependent resection of 5' on both sides of the DNA break site subsequently occurs to exposure single-stranded DNA (ssDNA). Exposed ssDNA regions then attract BRCA2 and RAD51, which lead to seeking the homologous template. DNA polymerases use the homologous DNA sequence as a template and the invaded ssDNA as a primer to synthesize new DNA. DNA ligases and endonucleases are responsible for final end-processing and ligation [114]. Replication protein A (RPA) is considered an accessory of RAD51 and facilitates ssDNA stability [107,115].

MMR in eukaryotes involves MutS homologs, either MSH2-MSH6 (MutSα) or MSH2-MSH3 (MutSβ). These MSH binds to a mismatch site to facilitate repair [116,117,108]. PMS1 in S. cerevisiae (PMS2 is the human homolog) is also reported to promote MMR [116].

Molecules responsible for DR include mammalian 3-methyladenine-DNA glycosylase (MAG) and O-6-methylguanine-DNA methyltransferase (MGMT) when the lesion is in DNA double-strand [109,118,119,120]. 1meA/3meC-DNA dioxygenase ABH2 and ABH3 repairs mismatch damage when the lesion of alkylation happens in ssDNA [118].

2. EGFR promotes DNA Repair in HSCs

Chapter 2 is adapted from a publication based on the thesis project by Tiancheng Fang et al. [121].

2.1. Hypothesis

Ionizing radiation (IR) and alkylator chemotherapy agents cause DNA damage in HSPCs, thereby contributing to risk for HSC dysfunction, accelerated aging, and risk for malignant transformation over time [122,123,124,125,126]. Eukaryotic cells repair DNA damage primarily through HR and NHEJ repair mechanisms [122,123]. HSCs, which are mainly quiescent in steady-state, primarily undergo NHEJ repair in response to IR, whereas proliferating HSCs and progenitor cells can undergo HR [122]. NHEJ repair is considered a more error-prone mechanism than HR due to lack of a homologous DNA template, potentially resulting in increased deletions, insertions, translocations, and genomic instability [123,124]. Mohrin et al. reported that NHEJ repair in quiescent HSCs was associated with increased genomic rearrangements that persisted in vivo [122].

Since IR and alkylator chemotherapy can induce genomic instability in HSCs and increase the risk for malignant transformation, the development of therapies capable of reducing DNA damage or increasing DNA repair in HSCs could be highly beneficial. Recently, de Laval et al. demonstrated that thrombopoietin (TPO), the c-Mpl ligand, stimulated DNA repair in HSCs via augmentation of DNA-PKcs-dependent NHEJ, and this DNA-PKcs activation was dependent on Erk and NFkB pathway activation [127,128]. The broader role of the BM microenvironment in regulating DNA repair in HSCs remains poorly understood [127,128]. The Chute lab previously showed that high dose total body irradiation (TBI) depletes BM HSCs in mice and accelerates the development of hematopoietic aging, characterized by myeloid skewing and immune cell depletion [43]. Systemic administration of EGF, which is expressed by BM ECs, mitigated these effects of TBI and promoted hematopoietic regeneration in vivo [43]. However, the precise

molecular mechanisms through which EGF promoted hematopoietic regeneration remained unclear. In tumor cells, EGFR can promote DNA repair via activation of DNA-PKcs [129,130,131]. Therefore, I hypothesize that EGFR signaling promotes NHEJ DNA repair pathway in HSCs via activation of DNA-PKcs.

2.2. Materials and Methods

2.2.1. Animals

Eight to 12 weeks old C57BL/6J (CD45.2), B6.SJL-Ptprca Pepcb/BoyJ (CD45.1) and B6;SJLF1/J mice were purchased from the Jackson Laboratory (Bar Harbor, ME) and the UCLA Radiation Oncology Animal Core. Tal1-tTA (SCL-tTA, B6.Cg-Tg(Tal1-tTA)19Dgt/J, Jackson Lab, stock #017722) mice and TRE-EGFR-tr (B6;SJL-Tg(tetO-Egfr*)2-9Jek/J, Jackson Lab, stock #010575) mice were purchased from the Jackson Laboratory. Mice were genotyped for the SCL-tTA transgene and TRE-EGFR-tr transgene by Transnetyx, Inc. (Cordova, TN) [132]. Littermates with the Tal1-tTA+/TRE-EGFR-tr+ genotype were fed with 0.2 g/L Doxycycline (Sigma-Aldrich, St. Louis, MO) water from birth, and half of them were changed to be fed with regular water at 4-6 weeks of age for at least four weeks. SCL-tTA mice were crossed with EGFR-TRE-tr mice, which express a mutant, dominant-negative EGFR lacking an intracellular protein kinase domain (EGFR-DN), to generate mice in which the expression of EGFR-DN in HSCs is controlled by doxycycline (DOX-off, EGFR-DN mice) [133,134,135]. Doxycycline treated SCL-tTA;EGFR-DN mice will have suppression of the EGFR-DN protein kinase (EGFR-WT mice). All animal procedures were performed under a protocol approved by the UCLA Animal Care and Use Committee (Protocol #2014-021-13O).

2.2.2. Validation of the EGFR DN mouse model

TRE-EGFR-tr mice ectopically express a truncated form of EGFR that lacks the intracellular signaling domain [136]. Overexpression of dominant-negative EGFR under doxycycline control was examined by PCR. Primers for probing the extracellular (Mm01187861_m1) and intracellular (Mm01187868_m1) domains of EGFR were purchased from ThermoFisher Scientific. PCR reaction conditions were set at 50°C for 2 minutes, 95°C for 10 minutes followed by 40 cycles of 95°C for 15 seconds and a 60°C anneal–extend step for 1 minute. Deficiency in EGFR activation after EGF stimulation was measured by flow cytometric analysis of p-EGFR (Tyr1173) in $CD150^{+}CD48^{-}CD41^{-}$ KSL cells from EGFR-WT mice and EGFR-DN mice.

2.2.3. Human BM cell culture and transplantation

Cryopreserved Human BM CD34+ cells were purchased from StemCell Technologies. Cells were recovered and cultured in human TSF media (IMDM supplemented with 10% FBS and 20 ng/ml recombinant human Thrombopoietin, 125 ng/ml recombinant human Stem Cell Factor and 50 ng/ml Flt-3 ligand. R&D Systems, Minneapolis, MN). Recovered cells were cultured for 36 hours after 300cGy radiation before collected for transplantation, % $CD34^{+}CD38^{-}$ analysis, and CFC. Progeny of 2 x 10^5 CD34+ cells were transplanted into NSG-SGM3 mice preconditioned with 225cGy TBI through intravenous injection. Peripheral blood from recipient mice was collected 8, 12, and 16 weeks post-transplantation to measure multi-lineage human cell engraftment. Cells were stained with APC anti-human CD3 (Biolegend), PE anti-human CD13 (Biolegend), PE anti-human CD33 (Biolegend), APC/Cy7 anti-human CD19 (Biolegend),

V450 anti-Human CD45 (BD Biosciences), and Brilliant Violet 605 anti-mouse CD45 (Biolegend) and analyzed with flow cytometry.

2.2.4. Flow Cytometry Analysis

BM cells from femurs and tibia were collected with IMDM with 10% FBS and 1% penicillin-streptomycin, following red blood cell lysis with ACK Lysis Buffer (Sigma-Aldrich). Cells were stained with V450 mouse Lineage Antibody Cocktail (BD Biosciences, San Jose, CA), c-kit (CD117) PE Rat anti-Mouse (BD Biosciences), and Sca-1 (Ly-6A/E) APC-Cy7 Rat anti-Mouse (BD Biosciences) for measuring the percentage of KSL cell. Cells were stained with antibodies mentioned above plus Alexa Fluor 488 anti-mouse CD41 Antibody (Biolegend, San Diego, CA), FITC Hamster Anti-Mouse CD48 (BD Biosciences), and CD150 Alexa Fluor 647 Rat anti-Mouse (BD Biosciences) to measure the percentage of $CD150^{+}CD48^{-}CD41^{-}KSL$ [137,138]. For the donor hematopoietic cell engraftment and lineage analysis, Brilliant Violet 605 CD45.1 (Biolegend), FITC CD45.2 (BD Biosciences), PE Mac-1 (CD11b) (BD Biosciences), PE Gr-1 (Ly-6G and Ly-6C) (BD Biosciences), V450 CD3 (BD Biosciences), and APC-Cy7 B220 (CD45R) (BD Biosciences) were used. For phospho-cytometric analysis of p-EGFR, p-Akt, p-DNA-PKcs, and p-Artemis, cells were permeabilized with 0.5% Triton X-100 (ThermoFisher Scientific, Waltham, MA) and 1% BSA (ThermoFisher Scientific) in PBS, and fixed with ice-cold methanol (ThermoFisher Scientific) for 10 minutes. Cells were stained with 1:100 primary antibody for 60 minutes at 4°C, washed with PBS, and stained with 1:100 Alexa Fluor 488 goat anti-Rabbit IgG(H+L) secondary antibody (ThermoFisher Scientific) for 30 minutes at RT prior to flow cytometric analysis. 7-AAD (BD Pharmingen) was used to exclude dead cells for live cell staining.

To measure the percentage of $CD34^+CD38^-$ cells in cultured human cells, the progeny of human $CD34^+$ cells were stained with FITC anti-human CD34 (Biolegend) and APC anti-human CD38 (BD Biosciences). All analyses were performed on a BD Canto II FACS instrument with BD FACS DIVA software. Data were analyzed using BD FACSDiva™ software (BD Biosciences) and Flowjo (Flowjo, LLC, Ashland, OR).

2.2.5. Immunohistochemistry

Lepr-cre; tdTomato conditional reporter mice at C57BL/6J background were used for this assay. Mice were irradiated at 500cGy TBI followed by ten days of EGF or saline treatment. The bone marrow niche was analyzed at day ten post-radiation. 1.25 mg/kg Alexa Fluor 647 CD144 (VE-cadherin) antibody was intravenously injected into each live mouse for endothelial cell staining. Femurs were collected and were fixed with 4% PFA overnight at 4°C. Fixed bones were washed three times with cold PBS to remove residual PFA and were decalcified in 10% EDTA for three days at 4°C. Specimens were submerged in 20% sucrose for 24 hours at 4°C. Specimens were then placed in Tissue-Tek® Cryomold® (Electron Microscopy Sciences, Hatfield, PA) embedded in pre-chilled Tissue-Plus™ O.C.T. Compound (Fisher Scientific. Waltham, MA) and snap-frozen. Specimens were sectioned into 8μm thickness in the CM3050S cryostat (Leica, Wetzlar, Germany) and were transferred onto a poly-L-lysine-coated microscope slide. Slides were mounted with ProLong® Gold Antifade Reagent with DAPI to stain the cell nucleus and were sealed with cover slide. For quantification of bone marrow vasculature and $LepR^+$ stromal cell, images were analyzed using ImageJ software. The VE-Cadherin fluorescence was thresholded for each image using the same parameters, and the thresholded area was quantified.

2.2.6. Immunofluorescence for EGFR nuclear localization

KSL cells were sorted from EGFR-WT and EGFR-DN mice and plated on fibronectin-coated Lab-Tek™ II CC2™ Chamber Slide™ (VWR, Radnor, PA). Cells were serum-starved for 45 minutes, irradiated at 300cGy, and treated with EGF and/or MK2206 for 20 minutes. Cells were then fixed with 4% PFA, permeabilized with 0.5% TritonX-100 and blocked with 5% FBS. Cells were stained with p-EGFR Thr2609 (Abcam) followed by Alexa Fluor 488 goat anti-Rabbit IgG(H+L) secondary antibody (ThermoFisher Scientific). Slides were imaged with Leica TCS SP8 confocal microscopy at a 63x objective lens. p-EGFR nuclear localization was quantified using ImageJ.

2.2.7. Retroviral packaging and transduction of cells

The vectors used include pMSCV-IRES-GFP (Addgene plasmid # 20672, a gift from Dr. Tannishtha Reya) and pMSCV HOXA9-IRES-MEIS1 neo [139] (a gift from Guy Sauvageau, Department of Medicine, Faculty of Medicine, Université de Montréal, Montreal, Quebec, Canada). Retrovirus was packaged in 293T cells (ATCC, Manassas, VA) using Ecopack packaging plasmid (pCL-Eco, Clonetech) and respective viral vectors. Lipofectamine 3000 (ThermoFisher Scientific) was used to facilitate transduction. Viral supernatants were collected at 48 hours and 72 hours after transduction and used for transducing primary cells. 120 µl cell suspensions in StemSpan (StemCell Technology, Vancouver, BC, Canada) were supplemented with 10 ng/ml IL-3 and IL-6, and 100 ng/ml SCF and 80 µl of viral supernatant were added to each well of a 96-well plate pre-coated with retronectin (Takara Bio, Mountain View, CA). Spinfection was conducted by centrifuging a cell-virus mixture at 1,000 g for 1 hour at 32°C. GFP-expressing KSL cells were sorted by FACS two days post-viral transfection. Positively transduced leukemic

cells were selected in RPMI media supplemented with Geneticin 1mg/mL (Sigma Aldrich, St. Louis, MO), 10%FBS, 10 ng/mL mouse SCF, 6 ng/mL mouse IL-3 and 5 ng/mL mouse IL-6 for four days before transplantation.

2.2.8. CFC assay

CFC Assays for Colony Forming Unit - Granulocyte Monocyte (CFU-GMs), Burst Forming Unit - Erythroid (BFU-Es), and Colony Forming Unit - Granulocyte, Erythroid, Monocyte, Megakaryocyte (CFU-GEMMs) were performed. Briefly, 100 BM KSL cells or 3 x 10^4 BM cells were plated per dish. For analysis of EGFR-WT mice and EGFR-DN mice following TBI, 10^5 BM cells were plated per dish. For human cells, 2 x 10^4 BM CD34+ cells were plated per dish. Colonies were cultured in MethoCult medium (StemCell Technologies) at 37°C, 5% CO_2, and counted on Day +14.

2.2.9. Annexin V assay

Annexin V apoptosis assay was performed using FITC Annexin V Apoptosis Detection Kit I (BD Biosciences). BM cells were collected with IMDM with 10% FBS and 1% penicillin-streptomycin, followed by red blood cell lysis with ACK Lysis Buffer (Sigma-Aldrich). Cells were stained with V450 mouse Lineage Antibody Cocktail (BD Biosciences), c-kit (CD117) PE Rat anti-Mouse (BD Biosciences), and Sca-1 (Ly-6A/E) APC-Cy7 Rat anti-Mouse (BD Biosciences) for 30 minutes at 4°C. Cells were rinsed with 3ml 1x Ca^{2+} free, Mg^{2+} free PBS (ThermoFisher Scientific), spun down at 1,400 rpm for 5 minutes at 4°C. Annexin V Binding Buffer was made fresh by diluting 10x Annexin V Binding Buffer with distilled water. Samples were resuspended with 300µl 1x Annexin V Binding Buffer. 5µl FITC Annexin V and 5µl 7-AAD were added to each sample and

incubated for 15 minutes in the dark at room temperature. Flow cytometric analysis was performed on a BD Canto II FACS instrument.

2.2.10. Comet assay

For in vitro studies, BM KSL cells were cultured with EGF and/or NU7441 in TSF media at 37°C for 1 hour before analysis. For in vivo analyses, C57BL/6J mice were irradiated with 500cGy, and subsequently treated with EGF and/or NU7441. KSL cells were analyzed at +4 hours post-irradiation. Neutral Comet Assay was performed using the Comet Assay Kit (Trevigen Inc., Gaithersburg, MD, USA). Briefly, cells were resuspended in CometAssay® LMAgarose (Trevigen Inc.) and spread on CometSlide™ (Trevigen Inc.). Slides were immersed in Lysis Solution (Trevigen) overnight. Electrophoresis was performed with 1X Neutral Electrophoresis Buffer (100mM Tris Base, 300mM Sodium Acetate, pH = 9.0). Slides were then immersed in DNA Precipitation Solution (1M Ammonium Acetate, 82% ethanol) for 30 minutes, and transferred to 70% ethanol for 30 minutes at RT. After drying, slides were stained with SYBR® Gold Nucleic Acid Gel Stain (ThermoFisher Scientific). Comet tails were visualized by a fluorescent microscope Zeiss Axio Imager M2 (ZEISS, Oberkochen, Germany) driven by ZEN software (ZEISS) with a 10x objective and analyzed with Comet Analysis Software (Trevigen).

2.2.11. Quantitative RT-PCR

RNA was isolated using the QIAGEN RNeasy micro kit (QIAGEN, Hilden, Germany). RNA concentrations were measured with NanoDrop 2000 (ThermoFisher Scientific). RNA was reverse transcribed into cDNA using a High-Capacity cDNA Reverse

Transcription Kit (ThermoFisher Scientific). Real-time PCR was performed using Taqman Gene Expression assays (Life Technologies, Carlsbad, CA). Transcript levels of target genes were normalized to GAPDH and control group using the delta-delta Ct method.

2.2.12. Measurement of telomere length

Telomere length was measured using real-time PCR as previously described [140]. Briefly, the genomes of BM KSL cells were extracted with PureLink Genomic DNA Mini Kit (ThermoFisher Scientific). The acidic ribosomal phosphoprotein PO (36B4) gene is a single-copy gene utilized as the reference gene. Forward and reverse primers for the 36B4 portion were 5′ ACT GGT CTA GGA CCC GAG AAG 3′ and 5′ TCA ATG GTG CCT CTG GAG ATT 3′, respectively. The reaction for the 36B4 portion contained 12.5µl Syber Green PCR Master Mix (Applied Biosystems), 300 nM forward primer, 500 nM reverse primer, 20 ng genomic DNA, and double-distilled H_2O to yield a 25 µl reaction. Conditions were set at 95°C for 10 min followed by 35 cycles of data collection at 95°C for 15 s, with 52°C annealing for 20 s, followed by extension at 72°C for 30 s.

Forward and reverse telomeric primers were 5′ CGG TTT GTT TGG GTT TGG GTT TGG GTT TGG GTT 3′ and 5′ GGC TTG CCT TAC CCT TAC CCT TAC CCT TAC CCT TAC CCT 3′ respectively. Each reaction for the telomere portion of the assay included 12.5 µl Syber Green PCR Master Mix (Applied Biosystems), 300 nM each of the forward and reverse primers, 20 ng genomic DNA, and double-distilled H_2O to yield a 25 µl reaction. PCR reaction conditions were set at 95°C for 10 minutes followed by 30 cycles of data collection at 95°C for 15 s and a 56°C anneal–extend step for 1 minute.

Calculation of the relative telomere length was performed by dividing the quantity of telomeric DNA by the quantity of 36B4.

2.2.13. Chemotherapy model

C57BL/6J mice were injected with one dose of 20 mg/kg Doxorubicin intravenously followed by daily injection of EGF or saline for 10 days. Complete blood count and bone marrow hematopoietic analysis were performed at day 10 post doxorubicin injection. Complete blood count was measured by a Hemavet 950 instrument (Drew Scientific, Miami Lakes, FL). For mechanistic studies phosphor-flow and comet assay, C57BL/6J mice were injected with one dose of 20 mg/kg Doxorubicin intravenously and one dose of EGF or saline subcutaneously. KSL cells from these mice were sorted at +12 hours post-Doxorubicin injection.

2.2.14. Acute myeloid leukemia model

C57BL/6J (CD45.2) BM Lin^- cells transduced with HOXA9/Meis1 and selected with Geneticin were used to generate leukemia in vivo. 0.5 x 10^6 transduced cells were transplanted into 850cGy TBI pre-conditioned B6.SJL (CD45.1) recipients together with 2 x 10^5 supportive BM cells from B6.SJL mice [139]. Peripheral blood was collected by retro-orbital bleeding to validate the leukemia burden at 3 weeks post-transplantation. Blood cells were stained with FITC CD45.2 (Biolegend), PE Gr-1 (BD Biosciences), APC Ter119 (BD Biosciences), APC-Cy7 CD27 (Biolegend), Brilliant Violet 605 CD11b (Biolegend), Alexa Fluor 700 CD23 (Biolegend) and V450 CD3 (BD Biosciences). Complete blood count was measured to assess white blood cell count and neutrophil count. Mice with AML burden were treated with cytarabine (SelleckChem) at 100 mg/kg dose for 5 days

through intraperitoneal injection [141]. Leukemic mice were stratified into saline and EGF groups to ensure similar levels of leukemic burden before EGF treatment. After cytarabine treatment, mice were injected with EGF or saline for 10 days. PB and BM of leukemia bearing mice were analyzed at 2 weeks post last day of cytarabine treatment.

2.2.15. EGF ELISA assay

EGFR-WT and EGFR-DN mice were irradiated at 500cGy TBI and collected at 10 minutes, 2 hours, or 10 days post-radiation. Bone marrow from 2 femurs per mouse was flushed with 1ml X-Vivo 10 media (Lonza, Basel, Switzerland). After 5,000 rpm centrifugation for 5 minutes, the supernatant was collected for measuring EGF level using Quantikine® ELISA mouse EGF kit (R&D Systems). The assay was performed according to the manufacture's manual. Optical density was measured using a Spark® microplate reader (Tecan, Morrisville, NC) set to 450 nm wavelength with correction set to 570 nm.

2.2.16. Sample preparation for whole-genome sequencing

C57BL/6J mice were irradiated with 500cGy and subsequently treated with EGF or saline. BM KSL cells were sorted from the BM of irradiated mice at 6 weeks post-TBI for whole-genome sequencing. Genomic DNA was extracted and purified using the PureLink Genomic DNA Mini Kit (ThermoFisher Scientific). Quality control of genomic DNA was done by electrophoresis using the Agilent 2200 TapeStation system (Agilent Technologies, Santa Clara, CA) and by measurement of DNA concentration with Qubit® 2.0 fluorometer (ThermoFisher Scientific). Libraries for DNA-Seq were prepared with KAPA Hyper DNA Prep Kit (KAPA Biosystem, Wilmington, MA). The workflow consists of DNA fragmentation, end-repair to generate blunt ends, A-tailing, adaptor ligation, and

PCR amplification. Different adaptors were used for multiplexing samples in one sequencing run. Library concentrations and quality were measured using the Qubit dsDNA HS Assay kit (Life Technologies) and Agilent Tapestation (Agilent Technologies). Sequencing was performed on NovaSeq6000 S4 for pair-end read 2x150 run. A data quality check was done on Illumina SAV. De-multiplexing was performed with the Illumina Bcl2fastq2 v 2.17 program.

2.2.17. Whole-genome sequencing analysis with control tissue

Paired and unpaired reads were separately mapped to the GRCm38.p4 mouse genome assembly with bwa mem version 0.7.17-r1188 [142]. Sequence alignment map (SAM) files created by bwa mem were converted to binary alignment map (BAM) files with samtools version 1.9 [143]. Resulting BAM files were sorted by chromosome coordinate, had PCR and optical duplicates marked, and individual sample and sequencing lane read group information was added to each BAM file with Picard version 2.9.0-1-gf5b9f50-SNAPSHOT (http://broadinstittute.github.io/picard). Genomic variants were called with GATK v3.5 [144], and subsequently split into files that contained only SNPs or INDELs. Variants were hard filtered for quality using these criteria for SNPs: QD < 2.0 || FS > 60.0 || MQ < 30.0 || HaplotypeScore > 13.0 || MQRankSum <-12.5 || ReadPosRankSum < -8.0; and, INDELs: QD < 2.0 || FS > 200.0 || ReadPosRankSum < -20.0. To determine treatment-specific variants, variants found in individual-matched genomic samples (tail) were removed from variants discover in treatment or control samples. The Program CNVnator [145] was used to call copy number variants for each sample using the same BAM files as described above. We attempted to call structural variants using the program

BreakDancer [146] but found variation in library insert size prohibited further analysis. All discovered variants were annotated using SnpEff [147].

2.2.18. RNA sequencing and data analysis

KSL cells were sorted from C57BL/6J mice at 6 weeks post-500cGy TBI and subsequent saline or EGF treatment. RNA was isolated using the Qiagen RNeasy Micro kit. Libraries were prepared with the Clonetech kit. Sequencing was performed on NextSeq500 for a pair-end 75bp read run. Data quality was checked on Illumina SAV. Demultiplexing was performed with Illumina Bcl2fastq2 v 2.17. The Partek flow (Partek Inc, St. Louis, MO) was used for bioinformatics methods. Reads were mapped to the latest UCSC transcript set using STAR – 2.7.2a and GRCm38.97 [148]. After obtaining gene counts, the counts were normalized by CPM (counts per million). The Principal Component Analysis (PCA) was applied to the transcript counts. The differential gene expressions were examined. Ingenuity Pathway Analysis (IPA) was used for data analysis [149]. For all results of differential gene expression analysis, the p-values and fold changes (FC) filters were applied. The filter values were $p<.05$ and $|FC|> 1.5$ for all differential gene expression results.

2.2.19. Statistics

Data are shown as means + SEM unless otherwise indicated in Figure Legend. We used the unpaired 2-tailed Student's t-test for simple comparisons. When making multiple comparisons on single data sets, one-way ANOVA was utilized. Two-way ANOVA was used when comparing the mean differences between groups that were split regarding two independent variables. Log-rank (Mantel-Cox) test was used for survival

analyses. Statistics were determined using GraphPad Prism 6 (GraphPad Software Inc., La Jolla, CA). All experiments were repeated to confirm the findings. Additional Methods are included in the Supplemental Data.

2.2.20. Data Availability

RNA sequencing data have been deposited into Gene Expression Omnibus (GEO) hosted by NCBI under accession number GSE146371. Whole-genome sequencing data have been deposited into The Sequence Read Archive (SRA) hosted by NCBI under project ID PRJNA612325.

2.3. Results

2.3.1. EGF decreases DNA damage in irradiated HSCs via activation of DNA-PKcs

IR causes DNA strand breaks that lead to cellular apoptosis and necrosis [150]. DNA damage responses are distinct between HSCs and committed progenitor cells [122, 151,152,153]. We sought to determine if EGFR signaling regulates the DNA damage response in HSCs following exposure to IR. Irradiation with 300 cGy increased y-H2AX foci, a sensitive marker of DNA double-strand breaks (DSB) [122,154] in BM ckit+sca-1+lin- (KSL) HSPCs, whereas treatment with 100 ng/ml EGF significantly decreased y-H2AX foci in irradiated KSL cells (Figure 2).

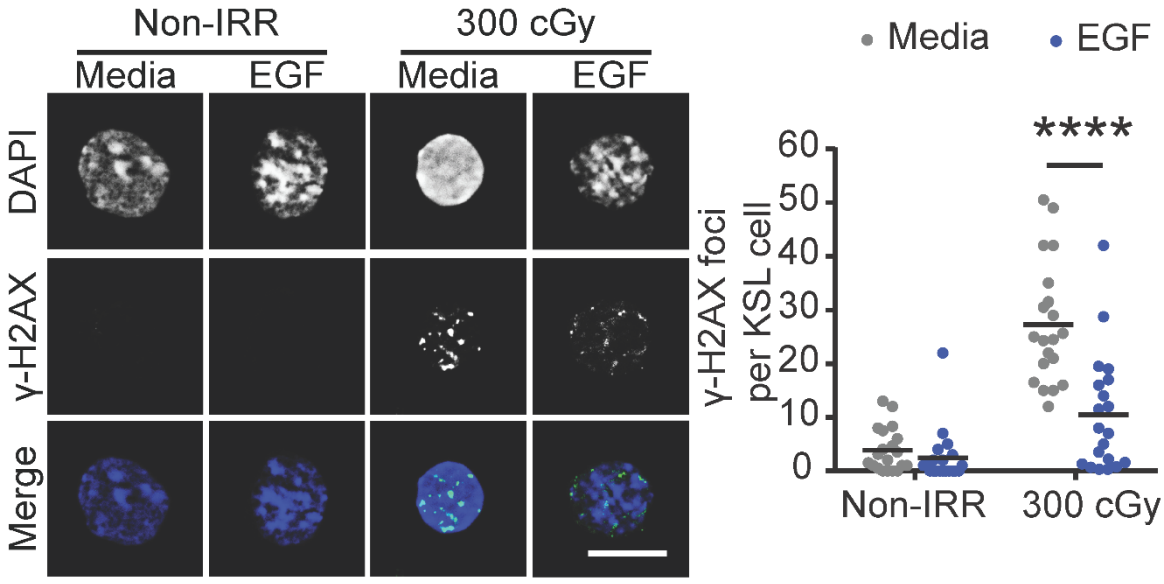

Figure 2. γ-H2AX foci in KSL cells with and without EGF treatment. At left, immunofluorescence microscopy of ionizing radiation-induced foci (IRIF) of γ-H2AX in non-irradiated (Non-IRR) and 300cGy-irradiated BM KSL cells cultured in complete media (Media) with and without 10 ng/ml EGF for 1 hour (scale bar = 10 μm). At right, numbers of foci per KSL cell are shown in non-irradiated and irradiated KSL cells (n = 20 replicates/group, two-way ANOVA, horizontal bars represent means. ****P < 0.0001.

Using the Comet assay, which detects DNA strand breaks as tail moments [155], 300 cGy irradiation increased tail moment length in KSL cells and EGF treatment decreased tail moment length (Figure 3). EGF treatment did not affect numbers of y-H2AX foci or tail moment lengths in non-irradiated KSL cells (Figure 2, 3).

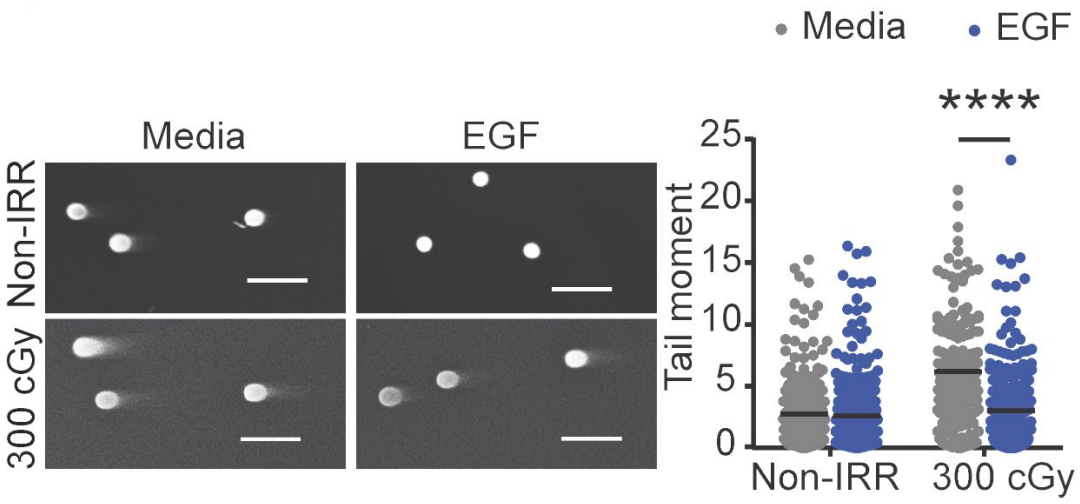

Figure 3. Comet tail of KSL cells with and without EGF treatment. At left, representative images of a Comet assay of non-irradiated and 300 cGy – irradiated BM KSL cells cultured in Media with and without EGF for 1 hour (scale bar = 100 μm). At right, quantification of tail moments in each condition (n = 179-256 cells/group, two-way ANOVA). ****P < 0.0001.

NHEJ is the predominant mechanism that regulates DNA repair following IR – induced DSB in quiescent HSCs [122,156,157]. DNA-PKcs is a principal enzyme effector of NHEJ in mammalian cells and, together with its regulator subunits, Ku70 and Ku80, stabilizes DNA breaks for repair [158,159,160,161]. Following 300 cGy irradiation, BM KSL cells displayed increased levels of phospho-DNA-PKcs (p-DNA-PKcs) at +1 hour compared to non-irradiated KSL cells (Figure 4).

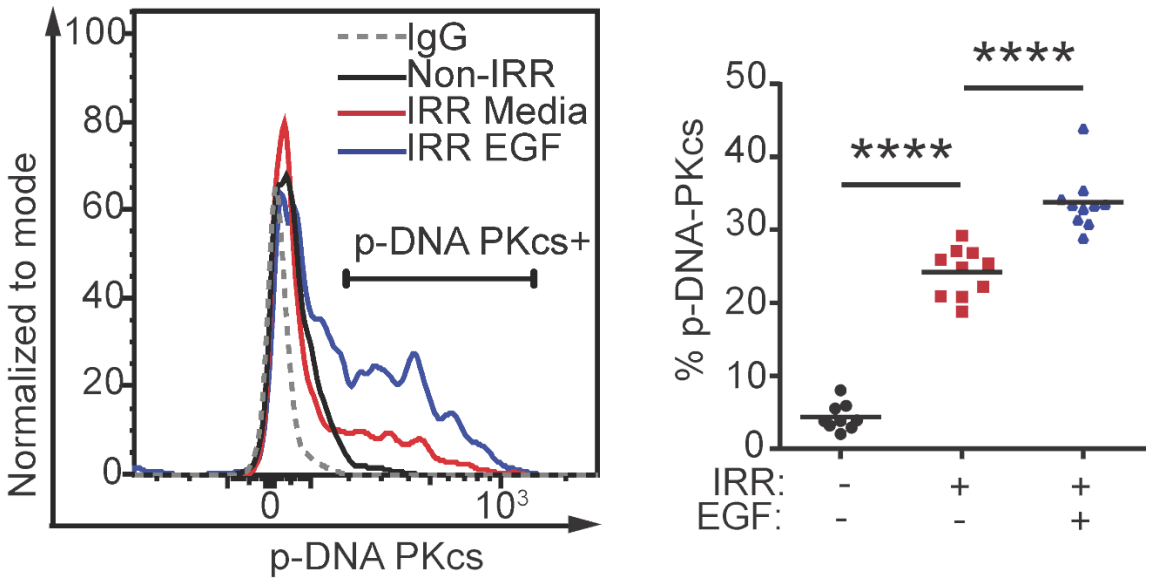

Figure 4. p-DNA PKcs in KSL cells. At left, flow cytometric analysis of p-DNA PKcs levels in non-irradiated KSL cells (black line), irradiated (100 cGy) KSL cells treated with Media alone (red) or Media plus EGF for 1 hour (blue). At right, %p-DNA PKcs+ KSL cells in each condition (n = 9-10/group, one-way ANOVA). ****P < 0.0001.

EGF treatment further increased p-DNA- PKcs levels in irradiated BM KSL cells compared to untreated KSL cells. EGF treatment also significantly increased the expression of X-ray repair cross complementing 6 (Xrcc6), which encodes the Ku70 protein (Figure 5) [162].

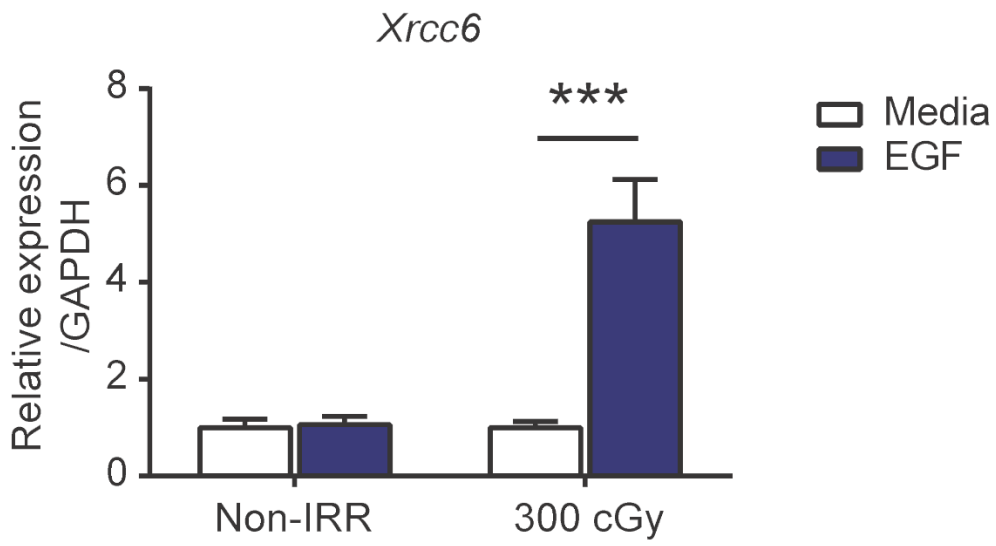

Figure 5. Xrcc6 RNA expression in cultured KSL cells. Gene expression of XRCC6 in non-irradiated KSL cells and at 1 hour following 300 cGy, treated with or without EGF (n=4/group, means + SEM, two-way ANOVA). ***P < 0.001

EGF treatment also increased phosphorylation of Artemis, a nuclease involved in end-trimming during NHEJ (Figure 6) [163].

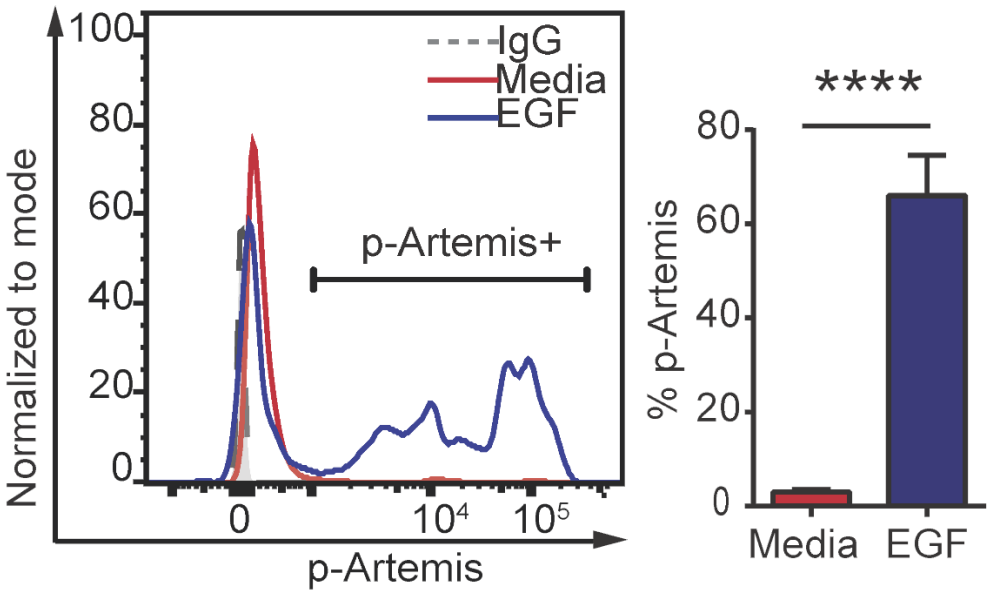

Figure 6. p-Artemis in KSL cells after radiation. (Left) representative histogram of p-Artemis (Ser516) in KSL cells irradiated with 300 cGy and then treated with or without EGF for 1 hour. (Right) %p-Artemis+ KSL cells (n=4/group, means + SEM, Student's t-test). ****P < 0.0001

Conversely, EGF treatment did not affect the expression of genes encoding proteins involved in HR, including replication protein A 1 (RPA1) and ataxia telangiectasia and rad3 – related protein (ATR) interacting protein (ATRIP), or foci of Rad51, a recombinase integral to HR, in irradiated KSL cells (Figure 7 - 9) [164,165].

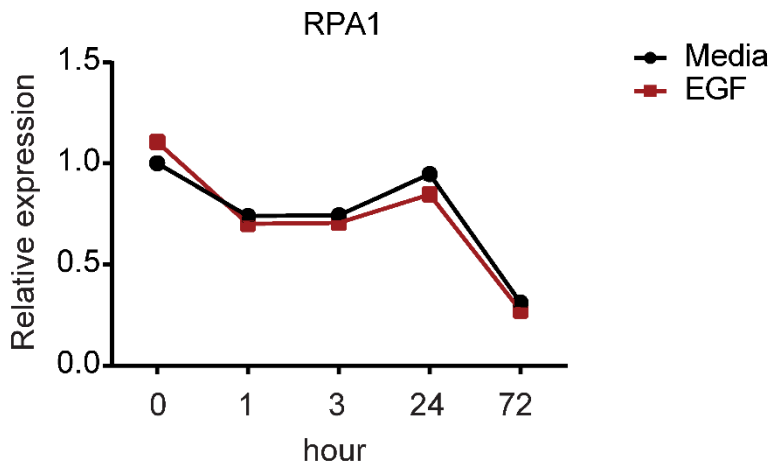

Figure 7. RPA1 RNA expression kinetics in KSL cells after radiation. Rpa1 gene expression in BM KSL cells over time in culture with complete media (Media) with or without 100 ng/ml EGF. The expression is relative to GAPDH (n=3/group, means ± SEM, Student's t-test).

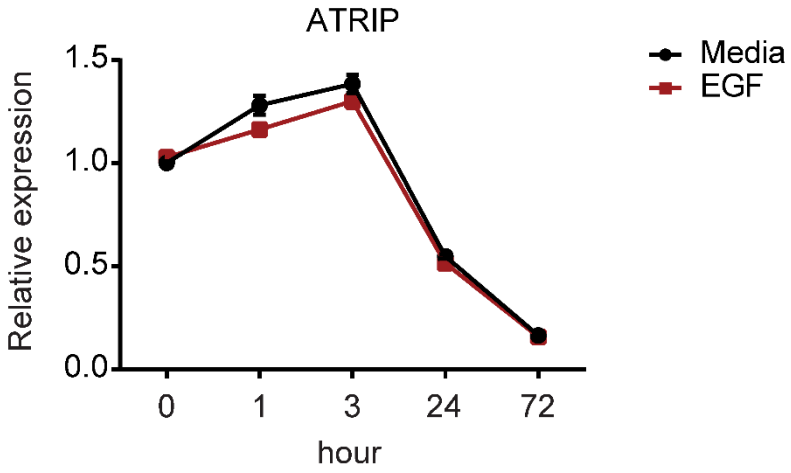

Figure 8. ATRIP RNA expression kinetics in KSL cells after radiation. Expression of the gene encoding ATR Interacting protein (Atrip) in BM KSL cells over time in culture with Media with or without EGF, relative to GAPDH (n=3/group, means ± SEM, Student's t-test).

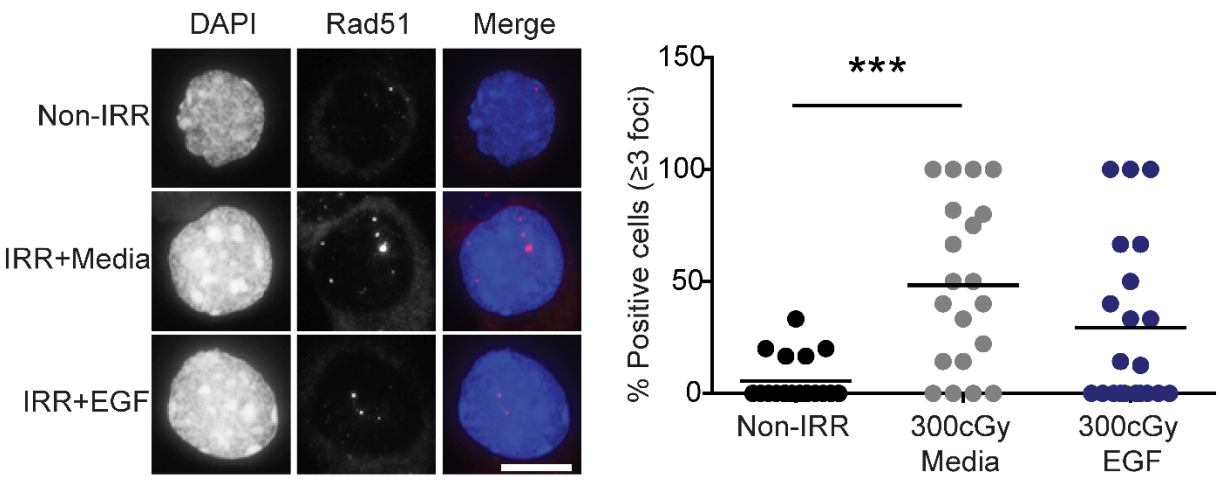

Figure 9. Rad51 foci in KSL cells. At left, immunofluorescence microscopy of Rad51 foci in non-irradiated and 300cGy-irradiated (IRR) KSL cells with or without EGF for 2 hours (scale bar = 10 μm). At right, percentage of Rad51+ KSL cells (≥3 foci/cell, n = 19-21 fields/group, one-way ANOVA). ***P < 0.001.

Taken together, these results suggest that EGF treatment activates the NHEJ machinery in HSCs, without effects on HR. Since cell cycle status impacts DNA repair processes [122,151], we evaluated the effects of EGF treatment on BM KSL cell cycle status. We observed no differences in the percentages of KSL cells in G0, G1, or G2/S/M phase between EGF – treated and saline-treated, irradiated cells (Figure 10).

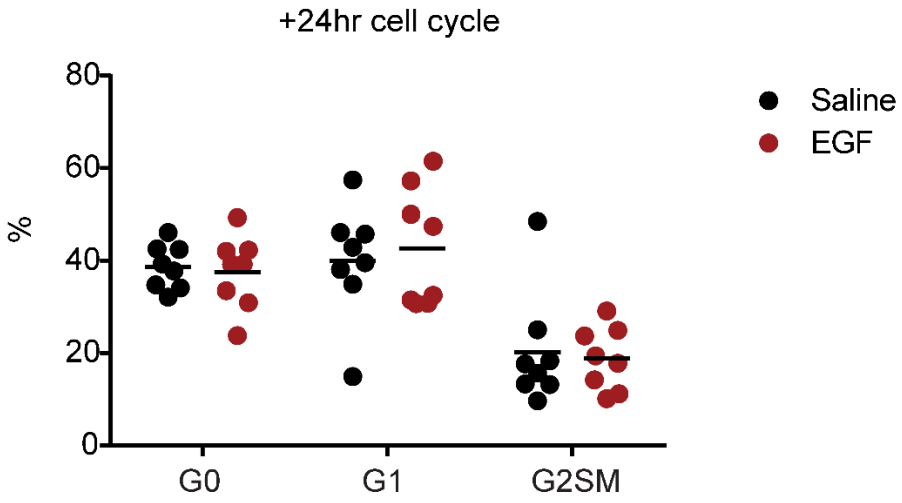

Figure 10. Cell cycle status of KSL cells after radiation. Cell cycle analysis of BM KSL cells collected at +24 hours from C57BL/6 mice irradiated with 500cGy TBI and treated with 0.5 μg/g EGF or saline (n=8/group, two-way ANOVA).

To determine if DNA-PKcs was necessary for EGF-mediated reduction in DNA damage in HSCs, we treated irradiated BM KSL cells with EGF with and without the selective DNA- PKcs inhibitor, NU7441 [166]. NU7441 treatment abrogated EGF-mediated DNA damage repair in irradiated KSL cells, as measured by γ-H2AX foci and the Comet assay (Figure 11, 12).

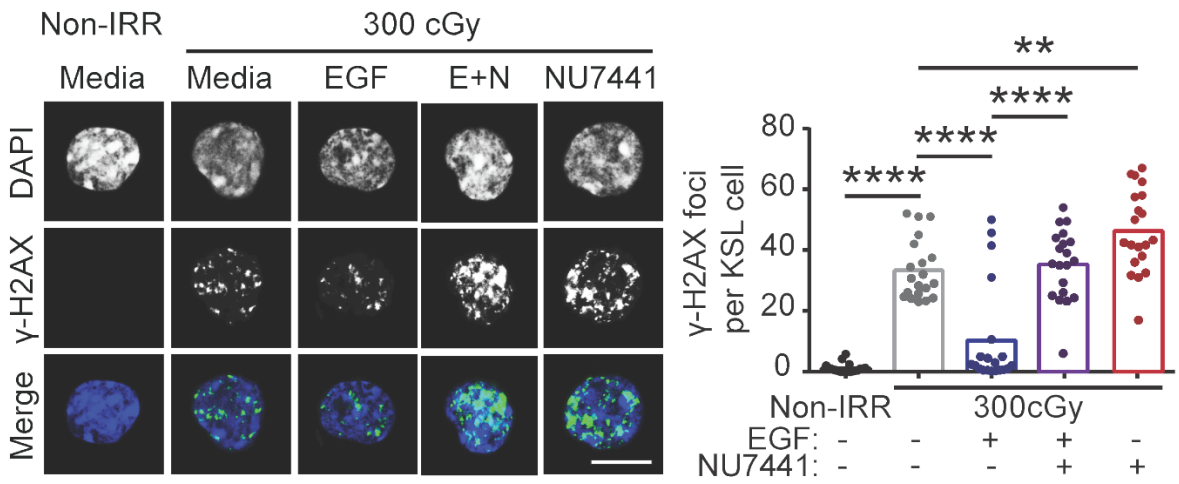

Figure 11. γ-H2AX foci in KSL cells treated with DNA PKcs inhibitor. At left, fluorescence microscopy images of γ-H2AX foci in non-irradiated KSL cells and irradiated KSL cells in Media +/- EGF +/- NU7441 (E + N, scale bar = 10 μm). At right, numbers of γ-H2AX foci per KSL cell in each condition (n= 20/group, Two way ANOVA). **P < 0.01, ****P < 0.0001

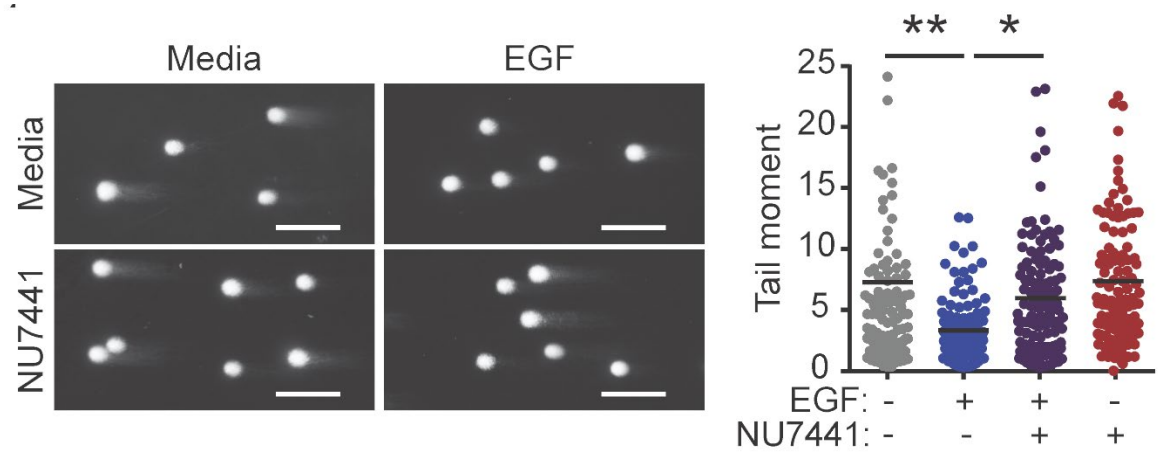

Figure 12. Comet tail of irradiated KSL cells treated DNA PKcs inhibitor. At left, representative images of Comet assay of 300cGy-irradiated KSL cells cultured with Media +/- EGF +/- NU7441 (scale bar = 100μm). A right, tail moments from KSL cells from each condition (n = 102-114 cells/group, One way ANOVA).

NU7441 treatment also suppressed the EGF-mediated recovery of colony-forming cells (CFCs) from irradiated KSL cells in culture, suggesting that DNA-PKcs activation was necessary for EGF-mediated hematopoietic regenerative effects (Figure 13).

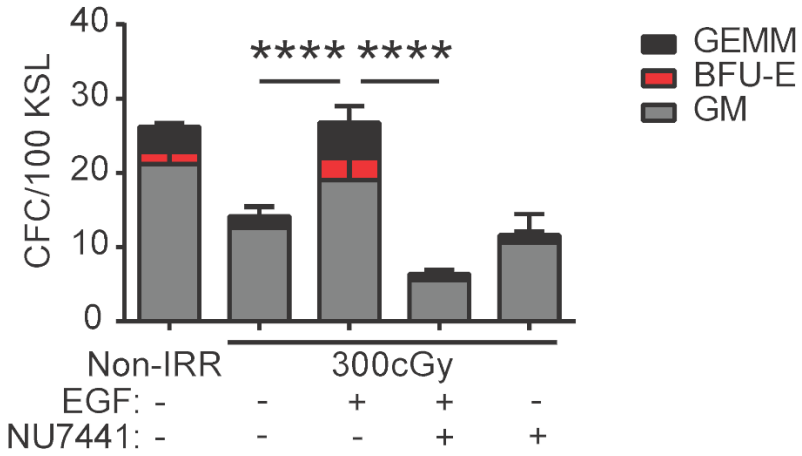

Figure 13. Colony-forming cells of irradiated KSL cells treated with EGF and DNA PKcs inhibitor. Numbers of CFCs from non-irradiated BM KSL cells and irradiated KSL cells cultured in Media +/- EGF +/- NU7441 for 72 hours (n = 6/group, means + SEM, Two way ANOVA). ****P < 0.0001.

2.3.2. EGF – mediated DNA repair in BM HSCs is dependent on Akt

In tumor cells, EGFR has been shown to regulate DNA-PKcs activity via two distinct mechanisms following irradiation. EGFR can bind with DNA-PKcs and physically translocate DNA-PKcs from the cytoplasm into the nucleus or increase DNA PKcs activity via induction of PI3k/Akt signaling [167]. Irradiation with 300 cGy did not increase Akt phosphorylation in BM KSL cells (Figure 14). However, the treatment of irradiated KSL cells with 100 ng/ml EGF increased Akt phosphorylation measured by microscopy and flow cytometry (Figure 14, 15).

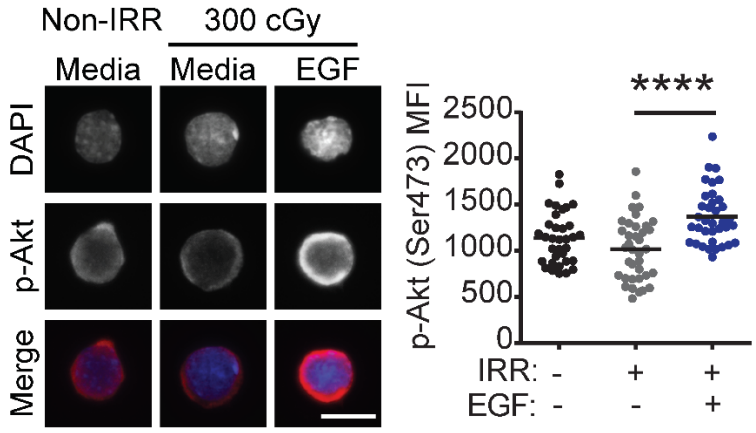

Figure 14. p-Akt(Ser473) in KSL cells. At left, representative microscopic images of p-Akt in non-irradiated and irradiated KSL cells cultured in Media +/- EGF for 5 minutes (scale bar = 10 μm). At right, p-Akt MFI in KSL cells in each condition (n = 34-37 cells/group, Student's t-test). ****P < 0.0001

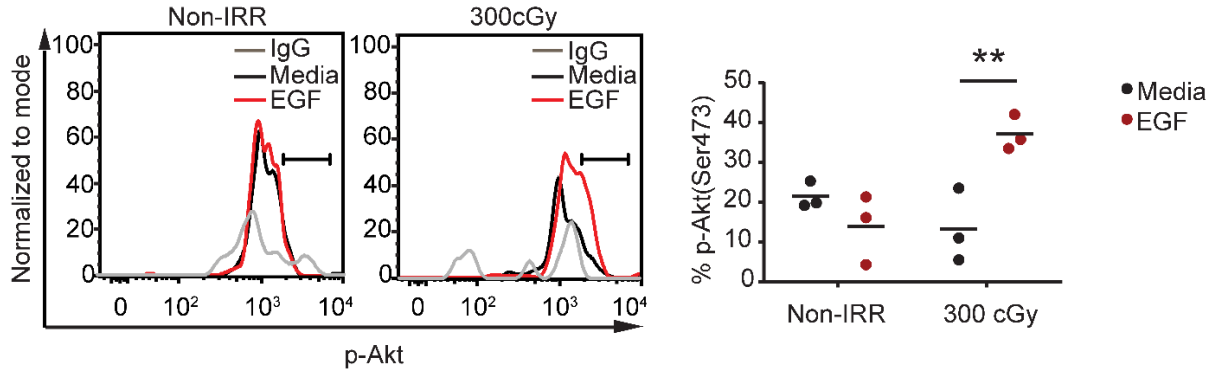

Figure 15. p-Akt(Ser473) in KSL cells after EGF treatment. Representative flow cytometric analysis of p-Akt (Ser473) in BM KSL cells at +5 minutes following treatment with 100 ng/ml EGF or saline treatment (n=3/group, two-way ANOVA). **P < 0.01

Treatment with a selective Akt inhibitor, MK2206, blocked EGF-mediated phosphorylation of Akt (Figure 16) [137].

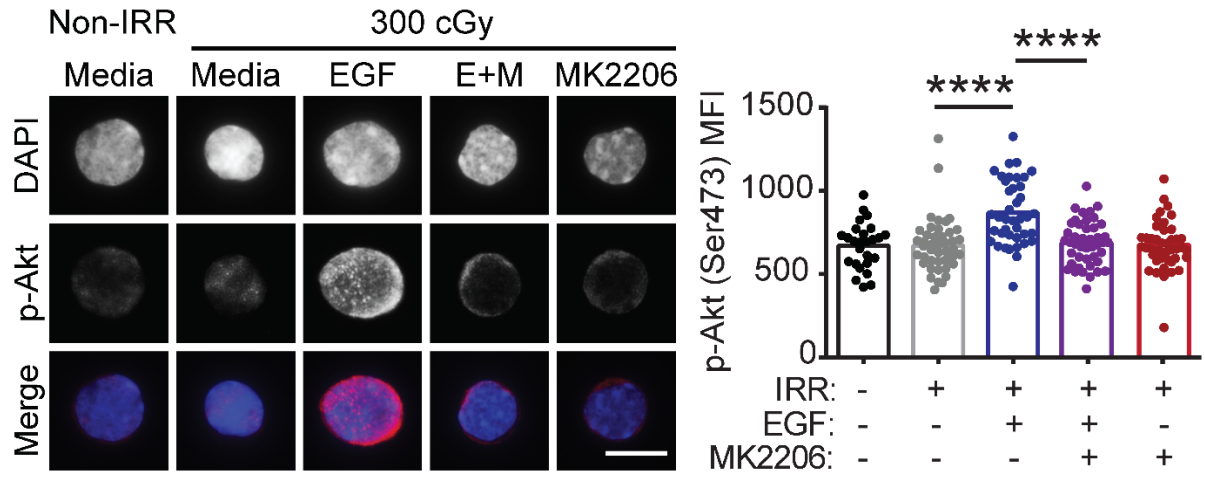

Figure 16. p-Akt(Ser473) in KSL cells treated with Akt inhibitor. At left, representative microscopic images of p-Akt in non-irradiated and irradiated KSL cells cultured with Media +/- EGF +/- MK 2206 for 5 minutes (scale bar = 10 μm). At right, p-Akt MFI in KSL cells in each condition (n = 26-44 cells/group, One way ANOVA). ****P < 0.0001

Treatment with MK2206 also abrogated EGF – mediated reduction in γ-H2AX foci in irradiated KSL cells (Figure 17).

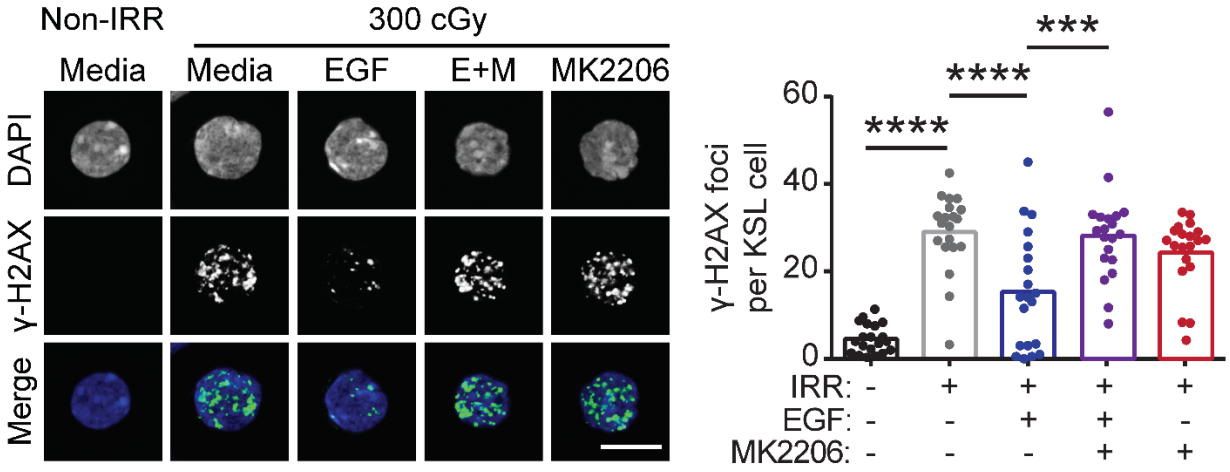

Figure 17. γ-H2AX foci in KSL cells treated with EGF and Akt inhibitor. At left, representative microscopic images of γ-H2AX foci in the conditions shown at 1 hour of culture (scale bar = 10

μm). At right, numbers of foci per KSL cell in each condition (n = 20 cells/group, One way ANOVA). ***P < 0.001, ****P < 0.0001

EGF-mediated phosphorylation of DNA-PKcs in irradiated KSL cells was also blocked by MK2206 (Figure 18).

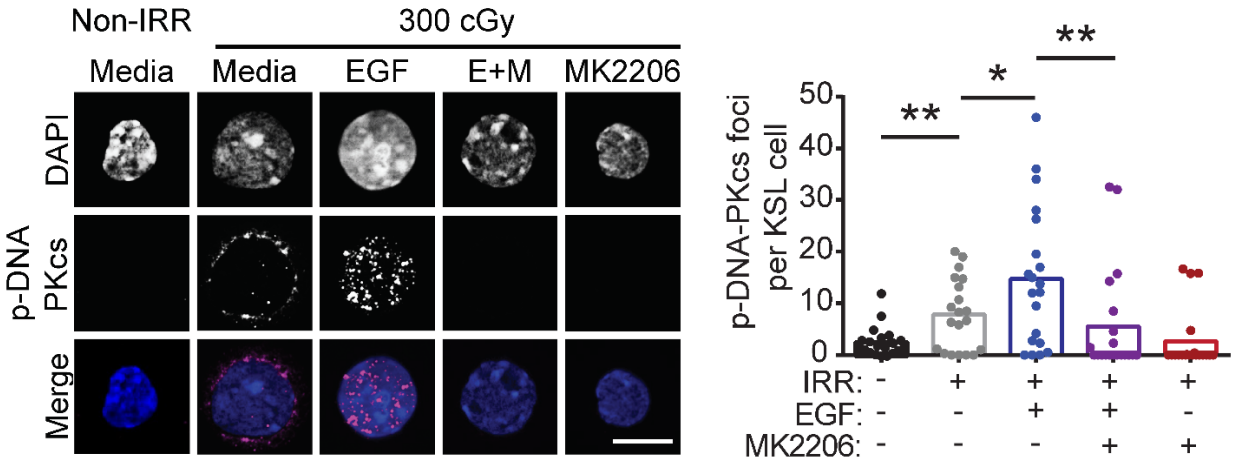

Figure 18. p-DNA PKcs in KSL cells treated with EGF and Akt inhibitor. At left, representative microscopic images of p-DNA PKcs foci in the conditions shown at (scale bar = 10 μm). At right, numbers of p-DNA PKcs foci per KSL cell in each condition (n = 20 cells/group, One way ANOVA). *P < 0.05, **P < 0.01

These results suggest that EGF-mediated activation of DNA-PKcs and DNA repair in irradiated HSCs is dependent on Akt. EGF-mediated recovery of CFCs from irradiated BM KSL cells was also blocked by Akt inhibition, suggesting a requirement for Akt in EGFR – mediated hematopoietic regeneration after irradiation (Figure 19).

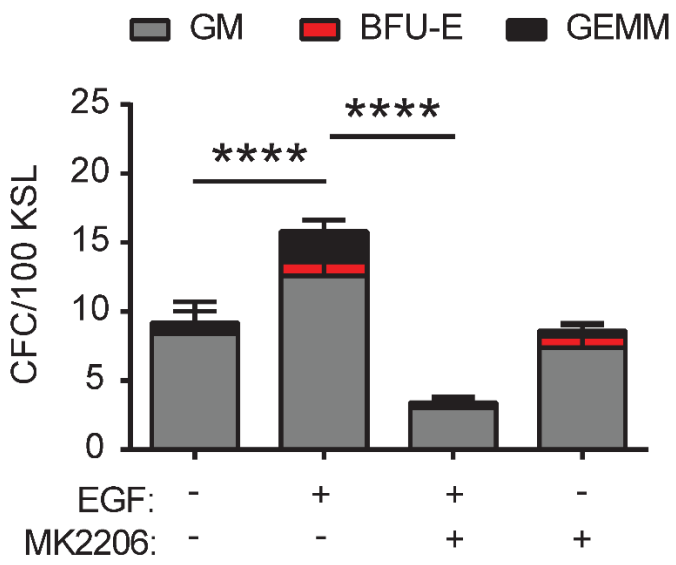

Figure 19. Colony-forming cells of KSL cells treated with EGF and Akt inhibitor. CFCs from KSL cells irradiated with 300cGy and cultured in Media +/- EGF +/- MK2206 (n = 6/group, means ± SEM, Two way ANOVA). ****P < 0.0001.

2.3.3. EGF promotes hematopoietic regeneration in vivo in a DNA-PKcs – dependent manner

To determine whether EGF regulates HSC DNA repair and DNA-PKcs in vivo, we irradiated mice with 500 cGy TBI and treated with 0.5 µg/g EGF or saline subcutaneously (SQ) x 1 and measured DNA damage in BM KSL cells at +4 hours (Figure 20).

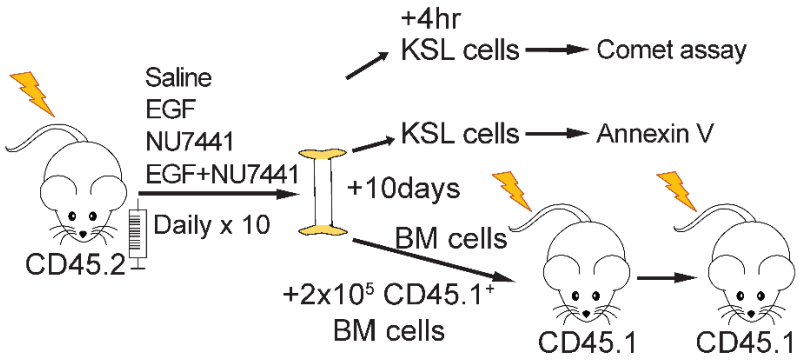

Figure 20. Schematic of irradiated mice treated with EGF and DNA PKcs inhibitor in vivo. Schematic of experimental design. C57BL/6 mice were irradiated at 500cGy TBI followed by daily injections of saline, EGF, NU7441, or EGF + NU7441 for 10 days. BM cells were collected at +4 hours for Comet assay, and at day +10 for Annexin V apoptosis assay and competitive repopulation assays.

EGF – treated mice demonstrated decreased DNA damage in BM KSL cells compared to control mice after 500 cGy (Figure 21). Systemic administration of the DNA-PKcs inhibitor, NU7441, abrogated EGF-mediated reduction in DNA damage in BM KSL cells (Figure 21).

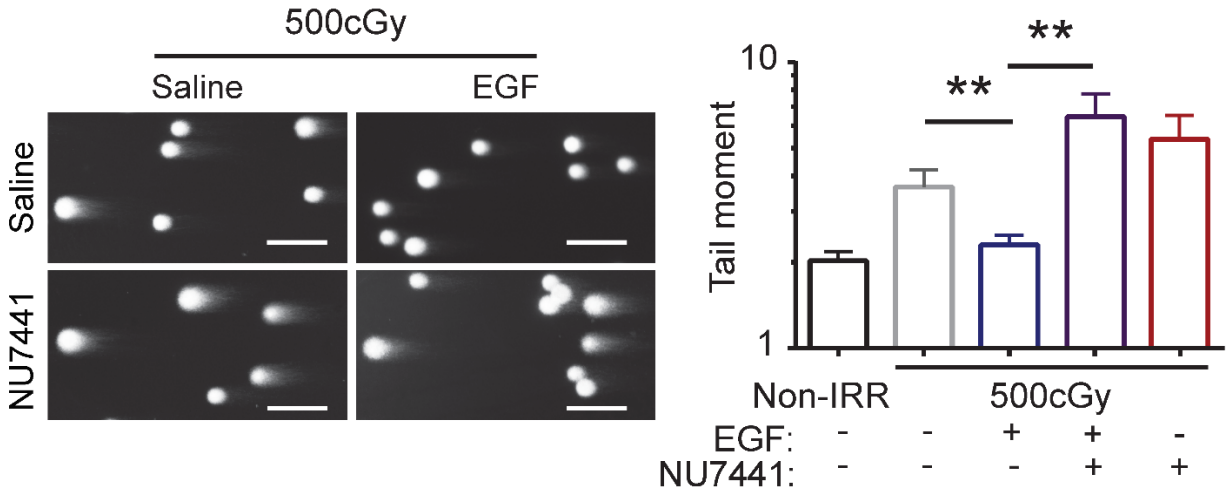

Figure 21. Comet tail of KSL cells isolated from irradiated mice treated with EGF and DNA PKcs inhibitor. At left, representative images of neutral Comet assay of BM KSL cells collected at +4 hours following 500cGy TBI and treatment with EGF +/- NU7441 (scale bar = 100μm). At right, measurements of the tail moment in KSL cells in each condition (n = 6-7 replicates/group, means ± SEM, Student's t-test). **P < 0.01

EGF treatment daily for 10 days decreased the percentages of Annexin V+ BM KSL cells in irradiated C57BL/6 mice compared to controls, and NU7441 treatment blocked this anti-apoptotic effect (Figure 22).

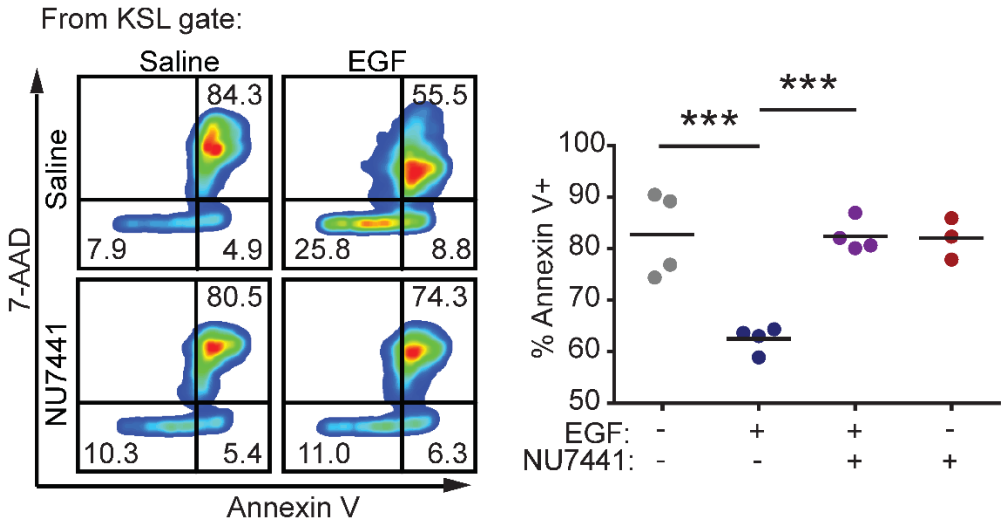

Figure 22. Annexin V cell death profile of KSL cells from irradiated mice after EGF and DNA PKcs inhibitor administration. (Left) representative flow cytometric analysis of Annexin V^+ and $7AAD^+$ of BM KSL cells at day +10 from mice described in (Figure 20). (Right) % Annexin V^+ KSL cells in each condition (n=3-4/group, One-way ANOVA). ***P < 0.001

Treatment of irradiated mice with NU7441 also blocked EGF – mediated recovery of BM CFCs (Figure 23).

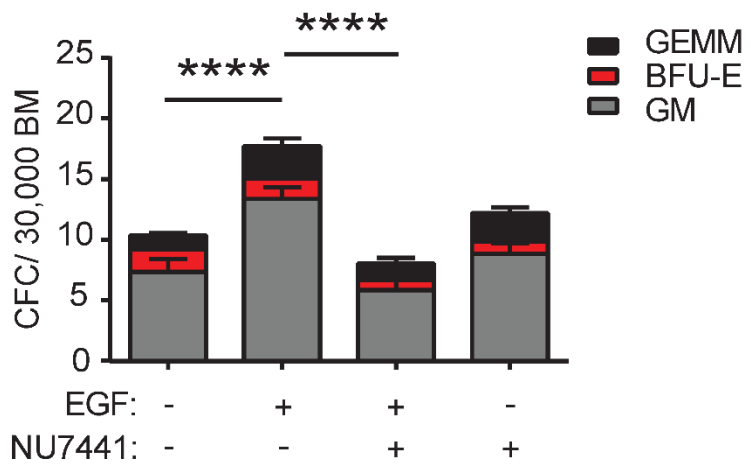

Figure 23. Colony-forming cells of BM from irradiated mice after EGF and DNA PKcs inhibitor administration. Numbers of CFCs in BM at day +10 from mice described in (Figure 20) (n=6/group, means ± SEM, Two-way ANOVA). ****P < 0.0001

EGF treatment increased the percentages of BM KSL cells and CD150+CD48-CD41-KSL HSCs [168] at day +10 following 500 cGy, and NU7441 treatment suppressed these effects (Figure 24).

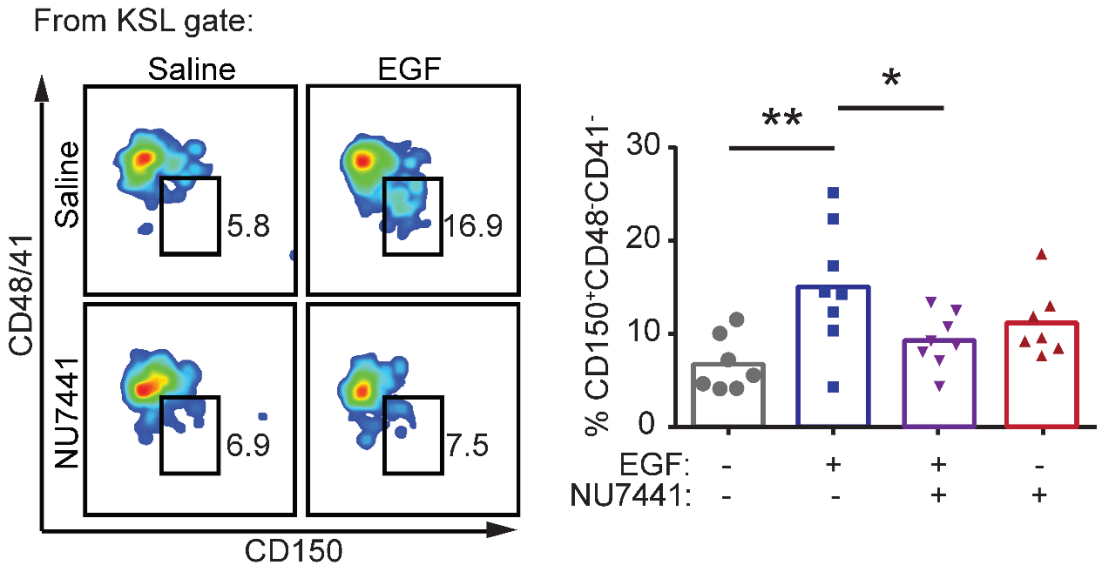

Figure 24. SLAM KSL cells from irradiated mice treated with EGF and DNA PKcs inhibitor. (Left) flow cytometric analysis of BM $CD150^{+}CD48^{-}CD41^{-}$ KSL cells at day +10 from mice described in (Figure 20). (Right) $\%CD150^{+}CD48^{-}CD41^{-}$ cells within the KSL population in each group (n=7-8/group, One-way ANOVA). *P < 0.05, **P < 0.01

EGF – mediated recovery of PB WBCs and lymphocytes was also blocked by NU7441 treatment (Figure 25).

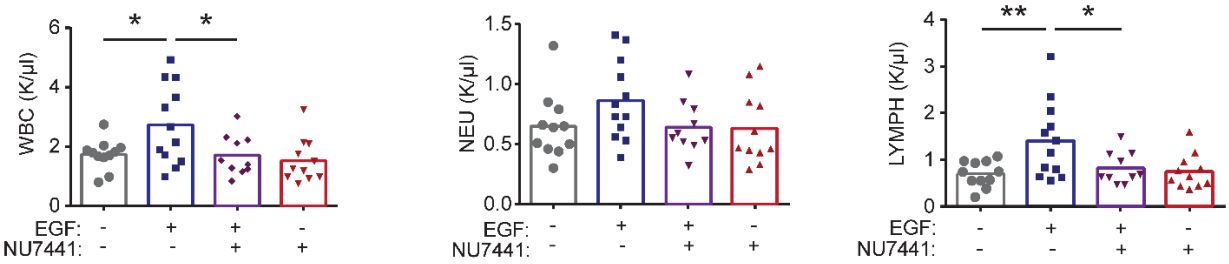

Figure 25. Peripheral blood counts of irradiated mice treated with EGF and DNA PKcs inhibitor. PB white blood counts (WBC), neutrophils (NEU), lymphocytes (LYMPH) in C57BL/6 mice at day +10 following 500 cGy TBI, and daily treatment with saline, EGF, NU7441 or EGF + NU7441 (n=10-12, one-way ANOVA). *P < 0.05, **P < 0.01

Competitive repopulation assays were performed to measure functional HSC content at day+10 following 500 cGy TBI. Primary recipient mice transplanted with BM cells from irradiated, EGF – treated mice displayed increased total donor CD45.2+ cell engraftment and multilineage engraftment in the BM at 16 weeks post-transplant compared to recipient mice transplanted with equal doses of BM from irradiated, control mice (Figure 26, 27).

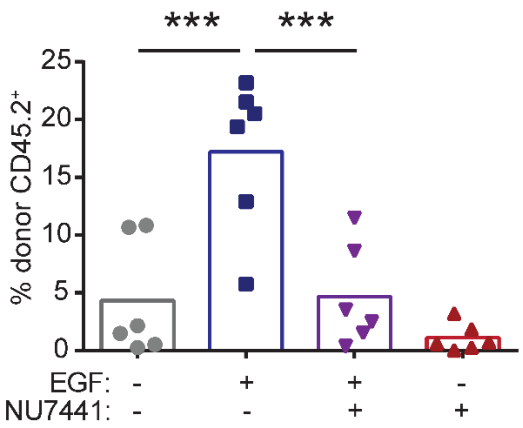

Figure 26. Engraftment of donor cells in primary recipients. Percentages of donor CD45.2+ cells in the BM of primary recipient mice at 16 weeks following transplant of BM cells collected at day +10 from the mice in (Figure 19)(n = 6 mice/group, two-way ANOVA).

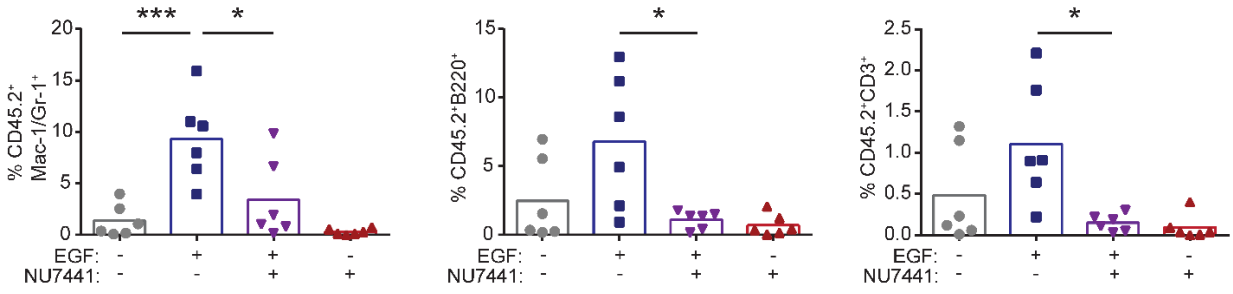

Figure 27. Multilineage engraftment of donor cells in primary recipients. Percentage donor CD45.2+ myeloid (Mac1/Gr1+) cells, CD45.2+B220+ B cells, CD45+CD3+ T cells in the PB of primary recipient mice at 16 weeks following transplantation of BM cells collected from irradiated

C57BL/6 at day +10 following the treatments shown in (B) (n=6/group, one-way ANOVA). *P < 0.05, ***P < 0.001

Recipient mice transplanted with BM cells from irradiated donor mice treated with EGF + NU7441 displayed no increase in engraftment of total cells, myeloid, B, or T cells compared to irradiated, controls. Secondary mice transplanted with BM cells from primary recipients in the irradiated, EGF – treatment group displayed increased total donor engraftment and multilineage engraftment at 16 weeks, but secondary recipient mice transplanted with equal doses of BM cells from irradiated mice treated with EGF + NU7441 demonstrated no differences in donor cell engraftment compared to the irradiated control group (Figure 28, 29).

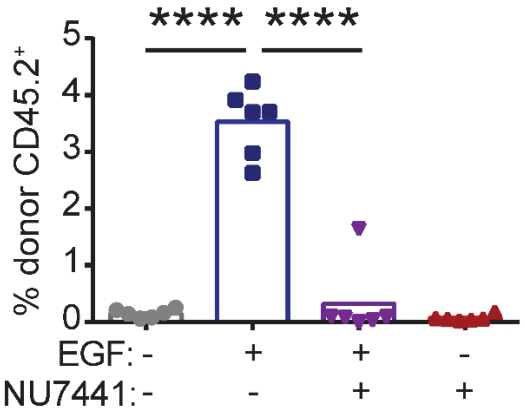

Figure 28. Engraftment of donor hematopoietic cells in secondary recipients. Percentages of donor CD45.2$^+$ cells in the BM of secondary mice at 16 weeks post-transplant. Secondary mice were transplanted with 5 x 10^6 BM cells collected from primary mice at 16 weeks post-transplant, along with 2 x 10^5 competitor BM (CD45.1$^+$) cells (n = 6/group, two-way ANOVA). ****P < 0.0001

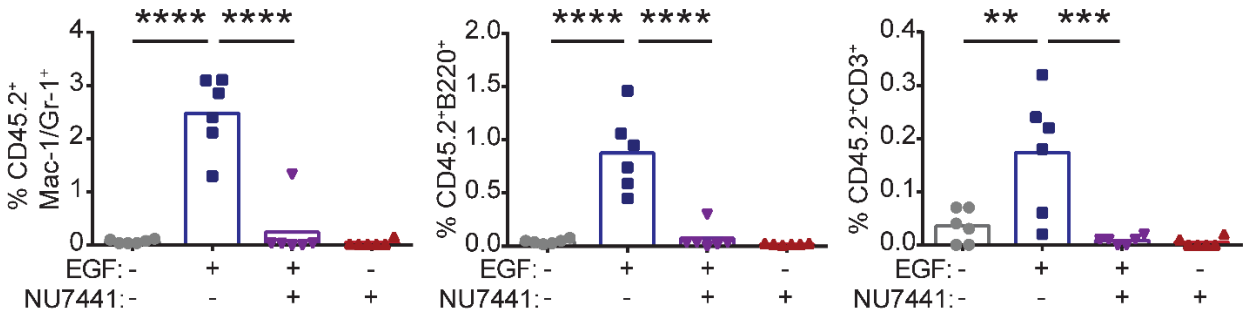

Figure 29. Multilineage engraftment of donor hematopoietic cells in secondary recipients. Percentages of $CD45.2^+Mac1/Gr1^+$ (myeloid) cells, $CD45.2^+B220^+$ (B) cells, and $CD45.2^+CD3^+$ T cells in the BM of secondary recipients at 16 weeks post-transplant (n=6/group, two-way ANOVA). **P < 0.01, ***P < 0.001, ****P < 0.0001

These results suggest that EGF – mediated HSC recovery in irradiated mice is dependent on DNA-PKcs activation. Of note, short-duration EGF treatment (2 doses, day +1, +2 after 500 cGy TBI) did not increase PB complete blood counts, BM cells, or HSCs in mice at day +10 compared to irradiated controls, suggesting that longer duration of EGF treatment was necessary for hematopoietic regeneration after TBI (Figure 30, 31).

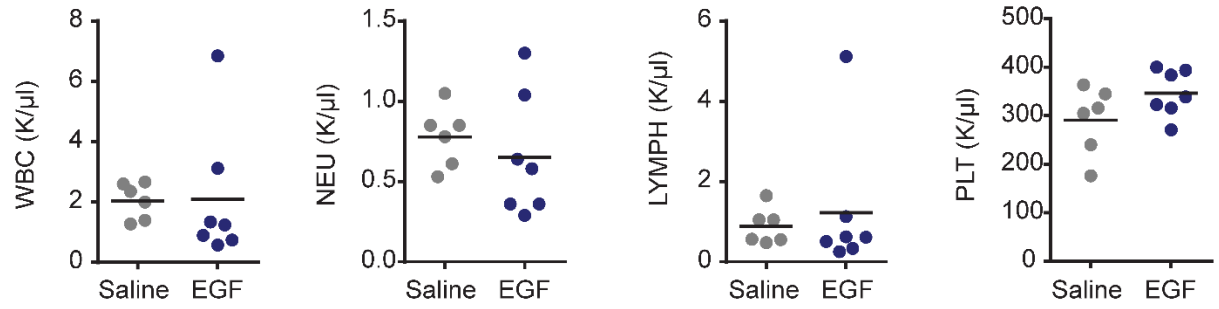

Figure 30. Peripheral blood counts in irradiated mice treated with two doses of EGF. PB complete blood count of WBC, NEU, LYMPH, PLT at + 10 days post-irradiation in 500cGy TBI irradiated mice treated with two doses of EGF (n=6-7, Student's t-test).

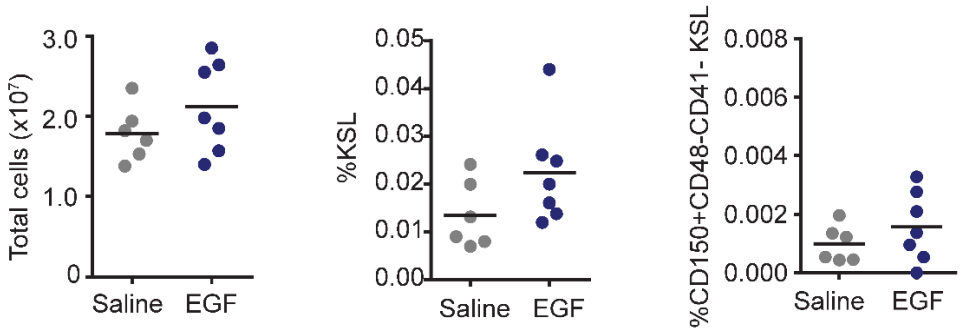

Figure 31. Bone marrow analysis of irradiated mice treated with two doses of EGF. (Left) Total bone marrow cell counts at + 10 days post-irradiation in 500cGy TBI irradiated mice treated with two doses of EGF (n=6-7, Student's t-test). (Middle) Frequency of KSL cells in total bone marrow cells at + 10 days post-irradiation in 500cGy TBI irradiated mice treated with two doses of EGF (n=6-7, Student's t-test). (Right) Frequency of $CD150^{+}CD48^{-}CD41^{-}$ KSL cells in total bone marrow cells at + 10 days post-irradiation in 500cGy TBI irradiated mice treated with two doses of EGF (n=6-7, Student's t-test).

2.3.4. EGF promotes hematopoietic regeneration following chemotherapy

To determine whether EGF treatment could promote hematopoietic regeneration following chemotherapy, we treated mice with an anthracycline, doxorubicin [169], followed by EGF or saline from day +1 to +10. Doxorubicin treatment caused pancytopenia in control mice at day +10; conversely, mice treated with doxorubicin followed by EGF displayed marked increases in PB WBCs, neutrophils, lymphocytes, and platelet counts compared to controls (Figure 32).

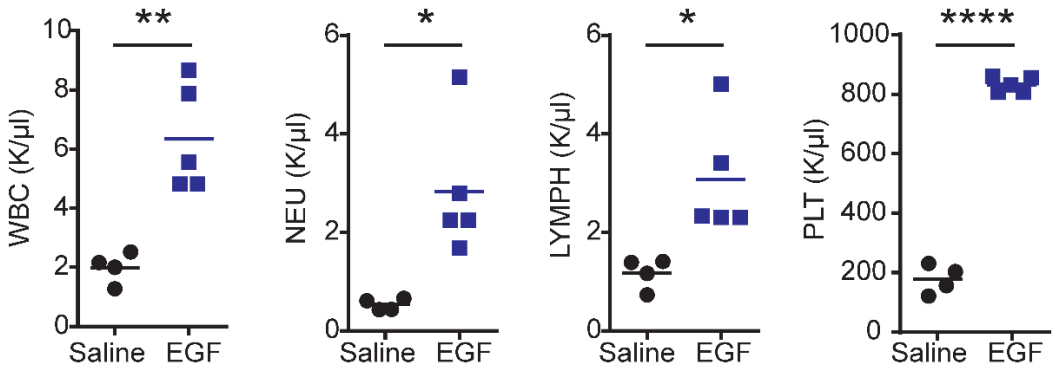

Figure 32. Peripheral blood counts of doxorubicin conditioned mice. C57BL/6J mice were injected with one dose of doxorubicin as chemotherapy followed by EGF or saline treatment. PB blood count of white blood counts (WBC), neutrophils (NEU), lymphocytes (LYMPH) of mice at +10 days post doxorubicin (n=4-5, Student's t-test). *P < 0.05, **P < 0.01, ****P < 0.0001

Concordantly, BM cell counts, KSL cells, and percentages of CD150+CD48-41-KSL cells were increased in EGF-treated mice compared to controls (Figure 33, 34).

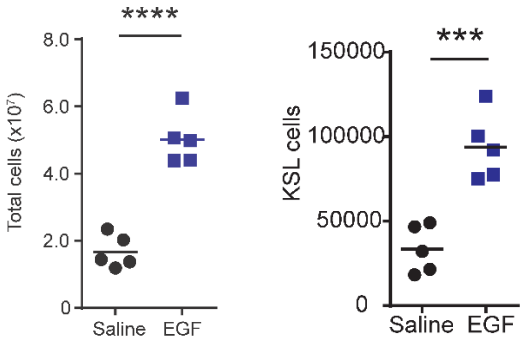

Figure 33. Bone marrow analysis of doxorubicin conditioned mice. C57BL/6J mice were injected with one dose of doxorubicin as chemotherapy followed by EGF or saline treatment. (Left) Total bone marrow cells from two femurs and two tibias per mouse at +10 days post doxorubicin (n=5/group, Student's t-test). (Right) The number of KSL cells per mouse at +10 days post doxorubicin (n=5/group, Student's t-test). ***P < 0.001, ****P < 0.0001

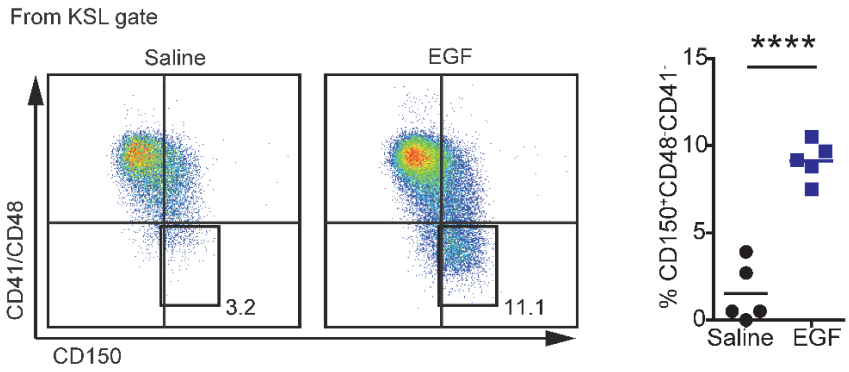

Figure 34. Bone marrow long-term HSC analysis of doxorubicin conditioned mice. (Left) Representative flow cytometry plot of $CD150^{+}CD41^{-}CD48^{-}$ cell in the bone marrow of mice at +10 days post doxorubicin. (Right) Percentage of $CD150^{+}CD41^{-}CD48^{-}$ cells out of KSL cell population at +10 days post doxorubicin (n=5/group, Student's t-test). **** $P < 0.0001$

BM KSL cells from doxorubicin – treated mice displayed increased y-H2AX foci and tail moments at +12 hours; EGF treatment decreased doxorubicin-mediated DNA damage and increased p-DNA-PKcs in BM KSL cells at +12 hours following doxorubicin exposure (Figure 35, 36, 37).

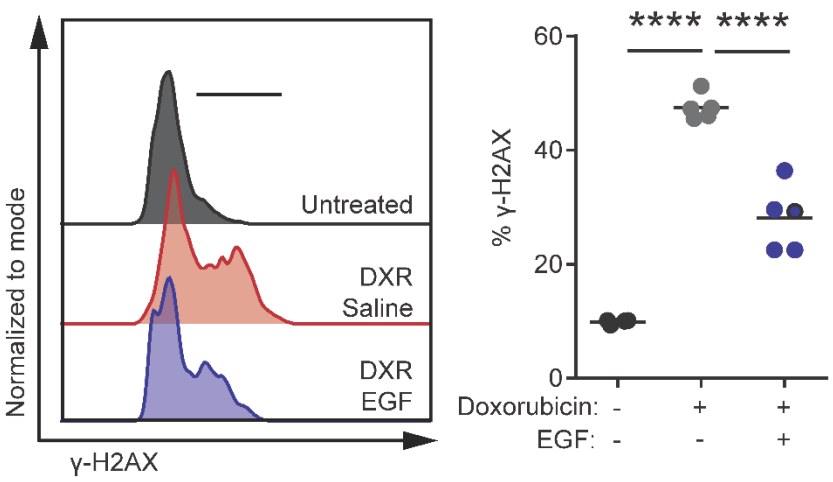

Figure 35. γ-H2AX foci in KSL cells collected from doxorubicin conditioned mice. (Left) Representative flow cytometry plot of γ–H2AX in KSL cells from mice collected at +12 hours post doxorubicin. Blackline in the plot demonstrates the gating of γ–H2AX. (Right) Quantification of γ–H2AX (n=3-5, One-way ANOVA). ****P < 0.0001

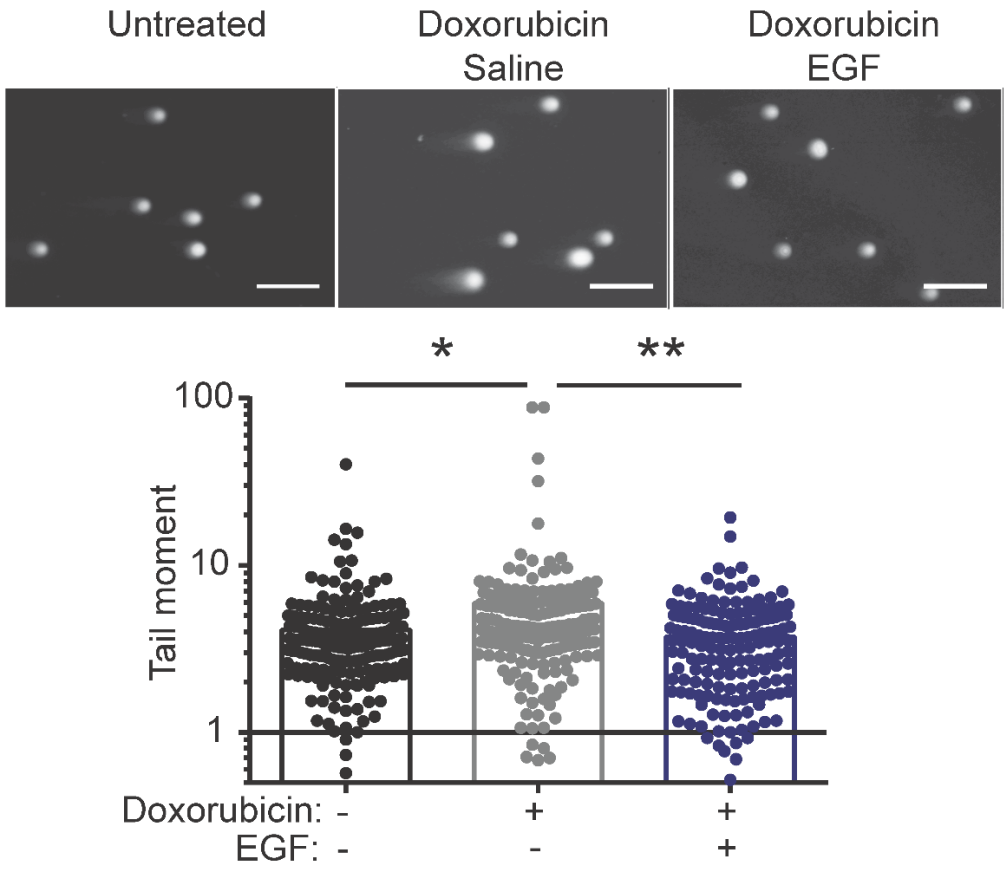

Figure 36. Comet tail of KSL cells sorted from doxorubicin conditioned mice. (Top) representative images of Comet assay. Mice were untreated, treated with doxorubicin and saline or doxorubicin, and EGF in vivo. KSL cells were sorted at +12 hours post doxorubicin for Comet assay (scale bar = 100 μm). (Bottom) quantification of tail moments in each condition (n = 161-184 cells/group, One-way ANOVA). *P < 0.05, **P < 0.01

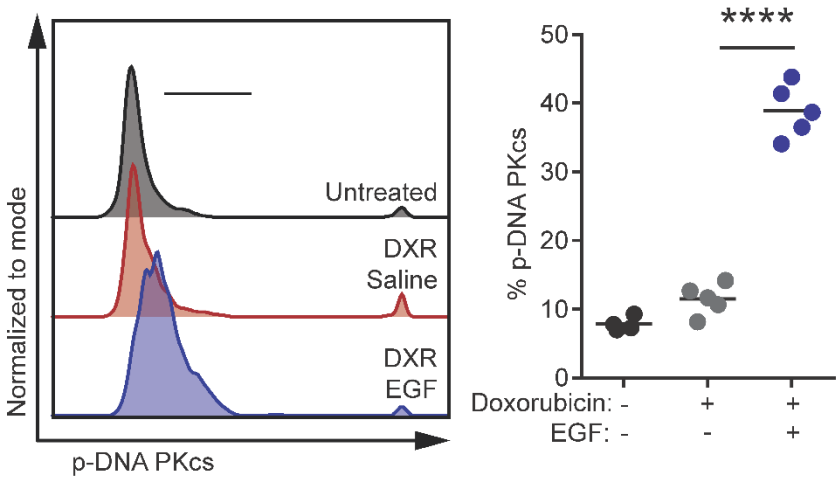

Figure 37. p-DNA PKcs in KSL cells from mice conditioned with doxorubicin. (Left) Representative flow cytometry plot of p-DNA PKcs in KSL cells from mice collected at +12 hours post doxorubicin. (Right) Percentage of p-DNA PKcs (n=3-5, One-way ANOVA). ****P < 0.0001

2.3.5. EGF administration does not promote leukemogenesis

To test whether EGF treatment might adversely promote tumor growth in vivo, we transplanted CD45.1+ B6.SJL mice with CD45.2+ BM lin- cells transduced with a retroviral HOXA9/MEIS1 vector that produces acute myeloid leukemia (AML) at 3-4 weeks post-transplantation [139]. Recipient mice demonstrated AML at 3 weeks post-transplant and were subsequently treated with cytarabine x 5 days to reduce tumor burden. Mice were then treated x 10 days with EGF or saline SQ daily and CD45.2+ AML cells and Mac1/Gr1+ myeloid cells were subsequently measured in the BM and PB. We observed no differences in percentages of CD45.2+ AML cell numbers or Mac1/Gr1+ cells in the BM or PB of EGF – treated versus saline-treated mice (Figure 38, 39, 40, 41).

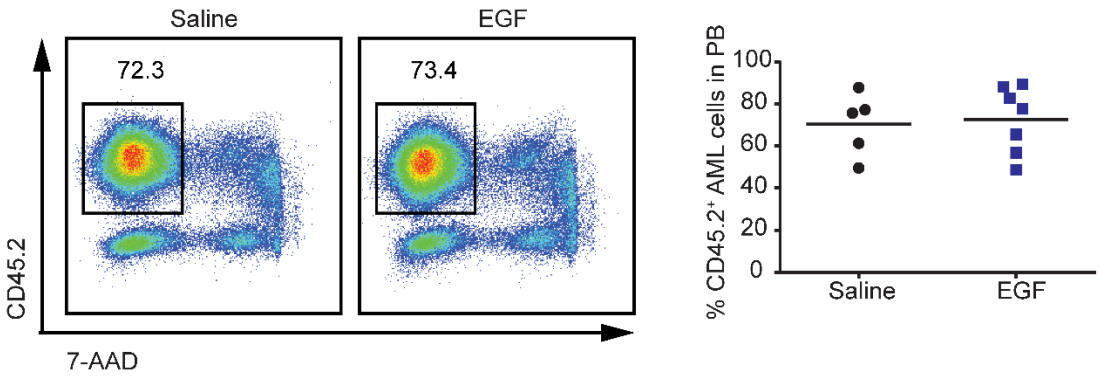

Figure 38. Transduced cells in the peripheral blood of mice with leukemia burden. (Left) Representative flow cytometry plot of HoxA9/Meis1 transduced cells ($CD45.2^+$) engraftment in the PB of recipients. (Right) Quantification of AML cells in the PB of recipients at 2 weeks post last dose of cytarabine (n=5-7, Student's t-test).

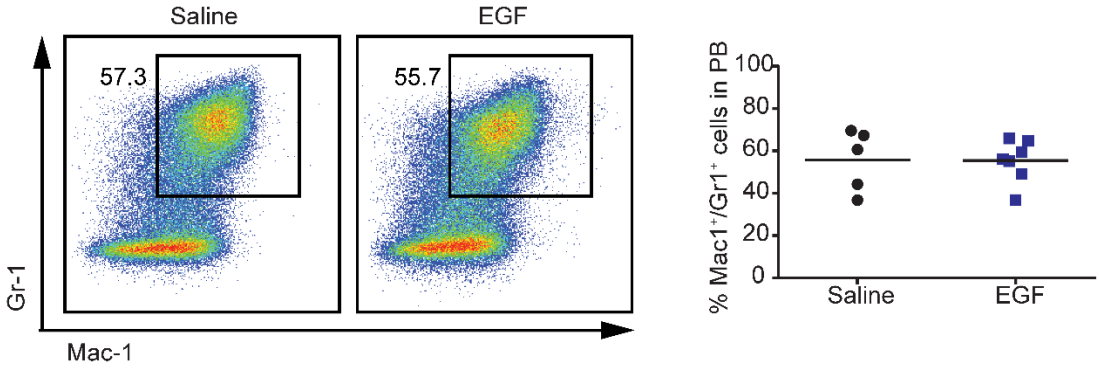

Figure 39. Myeloid transduced cells in the peripheral blood of mice with leukemia burden. (Left) Representative flow cytometric analysis of $Mac1^+Gr\text{-}1^+$ cells among total $CD45.2^+$ cells in the PB of leukemic mice at 2 weeks post last dose of cytarabine. (Right) Quantification of % $Mac1^+Gr\text{-}1^+$ myeloid cells (n=5-7, Student's t-test).

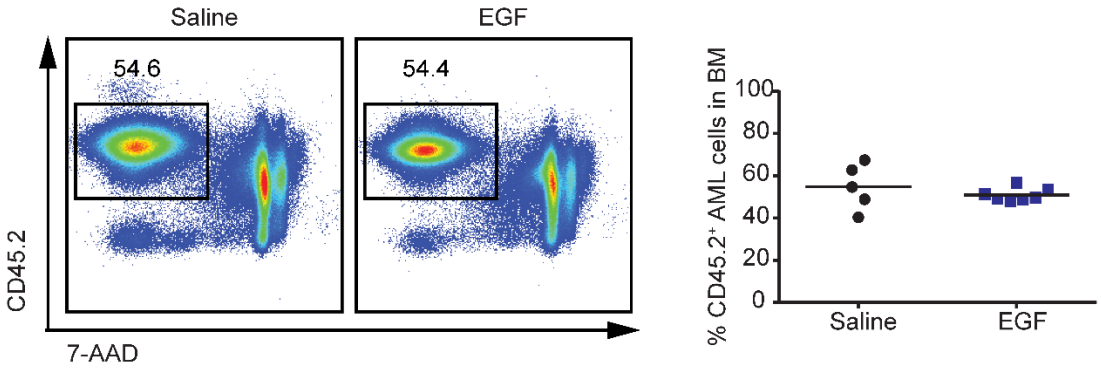

Figure 40. Transduced cells in the bone marrow of mice with leukemia burden. (Left) Representative flow cytometry plot of HoxA9/Meis1 transduced cells ($CD45.2^+$) engraftment in the BM of recipients at 2 weeks post the last dose of cytarabine. (Right) Quantification of AML cells in the PB of recipients (n=5-7, Student's t-test).

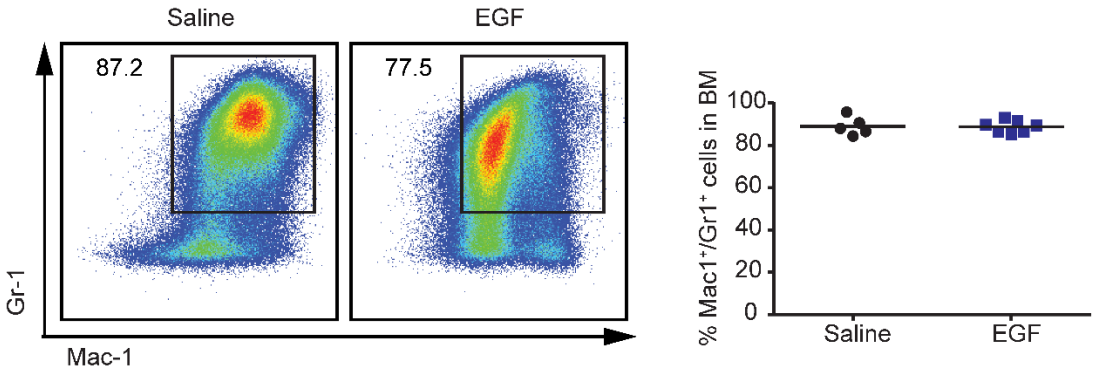

Figure 41. Myeloid transduced cells in the bone marrow of mice with leukemia burden. (Left) Representative flow cytometry plot of % $Mac1^+Gr\text{-}1^+$ cells among total $CD45.2^+$ cells in the BM of leukemic mice at 2 weeks post last dose of cytarabine. (Right) Quantification of $Mac1^+Gr\text{-}1^+$ cells percentage (n=5-7, Student's t-test).

2.3.6. EGF treatment effects on BM vascular endothelial cells (ECs) and stromal cells

Our prior studies [170] and a recent study by Tikhonova et al [171]. suggest that BM ECs and leptin receptor-positive (LepR+) stromal cells express EGFR, so systemic

administration of EGF may promote hematopoietic regeneration via indirect effects on the BM microenvironment. At day+10 following 500 cGy TBI and daily treatment with EGF or saline, we detected increased percentages of VE-cad+ BM ECs in both groups compared to non-irradiated mice (Figure 42).

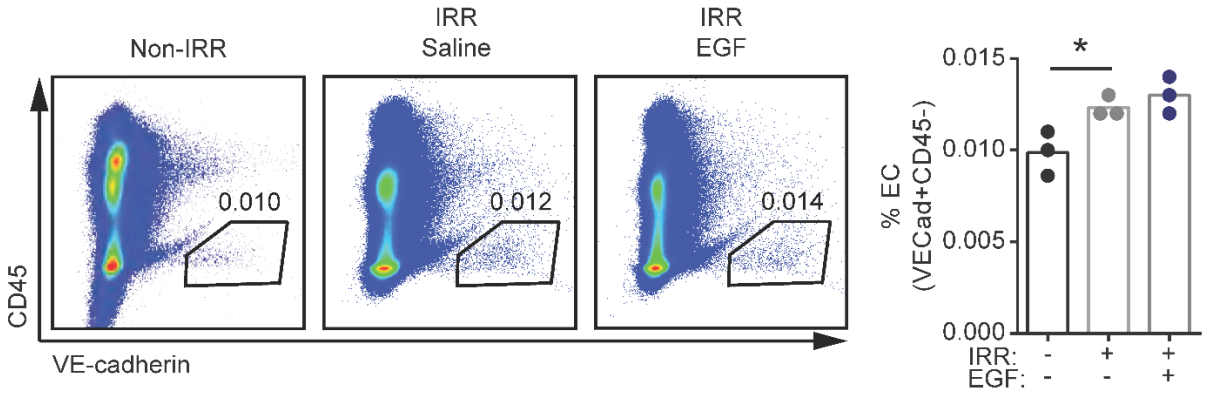

Figure 42. BM Endothelial cells increase in percentage after radiation. (Left) Flow cytometry plot of VE-cad^{+} ECs in the bone marrow of control irradiated treated with saline and irradiated treated with EGF mice. (Right) Quantification of VE-cad^{+} ECs (n=3/group, One-way ANOVA). *P < 0.05

Conversely, percentages of LepR+ BM stromal cells decreased following TBI in both groups of mice (Figure 43).

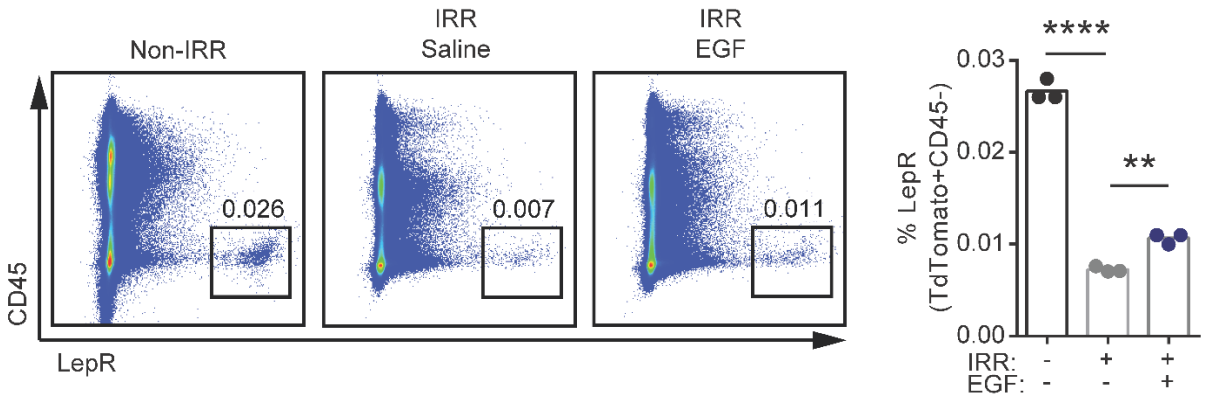

Figure 43. LepR⁺ stromal cells after radiation and EGF treatment. (Left) Flow cytometry plot of TdTomato-LepR⁺ cells in the bone marrow of control, irradiated treated with saline and irradiated treated with EGF mice. (Right) Quantification of TdTomato-LepR⁺ ECs (n=3/group, One-way ANOVA). **P < 0.01, ****P < 0.0001

To visualize the alteration of the bone marrow niche environment after EGF treatment, we utilized TdTomato-LepR⁺ mice and stained the endothelial cells by intravenous injection of anti-VEcadherin antibody (Figure 44).

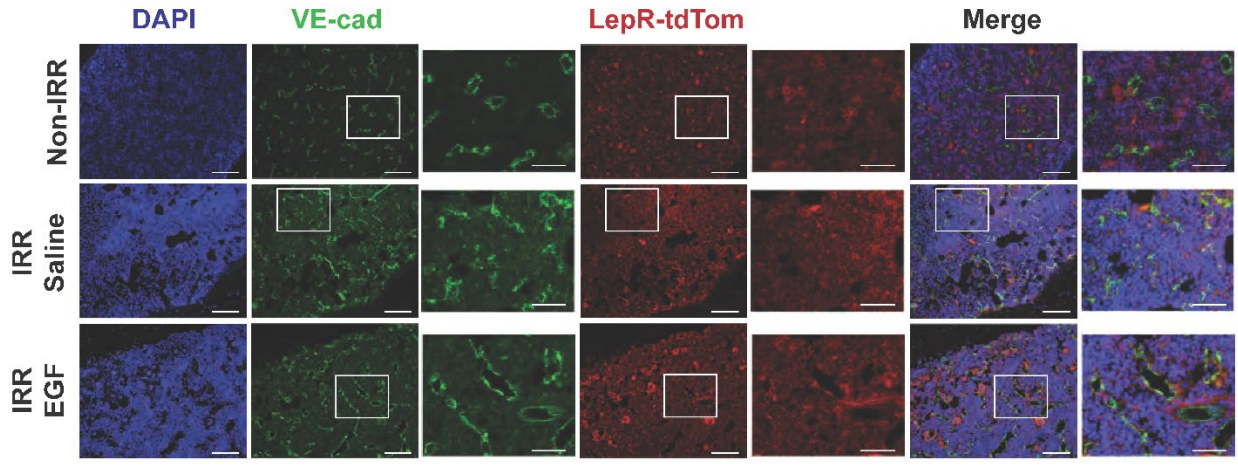

Figure 44. Morphology of endothelial cells and stromal cells in BM niche after radiation and EGF treatment. Immunofluorescence images of BM from non-irradiated Lepr-cre; tdTomato mice and irradiated Lepr-cre; tdTomato mice treated with EGF or saline. Femurs were collected at + 10

days post-radiation. Images were shown at low magnification (20X) and high magnification (63X) (scale bar = 100 μm for 20X images, scale bar = 40 μm for 63X images).

TBI caused an increase in mean fluorescence intensity (MFI) of VE-cad+ BM ECs and BM vascular area at day +10 in both EGF – treated and saline-treated mice (Figure 45).

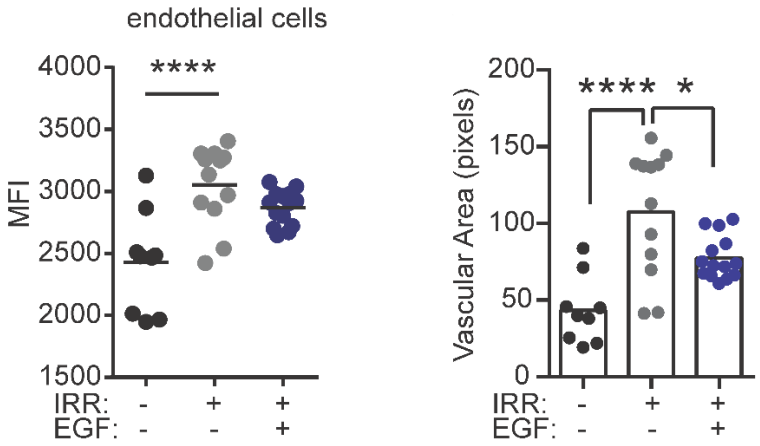

Figure 45. BM endothelial cell alteration after radiation and EGF measured by imaging. Quantification of bone marrow ECs cells from mice described in (Figure 43) (n=9-14, One-way ANOVA). (Left) Mean fluorescent intensity (MFI) of VE-cad^{+} cells. (Right) VE-cad^{+} vascular area in the BM. *P < 0.05, ****P < 0.0001.

However, EGF treatment decreased BM vascular area in irradiated mice, suggesting a beneficial effect of EGF treatment on BM vascular recovery after TBI [172]. We detected no effect of EGF treatment on the MFI of LepR+ stromal cells in the BM after TBI (Figure 46).

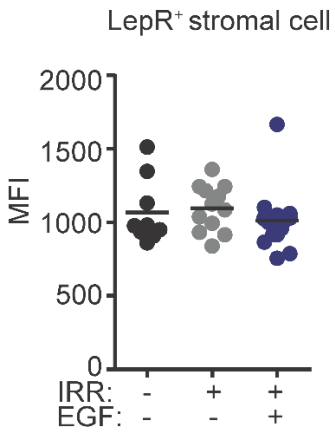

Figure 46. BM LepR$^+$ stromal cells after radiation and EGF measured by imaging. Quantification of mean fluorescence intensity of bone marrow TdTomato-LepR$^+$ cells from mice described in (Figure 43) (n=9-14, One-way ANOVA).

2.3.7. EGFR is necessary for HSC DNA repair and hematopoietic regeneration in vivo

To determine if EGFR signaling is necessary for HSC DNA repair and hematopoietic regeneration in vivo, we utilized EGFR-WT and EGFR-DN mice (Figure 47) [133,134,135].

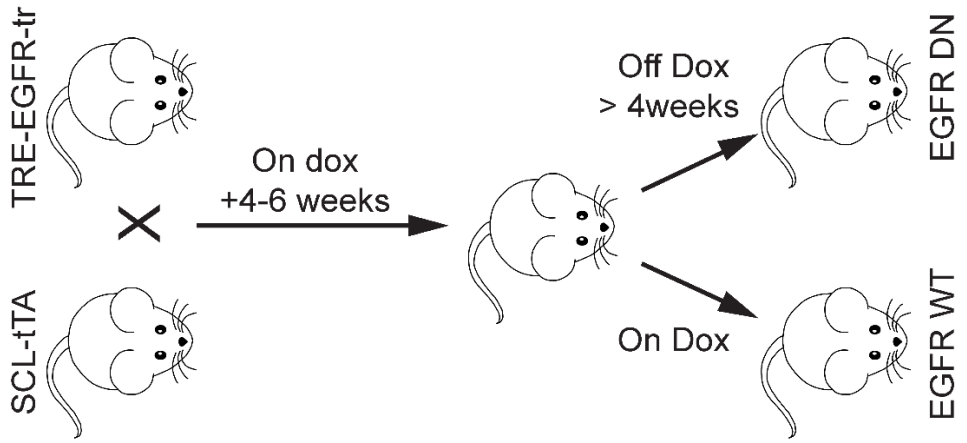

Figure 47. Schematic of the EGFR-DN model. Schematic of EGFR WT and EGFR DN mouse model using the Tet-off system. SCL-tTA mice were crossed with TRE-EGFR-tr mice to generate EGFR-DN mice. EGFR-DN mice were given doxycycline water from birth until week 6-8. Half of the mice were changed to regular water for more than 4 weeks to allow expression of EGFR-tr.

EGFR-DN mice expressed high levels of the EGFR mutant extracellular domain (Figure 48).

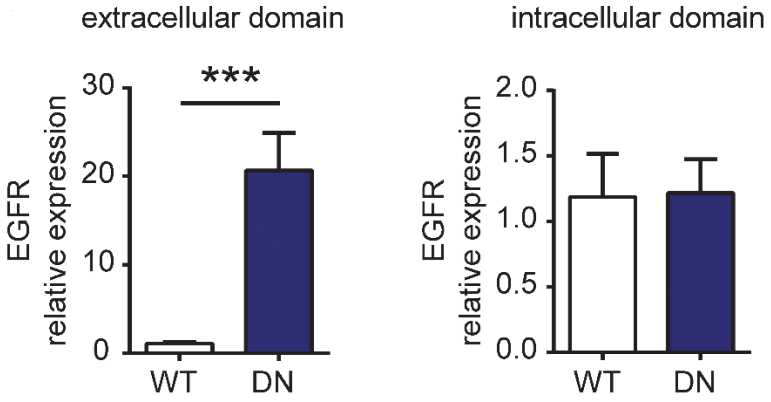

Figure 48. Validation of the EGFR-DN model by gene expression. Relative expression of the EGFR mutant extracellular domain (at left) and EGFR intracellular domain in KSL cells isolated

from EGFR-WT (WT) and EGFR-DN (DN) mice (n=10/group, means ± SEM, Student's t-test). ***P < 0.001

In response to EGF treatment, BM KSL cells from EGFR-WT mice displayed increased p-EGFR, whereas EGFR-DN mice failed to phosphorylate EGFR (Figure 49).

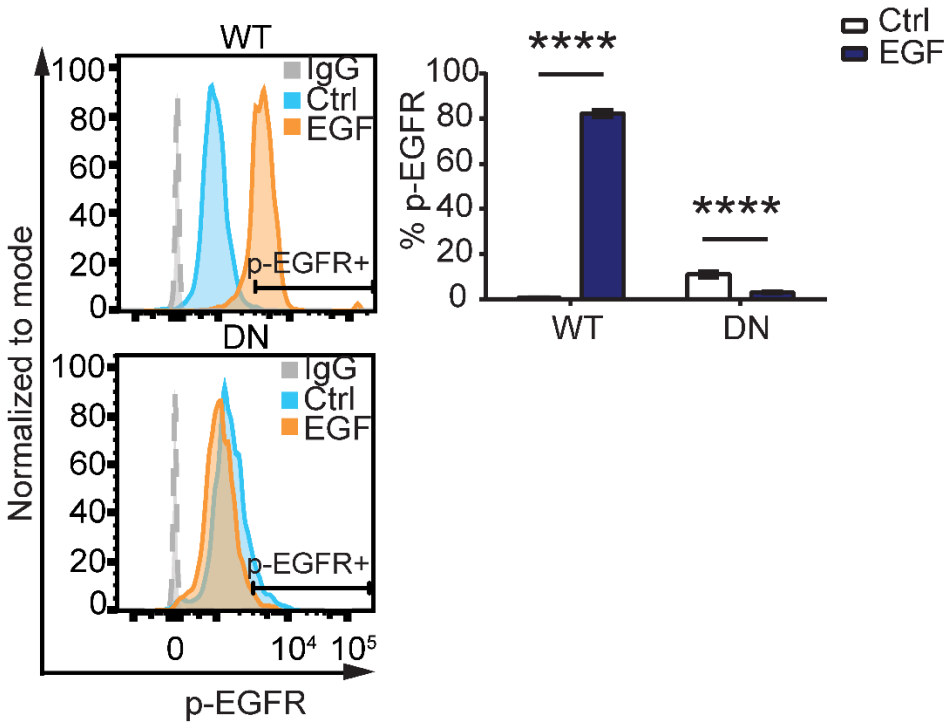

Figure 49. p-EGFR of long-term HSCs stimulated by EGF in EGFR-WT and EGFR-DN mice. (Left) Representative histograms of p-EGFR levels in BM KSL cells from EGFR-WT (WT) mice and EGFR-DN (DN) mice at 45 minutes following EGF treatment. (Right) %p-EGFR^{+} KSL cells in each condition (n = 6/group, means ± SEM, Two-way ANOVA). ****P < 0.0001

In steady-state, EGFR-WT mice and EGFR-DN mice demonstrated no differences in hematopoietic parameters or HSC repopulating capacity (Figure 50 - 55).

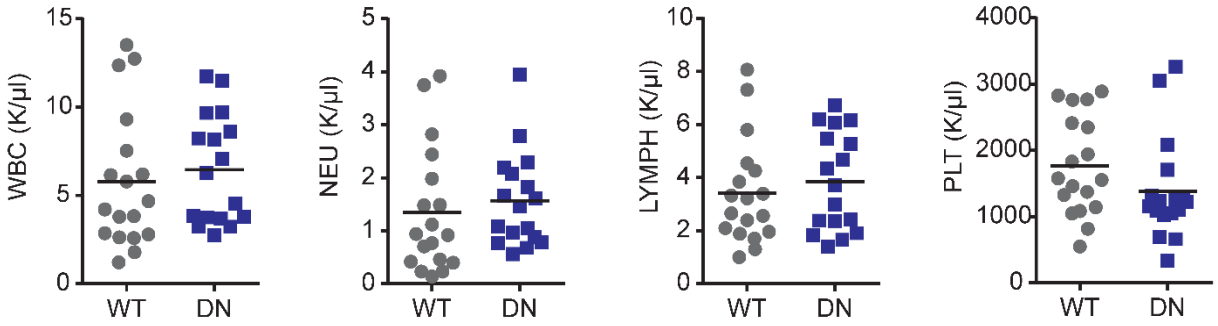

Figure 50. Peripheral blood counts of EGFR-WT and EGFR-DN at homeostasis. PB complete blood counts in WT and DN mice described in (Figure 47) (n = 17 – 18/group, Student's t-test).

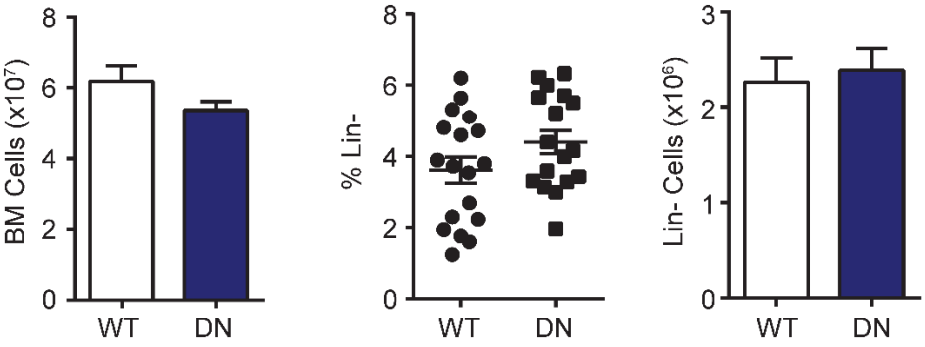

Figure 51. Bone marrow total cell count and Lin$^-$ cell counts. (Left) Bone marrow cellularity by cell count (Middle) percentage of BM lin- cells and (Right) BM lin- cell number of WT and DN mice described in (Figure 47) (WT n=18, DN n=17; error bar, SEM; unpaired t-test).

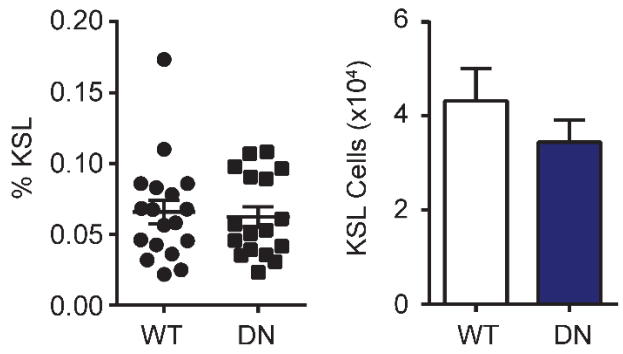

Figure 52. BM KSL percentage and cell number in EGFR-WT and EGFR-DN mice at homeostasis.

(Left) BM KSL percentage and (right) BM KSL cell number of WT and DN mice described in (Figure 47) (WT n=18, DN n=17; error bar, SEM; unpaired t-test).

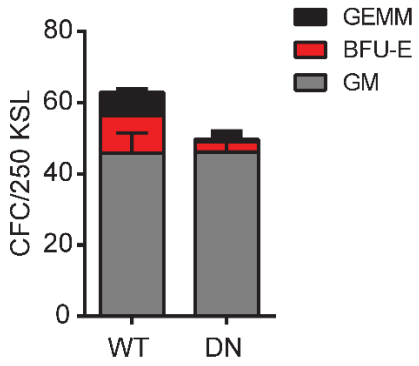

Figure 53. Colony-forming cells from KSL cells isolated from WT and DN mice at homeostasis.

Colony-forming unit of 250 sorted KSL cells isolated from the BM of WT and DN mice (n=6; error bar, SD; Two-way ANOVA). ** P=0.003 for BFU-E, * P=0.03 for GEMM

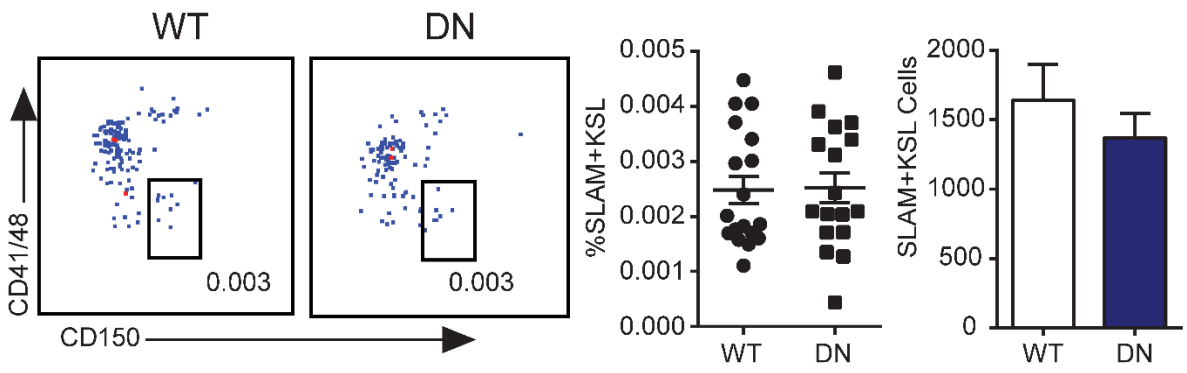

Figure 54. Long-term HSCs in the BM of WT and DN mice at homeostasis. (Left) Representative FACS plot of SLAM+KSL cell percentage in the BM of WT and DN mice. (Middle) Percentage of BM SLAM+KSL and (Right) BM SLAM+KSL cell number of WT and DN mice described in (Figure 47).

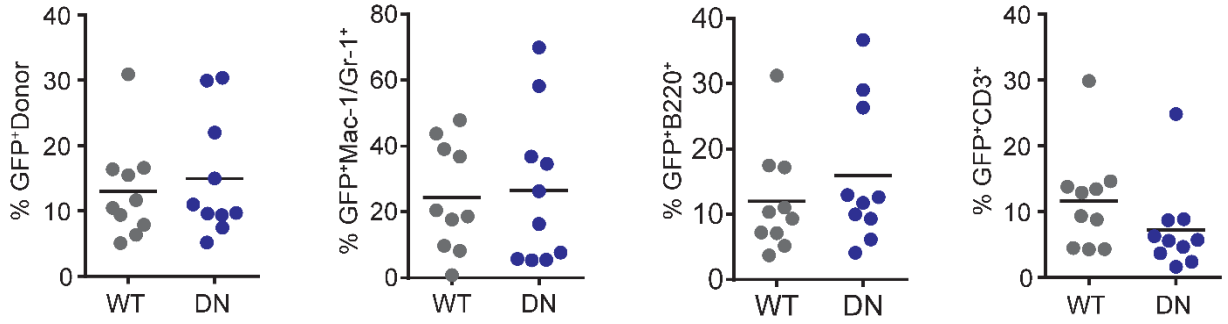

Figure 55. Engraftment of homeostatic WT and DN hematopoietic cells in primary recipients. Percentages of GFP^+ donor cells, $GFP^+Mac1/Gr1^+$, GFP^+B220^+ B cells, GFP^+CD3^+ T cells in the PB of primary recipient mice at 16 weeks following competitive transplantation of $2.5x10^4$ GFP^+ KSL isolated from WT or DN mice (n=10/group, Student's t-test).

However, at day +10 following 500 cGy TBI, EGFR-DN mice displayed decreased percentages of BM KSL cells and CD150+CD48-CD41- KSL HSCs and decreased BM CFCs compared to EGFR-WT controls, although PB CBCs were not substantially different (Figure 56, 57, 58).

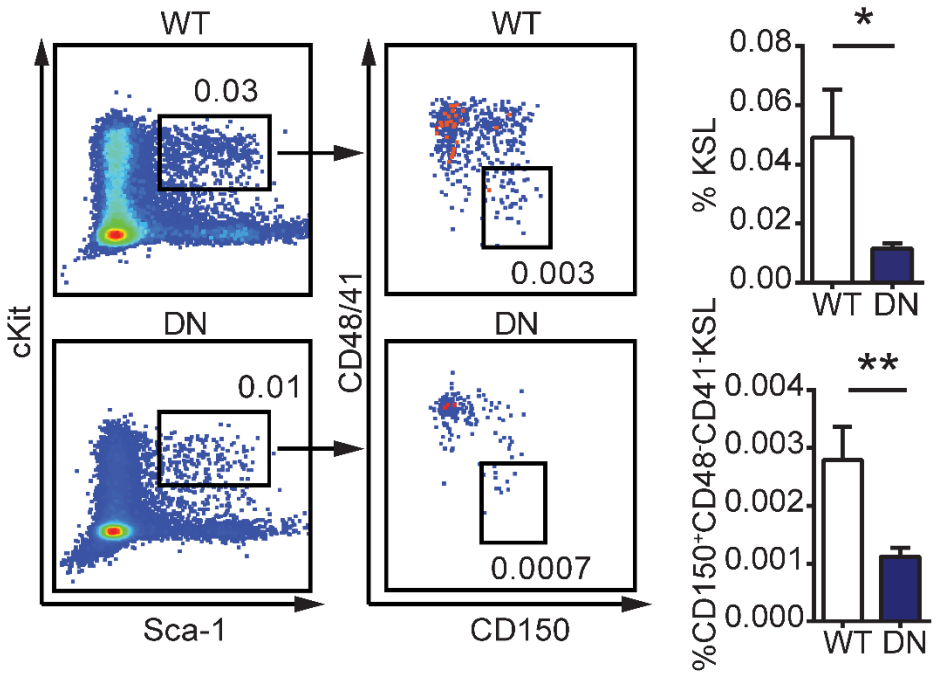

Figure 56. HSPCs and LT-HSCs in WT and DN mice after radiation in vivo. (Left) Representative flow cytometric analysis of percentages of BM KSL cells and $CD150^{+}CD48^{-}CD41^{-}$KSL HSCs in WT and DN mice at day +10 following 500 cGy TBI. (Right) %KSL cells and $\%CD150^{+}CD48^{-}CD41^{-}$KSL cells in each group (n = 14/group, means ± SEM, Student's t test). *P < 0.05, **P < 0.01

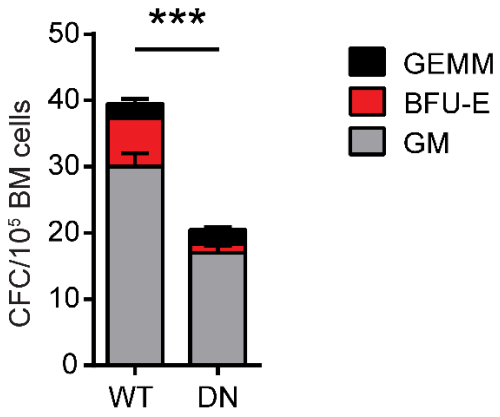

Figure 57. Colony-forming cells of BM from irradiated WT and DN mice. BM CFCs from WT mice and DN mice at day +10 following 500 cGy TBI (n = 6/group, means ± SEM, Student's t-test).

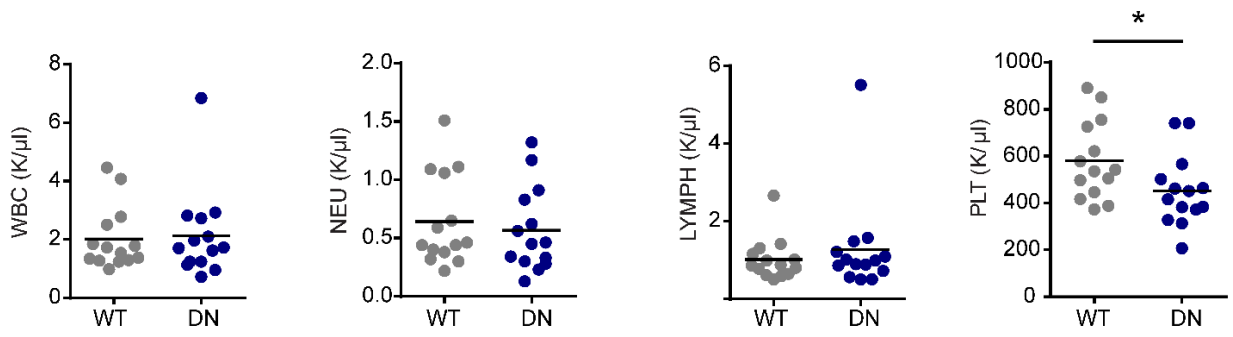

Figure 58. Peripheral blood counts of irradiated WT and DN mice. PB WBC, NEU, LYMPH, and PLT counts in WT and DN mice at day +10 following 500 cGy TBI (n=14/group, Student's t-test). *P < 0.05

To compare long term - HSC content, we transplanted 2.5 x 10^4 BM GFP+ KSL cells, labeled via transduction with MSCV-IRES-GFP (Addgene #20672, a gift from Dr. Tannishtha Reya), isolated at day +10 from 500 cGy-irradiated EGFR-DN mice or EGFR-WT mice into 950 cGy-irradiated F1 recipient mice, along with 2 x 105 competitor (F1) BM cells. At 16 weeks, recipient mice transplanted with KSL cells from EGFR-DN donors displayed decreased total donor cell and decreased donor myeloid, B cell, and T cell engraftment in the PB, and decreased donor KSL cells in the BM, compared to recipients transplanted with KSL cells from EGFR- WT mice (Figure 59, 60).

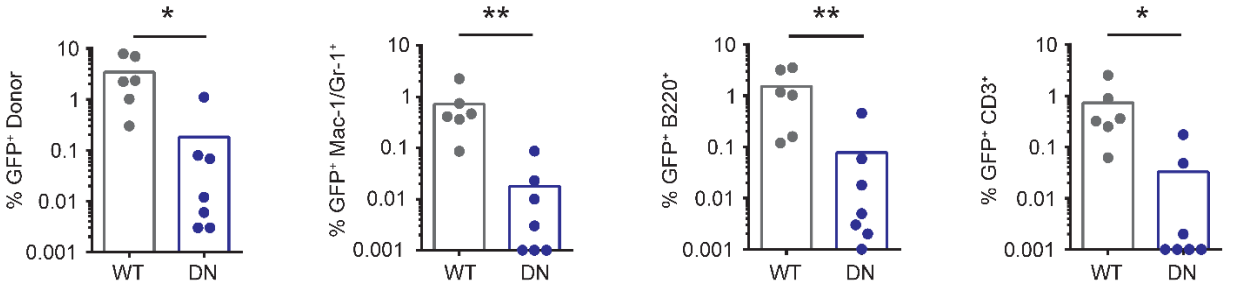

Figure 59. Total and multilineage reconstitution of donor WT and DN hematopoietic cells in the primary recipients. Percentages of total donor GFP⁺ cells, myeloid cells, B cells, and T cells in the

PB of recipient mice at 16 weeks following transplantation of 2.5 x 10^4 GFP^+ KSL cells collected from WT or DN mice at day +10 following 500 cGy TBI, coupled with 2x10^5 BM competitor cells (n = 6-7/group, Student's t-test). *P < 0.05, **P < 0.01

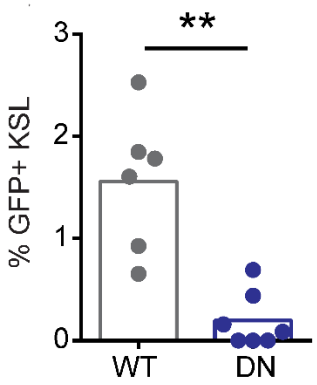

Figure 60. Donor KSL cell engraftments in the primary recipients. Percentages of GFP^+KSL cells in the BM of primary recipient mice at 16 weeks following competitive transplantation in the groups shown (n = 6-7/group, means ± SEM, Student's t-test). **P < 0.01

Separately, recipient F1 mice transplanted with BM cells collected at day +10 from 500 cGy – irradiated EGFR-DN mice displayed decreased survival compared to mice transplanted with BM cells from irradiated EGFR-WT mice, suggesting that EGFR deficiency in HSCs also caused a loss of radioprotective HSPCs after TBI (Figure 61).

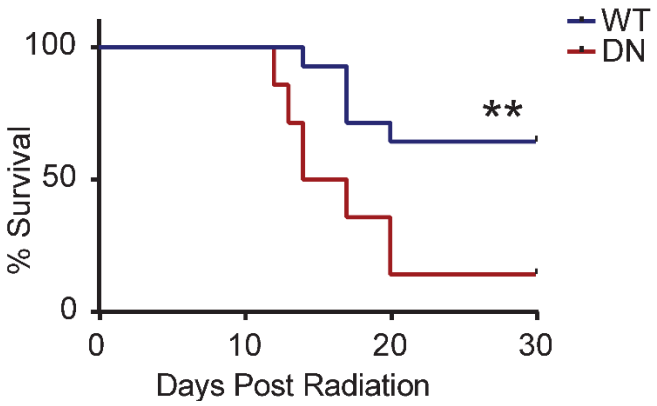

Figure 61. Survival curve of limiting dose transplantation with BM cells from irradiated WT and DN mice. Percent survival of recipient F1 mice over 30 days following 900 cGy TBI and transplantation with 5×10^5 BM cells collected from EGFR-DN or EGFR-WT mice at 24 hours post-500 cGy TBI (n=14 mice/group, Log-rank test). **P < 0.01

Following 300 cGy irradiation, BM KSL cells from EGFR-DN mice displayed increased γ-H2AX foci compared to irradiated KSL cells from EGFR-WT mice (Figure 62).

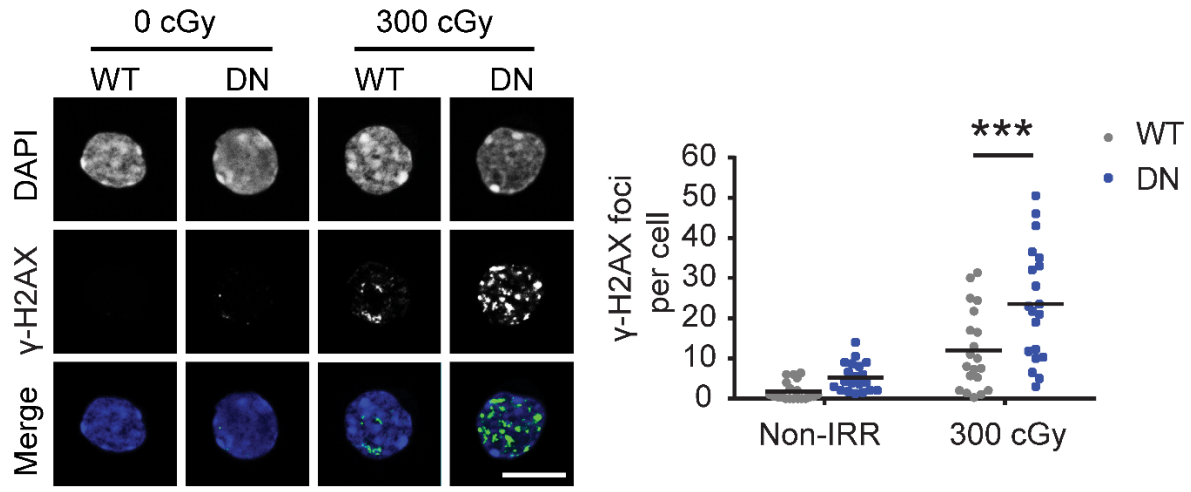

Figure 62. γ-H2AX foci in KSL cells from WT and DN mice. (Left) representative microscopic image of γ-H2AX foci in KSL cells from WT and DN mice cultured with TSF for 1 hour (scale bar

= 10μm). At right, foci numbers per KSL cell (n = 20 cells/group, means ± SEM, Two way ANOVA). ***P < 0.001

EGF treatment increased p-Akt in KSL cells from EGFR-WT mice, but no change in p-Akt was observed in KSL cells from EGFR-DN mice (Figure 63).

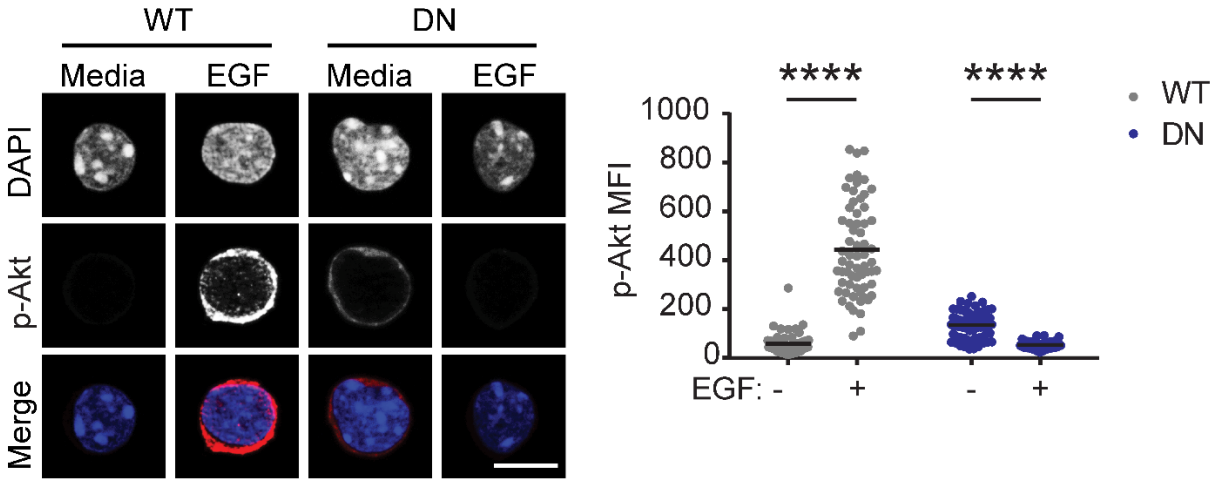

Figure 63. p-Akt(Ser473) in KSL cells from WT and DN mice. (Left) Microscopic images of p-Akt in KSL cells from WT and DN mice at 5 minutes following irradiation with 300 cGy and culture in Media ± EGF (scale bar = 10 μm). (Right) p-Akt MFI in KSL cells from each condition (n = 56-69 cells/group, means ± SEM, Two-way ANOVA). ****P < 0.0001

Similarly, p-DNA-PKcs levels increased in BM KSL cells from EGFR-WT mice following 300 cGy irradiation but did not increase in KSL cells from EGFR-DN mice (Figure 64).

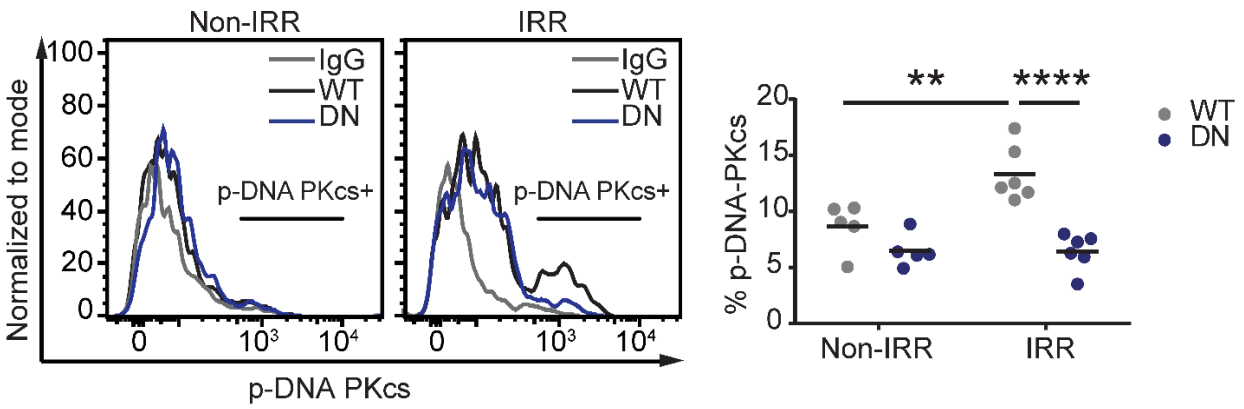

Figure 64. p-DNA PKcs in KSL cells from WT and DN mice. (Left) Representative histogram of p-DNA-PKcs levels in KSL cells from WT and DN mice at 1 hour following 100 cGy. (Right) %p-DNA-PKcs^{+} KSL cells in each condition at 1 hour post-irradiation (n=5-6/group, Two-way ANOVA). **P < 0.01, ****P < 0.0001

Therefore, EGFR was necessary for normal DNA-PKcs activation and DNA repair in irradiated HSCs.

2.3.8. EGF induces EGFR/Akt/DNA PKcs pathway activation in HSPCs in irradiated mice

In our comparison of EGFR-WT mice and EGFR-DN mice, we detected increased activation of DNA- PKcs in BM KSL cells in irradiated EGFR-WT mice in the absence of EGF treatment. This implies that endogenous EGF activates EGFR signaling and DNA-PKcs in HSPCs of EGFR-WT mice.

Indeed, following 500 cGy TBI, both EGFR-WT and EGFR-DN mice demonstrated EGF levels in the BM over time (range 22 – 5205 pg/ml, Figure 65).

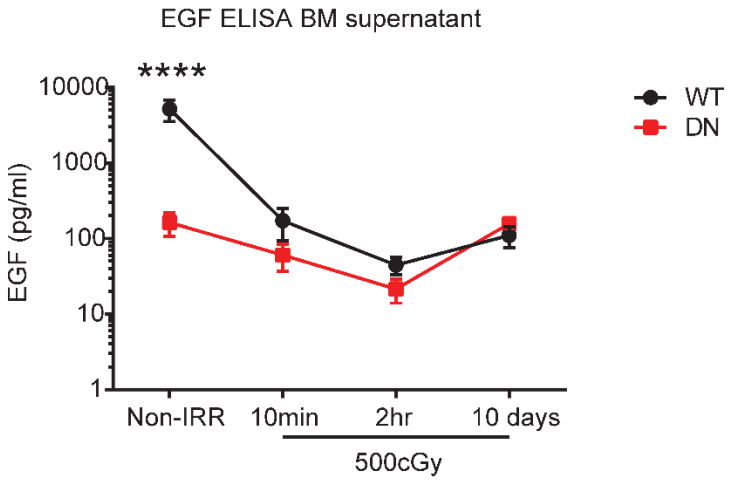

Figure 65. Endogenous EGF secretion in the BM of WT and DN mice. Time course of EGF levels in the bone marrow of EGFR-WT and EGFR-DN mice at steady-state and after radiation (n=5/group for each time point, Two-way ANOVA). ****P < 0.0001

In keeping with these results, EGFR- WT mice demonstrated increased p-EGFR, p-Akt, p-Artemis, and p-DNA-PKcs in BM KSL cells at 5 minutes following 500 cGy TBI, whereas EGFR-DN mice showed no activation of these targets (Figure 66, 67, 68, 69).

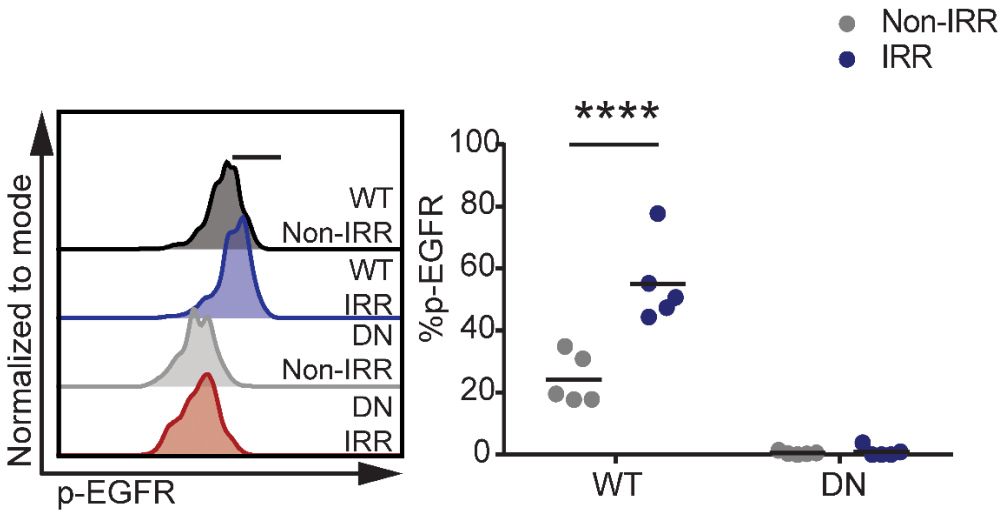

Figure 66. p-EGFR in KSL cells from WT and DN mice after radiation. KSL cells from EGFR-WT and EGFR-DN mice were analyzed at +10 minutes post 500cGy TBI for p-EGFR (n=5/group,

Two-way ANOVA). (Left) flow cytometry plot of p-EGFR in EGFR-WT and EGFR-DN mice. (Right) Quantification of %p-EGFR. ****P < 0.0001

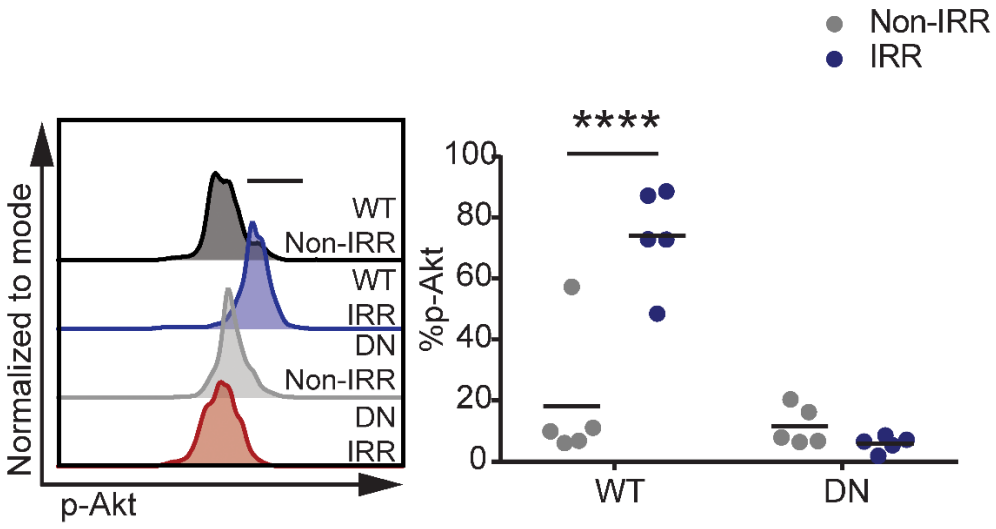

Figure 67. p-Akt in KSL cells from WT and DN mice after radiation. KSL cells from EGFR-WT and EGFR-DN mice were analyzed at +10 minutes post-500cGy TBI for p-Akt (n=5/group, Two-way ANOVA). (Left) flow cytometry plot of p-EGFR in EGFR-WT and EGFR-DN mice. (Right) Quantification of %p-Akt. ****P < 0.0001

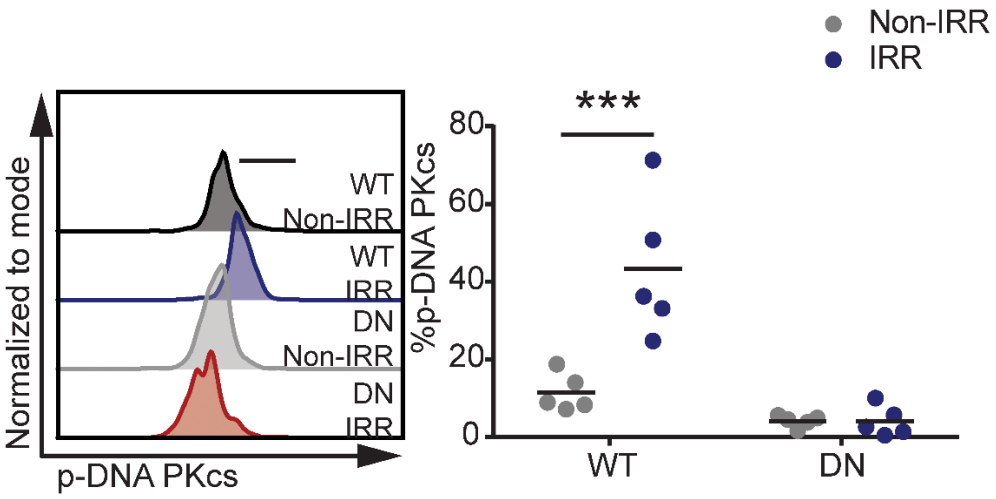

Figure 68. p-DNA PKcs in KSL cells from WT and DN mice after radiation. KSL cells from EGFR-WT and EGFR-DN mice were analyzed at +10 minutes post 500cGy TBI for p-DNA PKcs

(n=5/group, Two-way ANOVA). (Left) flow cytometry plot of p-EGFR in EGFR-WT and EGFR-DN mice. (Right) Quantification of %p-DNA PKcs. ***P < 0.001

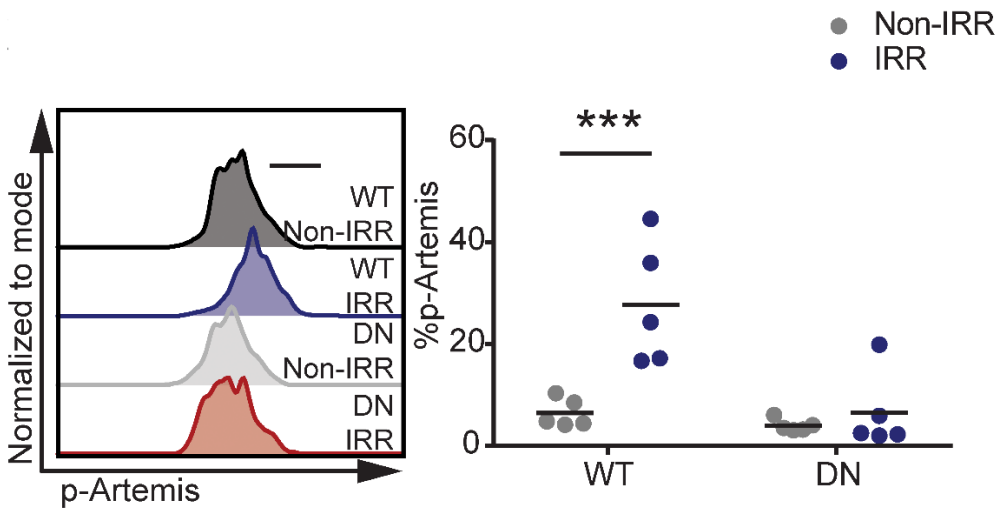

Figure 69. p-Artemis in KSL cells from WT and DN mice after radiation. KSL cells from EGFR-WT and EGFR-DN mice were analyzed at +10 minutes post 500cGy TBI for p-Artemis (n=5/group, Two-way ANOVA). (Left) flow cytometry plot of p-EGFR in EGFR-WT and EGFR-DN mice. (Right) Quantification of %p-Artemis. ***P < 0.001

We also treated BM HSCs with 100 pg/ml EGF in vitro and found that this dose of EGF induced phosphorylation of EGFR, Akt, Artemis, and DNA-PKcs in BM HSPCs compared to untreated BM HSPCs (Figure 70).

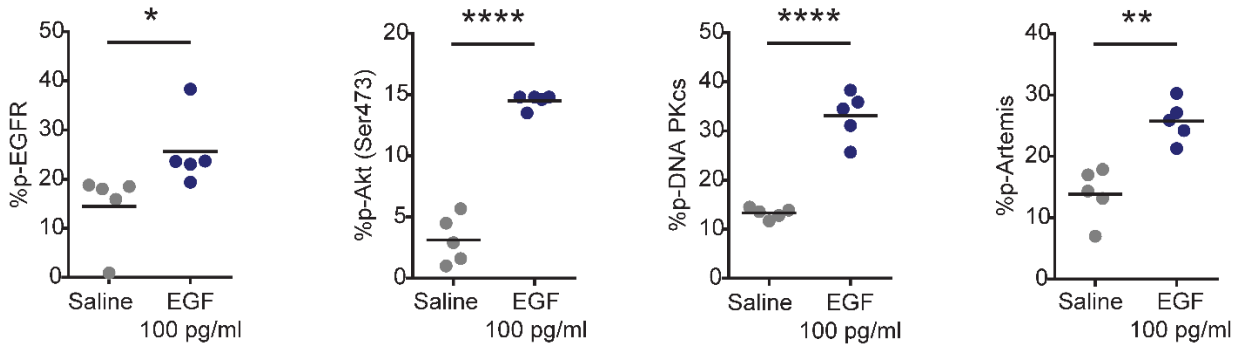

Figure 70. phosphorylation of EGFR signaling and NHEJ related proteins. Percentage of p-EGFR (Left), p-Akt (Middle left), p-DNA PKcs (Middle right), and p-Artemis (Right) measured by flow cytometry (n=5/group, Student's t-test). KSL cells were irradiated at 300cGy and treated with 100 pg/ml EGF or saline for 5 minutes before analysis. *P < 0.05, **P < 0.01, ****P < 0.0001

These data suggest that endogenous EGF promotes the activation of EGFR/Akt/DNA-PKcs pathway in BM HSPCs in irradiated EGFR-WT mice, whereas EGFR-DN mice fail to activate this pathway due to EGFR deficiency. Of note, we detected no differences in the nuclear localization of EGFR in response to irradiation or EGF treatment in EGFR-WT mice or EGFR-DN mice (Figure 71).

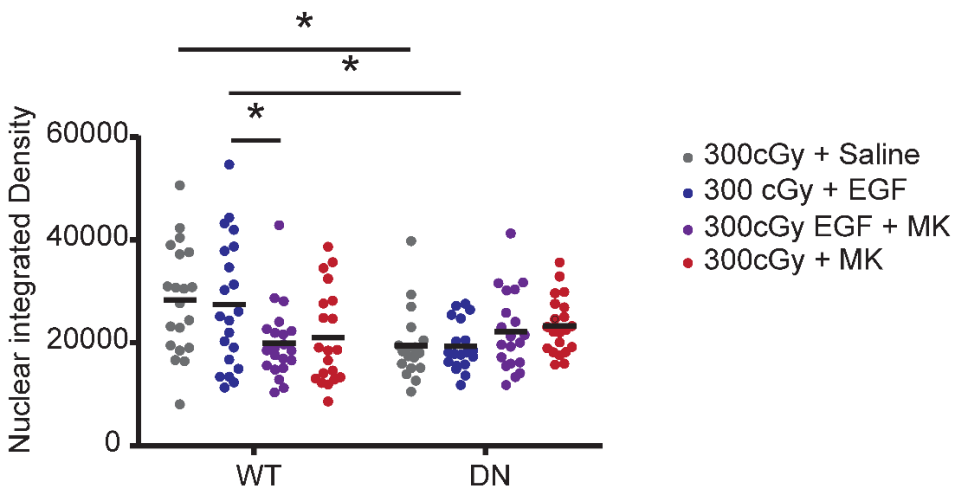

Figure 71. Nuclear p-EGFR in KSL cells after Akt inhibition. Nuclear localization of p-EGFR after 300cGy radiation and EGF and/or MK2206 treatment for 20 minutes. *P < 0.05

In a complementary study, we compared the phosphorylation of EGFR, Akt, Artemis, and DNA PKcs in BM KSL cells from C57BL/6 mice irradiated with 500 cGy TBI and treated x 1 with EGF versus irradiated C57BL/6 mice treated with saline. Both groups of irradiated mice displayed increased levels of p-EGFR, p-Akt, p-Artemis, and p-DNA PKcs in BM KSL cells compared to non- irradiated mice (Figure 72, 73, 74, 75). However, irradiated mice treated systemically with EGF demonstrated significantly increased levels of p-EGFR, p-Akt, p-Artemis, and p-DNA PKcs compared to irradiated control mice (Figure 72, 73, 74, 75).

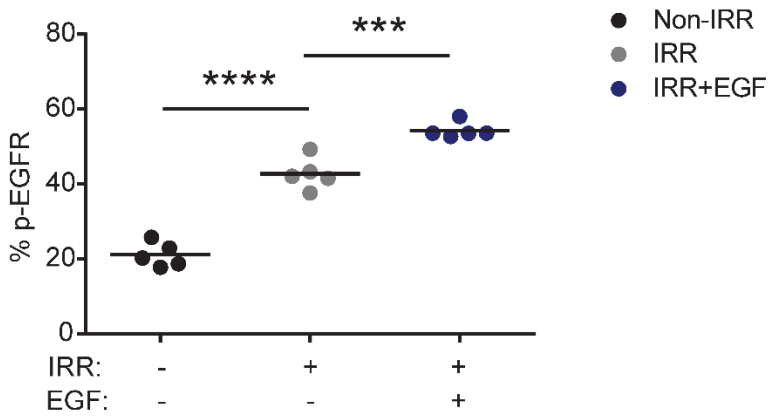

Figure 72. p-EGFR in KSL cells after radiation and EGF treatment. KSL cells of non-irradiated EGFR-WT mice, 500cGy TBI irradiated EGFR-WT mice treated with saline and 500cGy TBI irradiated EGFR-WT mice treated with EGF collected at + 2 hours post-radiation. Quantification of %p-EGFR by flow cytometry analysis (n=5/group, One-way ANOVA). ***P < 0.001, ****P < 0.0001

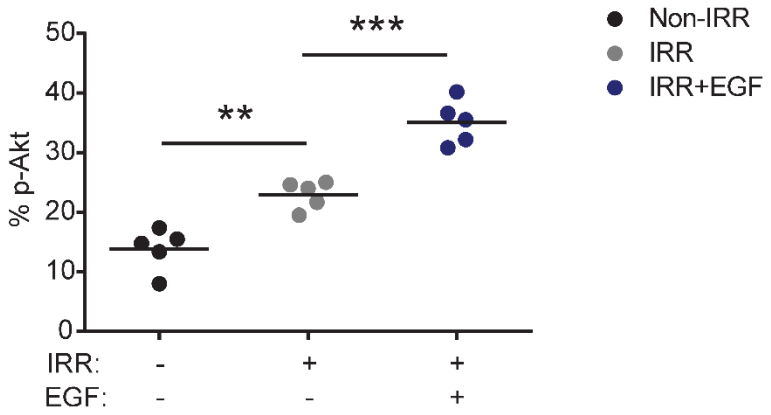

Figure 73. p-Akt in KSL cells after radiation and EGF treatment. KSL cells of non-irradiated EGFR-WT mice, 500cGy TBI irradiated EGFR-WT mice treated with saline and 500cGy TBI irradiated EGFR-WT mice treated with EGF collected at + 2 hours post-radiation. Quantification of %p-Akt by flow cytometry analysis (n=5/group, One-way ANOVA). **P < 0.01, ***P < 0.001

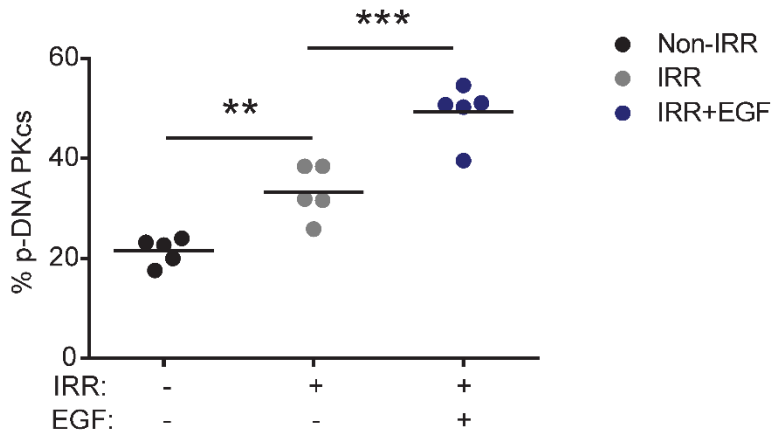

Figure 74. p-DNA PKcs in KSL cells after radiation and EGF treatment. KSL cells of non-irradiated EGFR-WT mice, 500cGy TBI irradiated EGFR-WT mice treated with saline and 500cGy TBI irradiated EGFR-WT mice treated with EGF collected at + 2 hours post-radiation. Quantification of %p-DNA PKcs by flow cytometry analysis (n=5/group, One-way ANOVA). **P < 0.01, ***P < 0.001

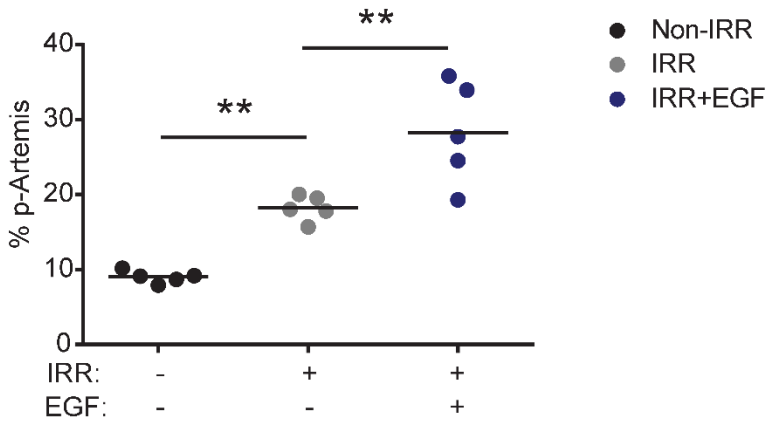

Figure 75. p-Artemis in KSL cells after radiation and EGF treatment. KSL cells of non-irradiated EGFR-WT mice, 500cGy TBI irradiated EGFR-WT mice treated with saline and 500cGy TBI irradiated EGFR-WT mice treated with EGF collected at + 2 hours post-radiation. Quantification of %p-Artemis by flow cytometry analysis (n=5/group, One-way ANOVA). **P < 0.01

2.3.9. EGF promotes human hematopoietic regeneration following irradiation

To test the therapeutic potential of EGF to promote human hematopoietic regeneration, we irradiated human BM CD34+ HSPCs with 300 cGy and cultured in media with or without 100 ng/ml EGF for 36 hours. Irradiation increased the numbers of y-H2AX foci per CD34+ cell at +1 hour and EGF treatment abrogated this effect (Figure 76).

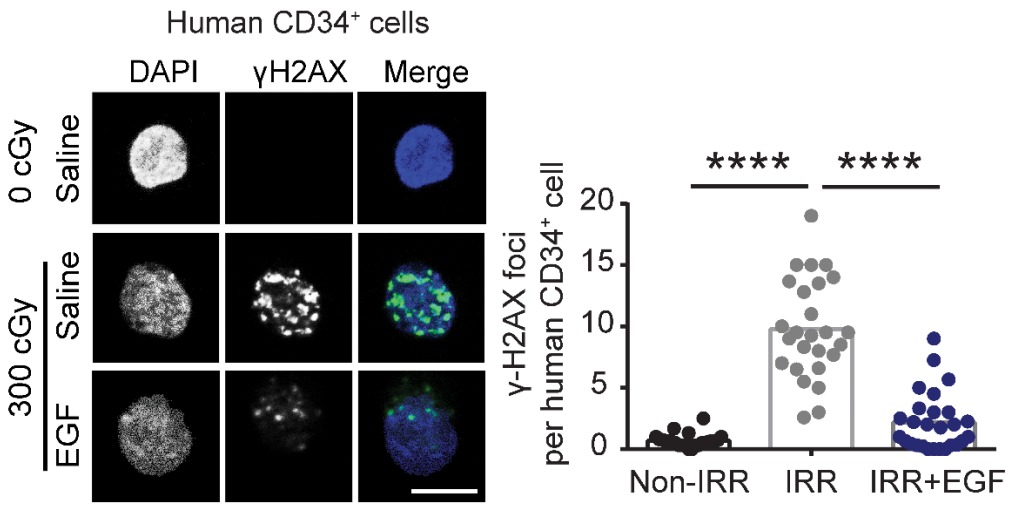

Figure 76. γ-H2AX foci in human HSPCs after EGF treatment. (Left)Immunofluorescence microscopy of ionizing radiation-induced foci of γ-H2AX in non-irradiated (Non-IRR) and 300cGy-irradiated human BM CD34⁺ cells cultured in complete media (TSF) with and without 100 ng/ml EGF for 1 hour (scale bar = 10 μm). (Right) Numbers of foci per cell are quantified (n = 24-27 fields of view, One-way ANOVA). ****P < 0.0001

EGF treatment significantly increased p-EGFR, p-Akt, p-Artemis, and p-DNA-PKcs, and increased expression of XRCC6 in irradiated human CD34+ cells (Figure 77 - 81).

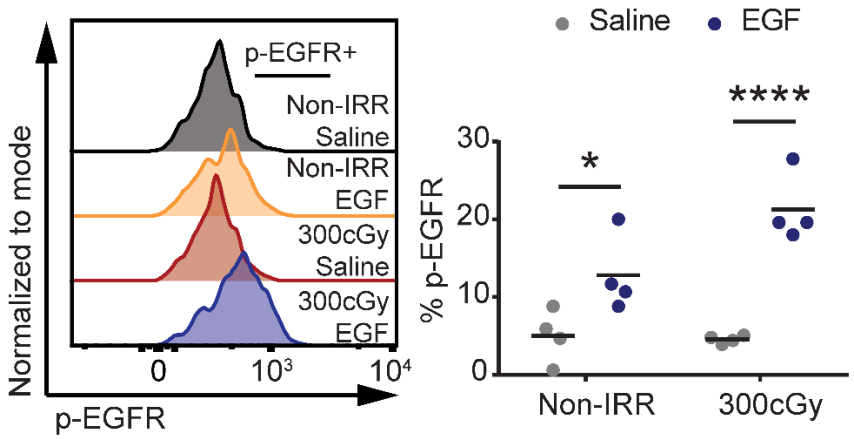

Figure 77. p-EGFR in human HSPCs after EGF treatment. Human Non-irradiated or 300cGy irradiated Human BM CD34⁺ cells were treated with saline or EGF for 5 minutes and were analyzed for p-EGFR (n=4/group, Two-way ANOVA). (Left) Flow cytometry plot of p-EGFR in Human BM CD34⁺ cells. (Right) Quantification of %p-EGFR. *P < 0.05, ****P < 0.0001

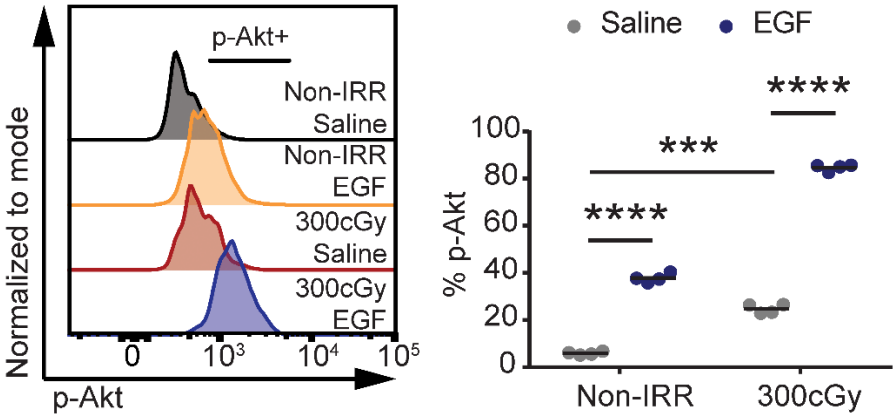

Figure 78. p-Akt in human HSPCs after EGF treatment. Human Non-irradiated or 300cGy irradiated Human BM CD34⁺ cells were treated with saline or EGF for 5 minutes and were analyzed for p-Akt (n=4/group, Two-way ANOVA). (Left) Flow cytometry plot of p-EGFR in Human BM CD34⁺ cells. (Right) Quantification of %p-Akt. ***P < 0.001, ****P < 0.0001

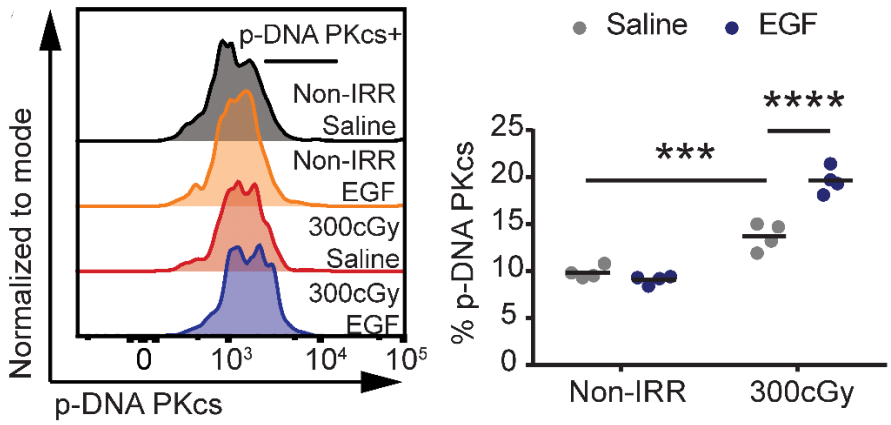

Figure 79. p-DNA PKcs in human HSPCs after EGF treatment. Human Non-irradiated or 300cGy irradiated Human BM CD34⁺ cells were treated with saline or EGF for 5 minutes and were analyzed for p-DNA PKcs (n=4/group, Two-way ANOVA). (Left) Flow cytometry plot of p-DNA PKcs in Human BM CD34⁺ cells. (Right) Quantification of %p-DNA PKcs. ***P < 0.001, ****P < 0.0001

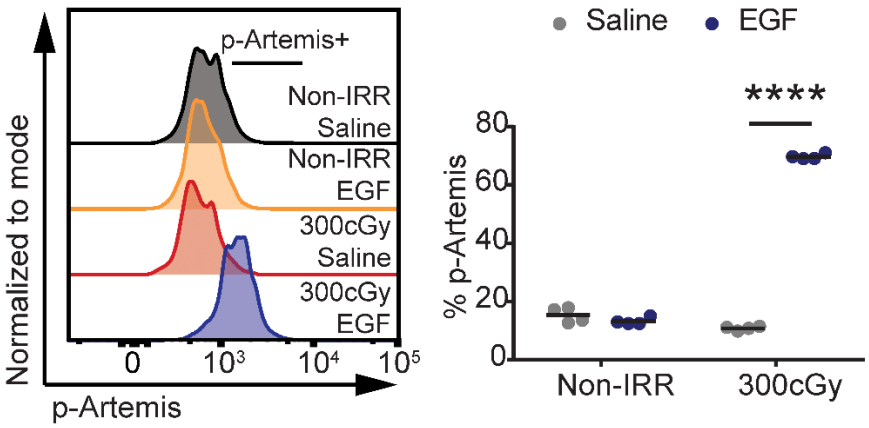

Figure 80. p-Artemis in human HSPCs after EGF treatment. Human Non-irradiated or 300cGy irradiated Human BM CD34⁺ cells were treated with saline or EGF for 5 minutes and were analyzed for p-Artemis (n=4/group, Two-way ANOVA). (Left) Flow cytometry plot of p-EGFR in Human BM CD34⁺ cells. (Right) Quantification of %p-Artemis. *P < 0.05, **P < 0.01, ***P < 0.001, ****P < 0.0001

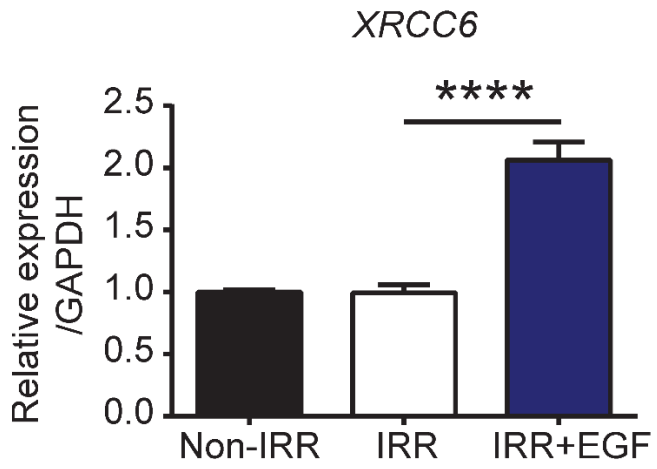

Figure 81. RNA expression of XRCC6 in human HSPCs after EGF treatment. XRCC6 gene expression from 300cGy irradiated human BM $CD34^+$ cells treated with saline or EGF for 1 hour. Non-irradiated human BM $CD34^+$ cells cultured for 1 hour were used as control (n = 3, means ± SEM, One-way ANOVA). ****P < 0.0001

EGF treatment also increased the percentages of CD34+CD38- HSPCs in the culture at +36 hours and increased CFC content compared to control cultures (Figure 82, 83). The addition of the DNA-PKcs inhibitor, NU7441, blocked EGF effects on the maintenance of HSPCs in culture and CFC recovery after irradiation (Figure 82, 83).

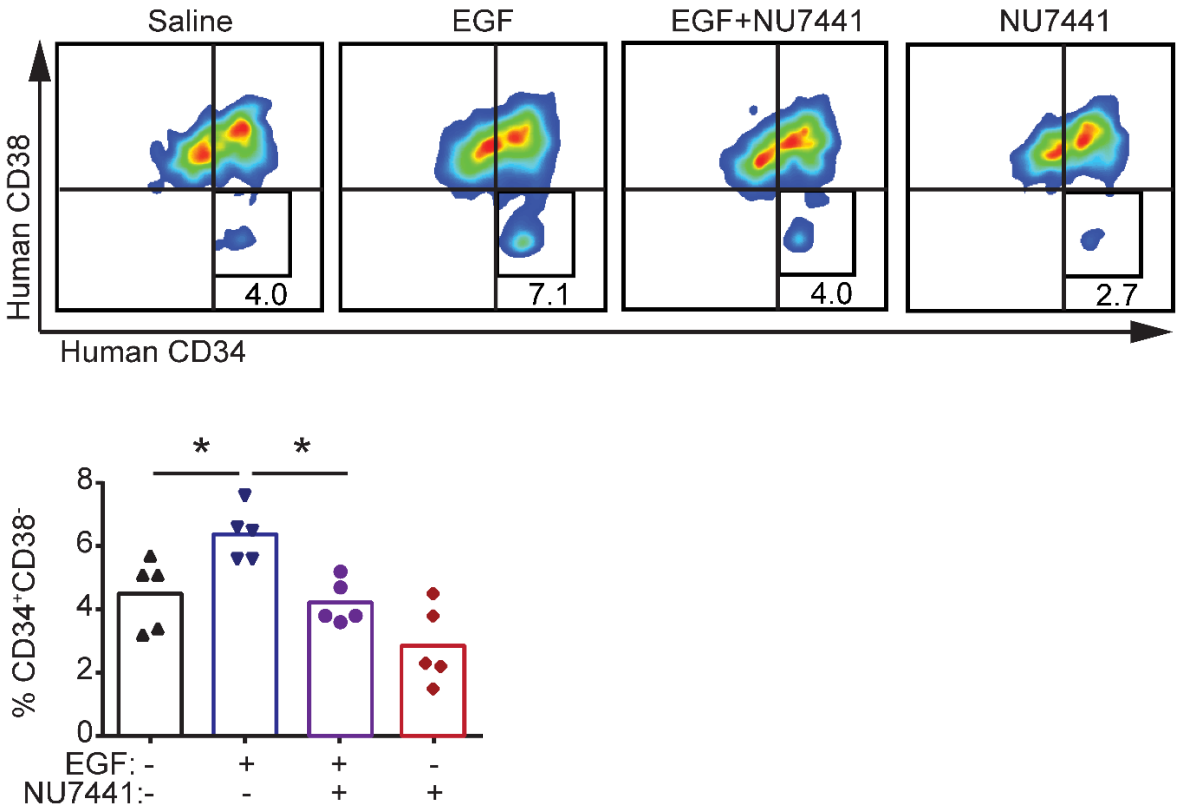

Figure 82. Human HSPCs after radiation and EGF or DNA PKcs inhibitor treatment. (Top) Flow cytometry plot of human $CD34^{+}CD38^{-}$ HSPCs from human BM $CD34^{+}$ cells irradiated at 300cGy and treated with saline, EGF, NU7441 and EGF + NU7441 respectively for 36 hours. (Bottom) Quantification of $CD34^{+}CD38^{-}$ cell percentage (n = 5/group, One-way ANOVA). *P < 0.05

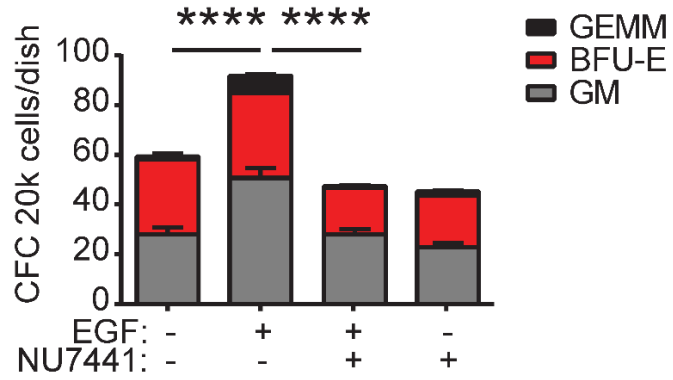

Figure 83. Colony-forming cells from irradiated human hematopoietic cells. Colony-forming units of human BM $CD34^{+}$ cells. 300cGy irradiated human BM $CD34^{+}$ cells were treated with saline or

EGF for 36 hour and progenies were collected and plated for CFC at 2 x 10^4 cells/dish (n = 6, means ± SEM, Two-way ANOVA). ****P < 0.0001

To determine if EGF treatment could promote the recovery of human HSCs with in vivo repopulating capacity, we transplanted NOD/SCID-Stem Cell Factor/Granulocyte Macrophage Colony Stimulating Factor/Interleukin-3 (NSG-S) mice [173] with the progeny of 2 x 10^5 CD34+ cells at 36 hours following 300 cGy irradiation and culture with and without 100 ng/ml EGF. Mice transplanted with the progeny of irradiated human CD34+ cells treated with EGF displayed significantly increased total human donor cell engraftment, myeloid engraftment, B cell engraftment, and T cell engraftment at 12 and 16 weeks post-transplant compared to mice transplanted with the progeny of irradiated human CD34+ cells cultured in media alone (Figure 84, 85).

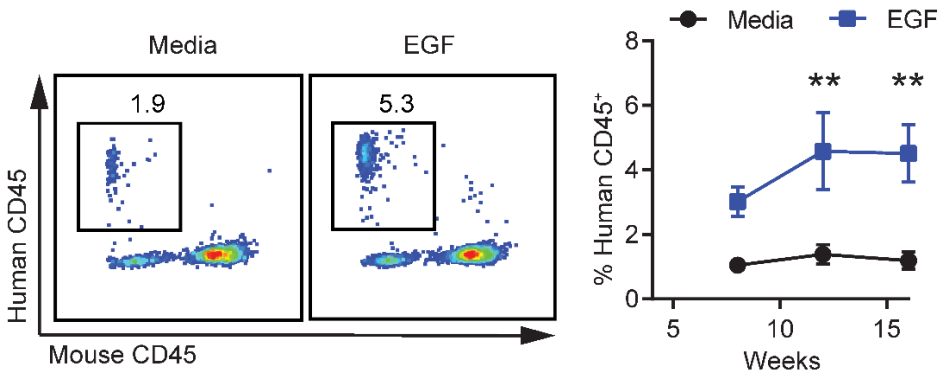

Figure 84. Human hematopoietic cell engraftment in the primary recipients. (Left) Flow cytometry plot of human cell engraftment in the peripheral blood of NSG-SGM3 mice at 16 weeks post-transplantation. (Right) Time course of human cell engraftment in the PB of NSG-SGM3 mice (n = 7-8, means ± SEM, Two-way ANOVA). **P < 0.01

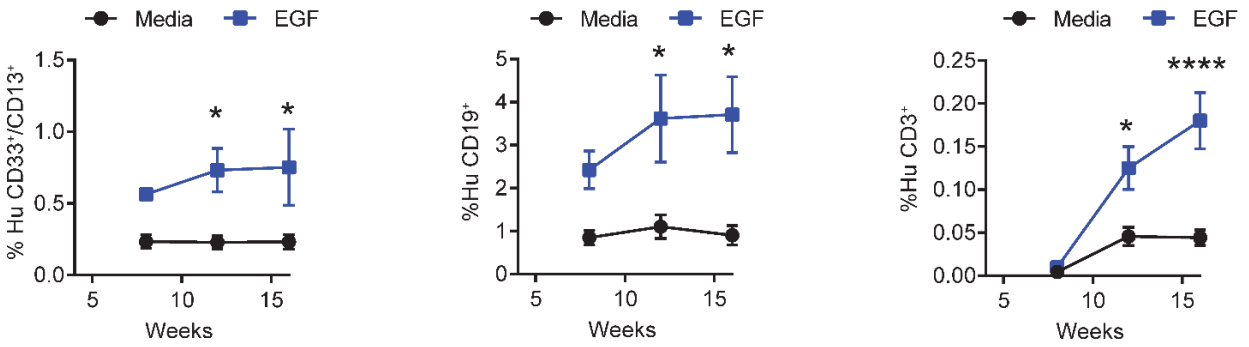

Figure 85. Multilineage reconstitution of human hematopoietic cells in the primary recipients. Time course of human lineage cells engraftment in the PB of NSG-SGM3 mice (n=7-8, means ± SEM, Two-way ANOVA) (Left) Time course of human $CD33^+/CD13^+$ myeloid cell engraftment. (Middle) Time course of human $CD19^+$ B cell engraftment. (Right) Time course of human $CD3^+$ T cell engraftment. *P < 0.05, ****P < 0.0001

These results suggest that EGF treatment promotes the recovery of human HSCs with multilineage repopulating capacity after irradiation.

2.3.10. Effect of EGF treatment on HSC mutagenesis and gene expression following TBI

Since EGF treatment increases NHEJ repair in KSL cells and NHEJ repair is considered error-prone, we sought to measure whether EGF treatment affected the frequency of somatic mutations in BM KSL cells following TBI. We irradiated C57BL/6 mice with 500 cGy TBI and treated SQ at +1 hour and +24 hours with EGF or saline, and BM KSL cells were collected at 6 weeks post-TBI for whole-genome sequencing (WGS). BM KSL cells from irradiated, EGF - treated mice displayed no differences in the total numbers of insertions or deletions (InDels), copy number variations (CNVs), or single nucleotide polymorphisms (SNPs) compared to KSL cells from irradiated, saline-treated controls (Figure 86, 87).

IRR, Saline

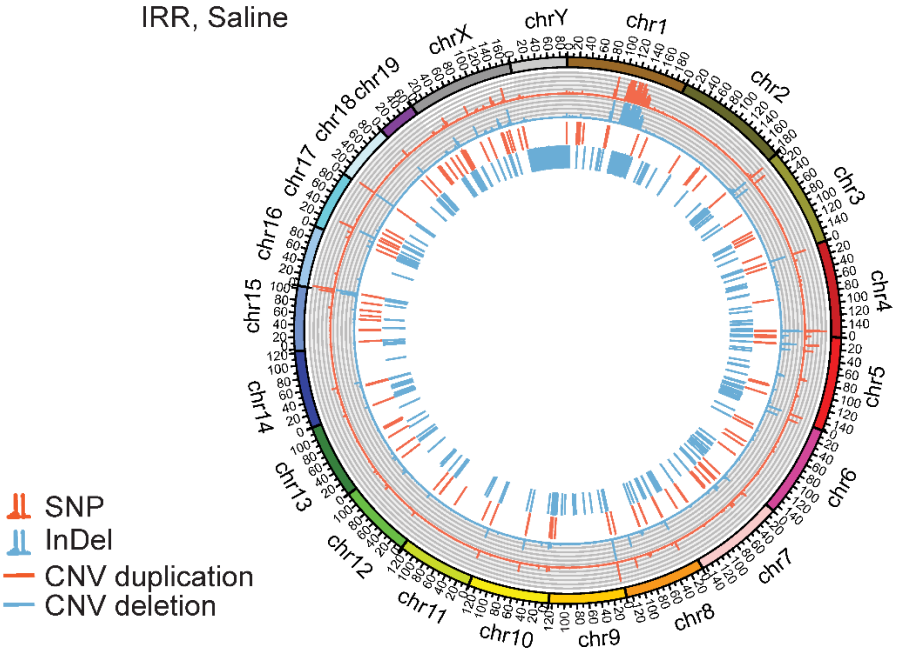

IRR, EGF

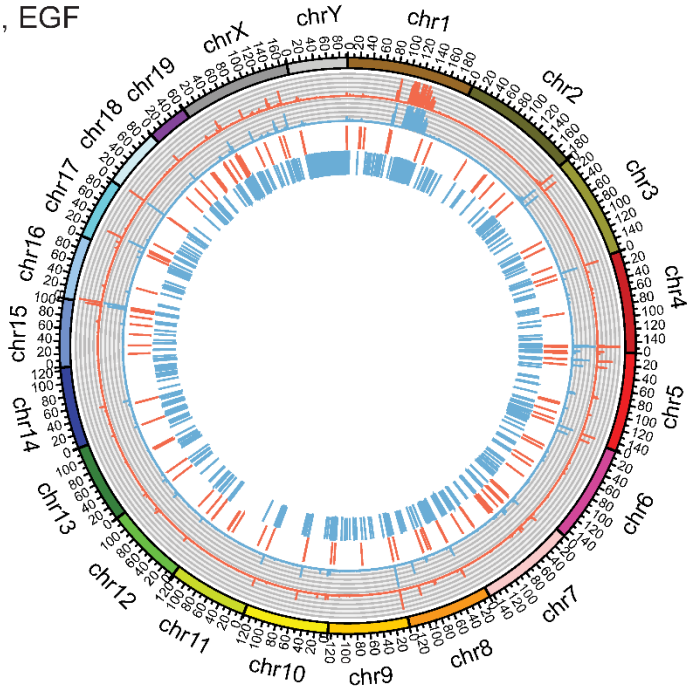

Figure 86. Whole-genome sequencing of KSL cells after radiation. Representative Circos plot of whole-genome sequencing of BM KSL cells collected from C57BL/6 mice at 6 weeks following 500cGy TBI and treatment with saline (Top) and EGF (Bottom).

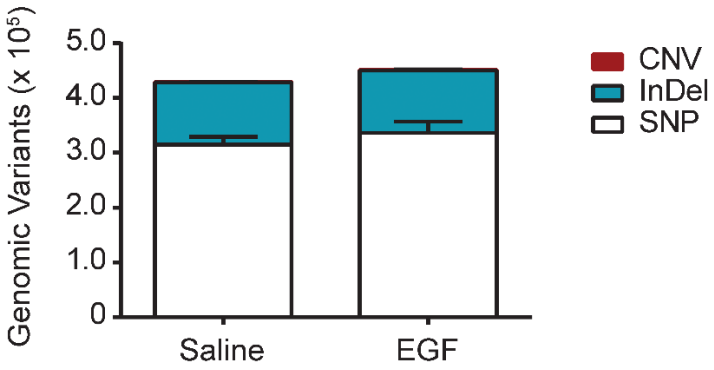

Figure 87. Total genomic variants from WGS. Total genome variant numbers categorized by mutation type (n = 5/group, means ± SEM, two-way ANOVA).

We also detected no differences in coding region mutations or intergenic SNPs or InDels between EGF-treated and saline-treated mice (Figure 88, 89, 90). However, we detected increased numbers of intergenic CNVs in KSL cells from EGF-treated mice (Figure 88).

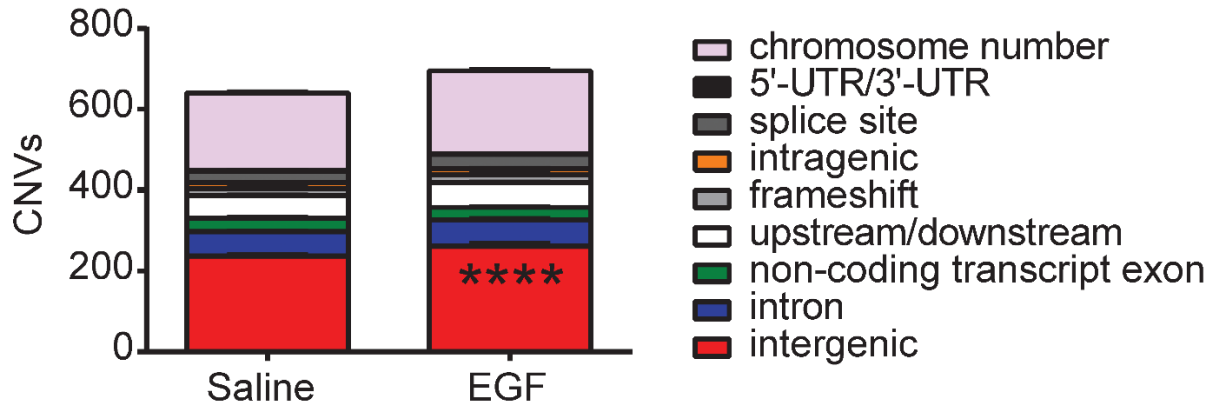

Figure 88. Copy Number Variants from WGS. Numbers of CNVs in BM KSL cells at 6 weeks following 500 cGy TBI and treatment with EGF or saline (n = 5/group, means ± SEM, two-way ANOVA). **** P < 0.0001 for intergenic CNVs

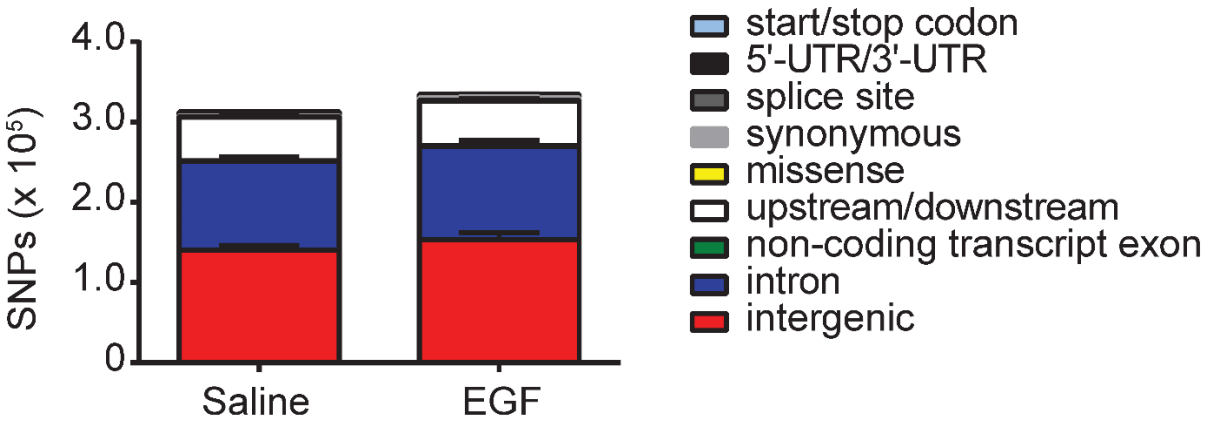

Figure 89. single nucleotide polymorphism (SNPs) from WGS. Numbers of SNPs in BM KSL cells at 6 weeks following 500 cGy TBI and treatment with EGF or saline (n = 5/group, means ± SEM, two-way ANOVA).

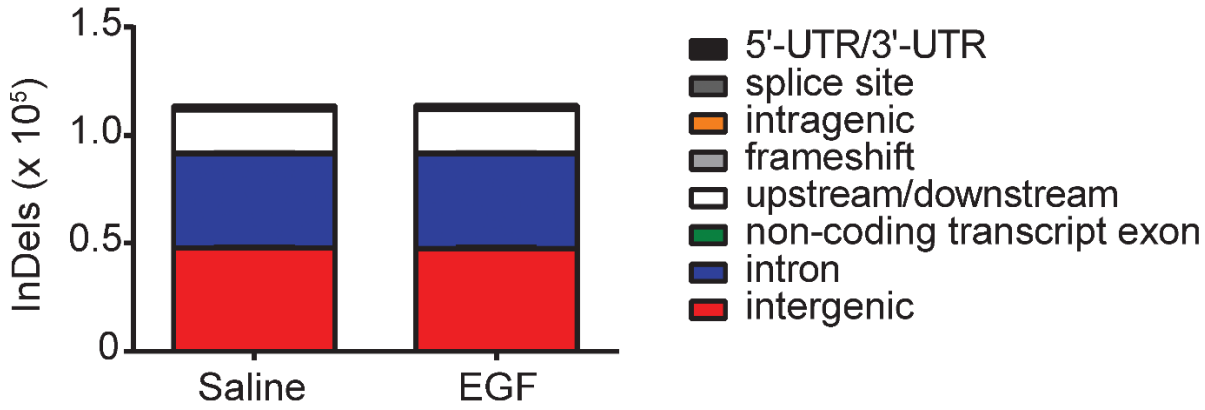

Figure 90. Insertions or deletions (InDel) from WGS. Numbers of InDels in BM KSL cells at 6 weeks following 500 cGy TBI and treatment with EGF or saline (n = 5/group, means ± SEM, two-way ANOVA).

We also evaluated the frequency of mutations in coding regions and non-coding regions of human acute myeloid leukemia (AML) oncogenes (Figure 91).

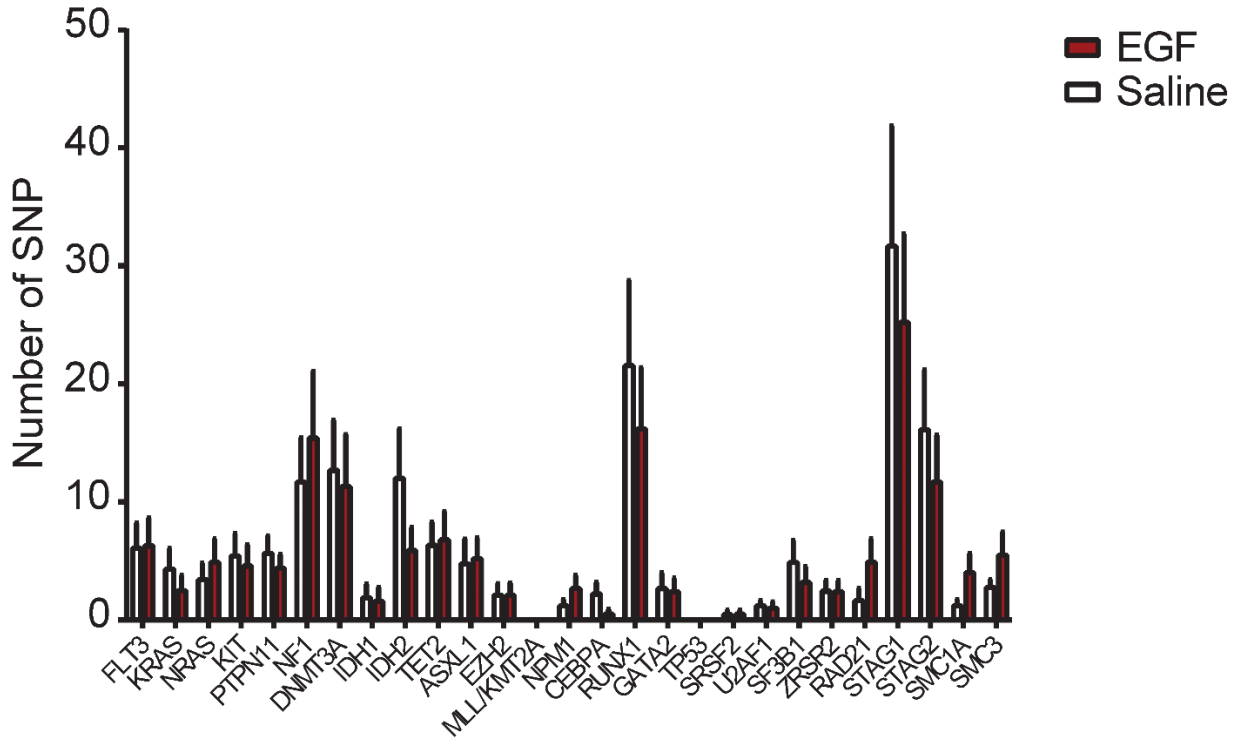

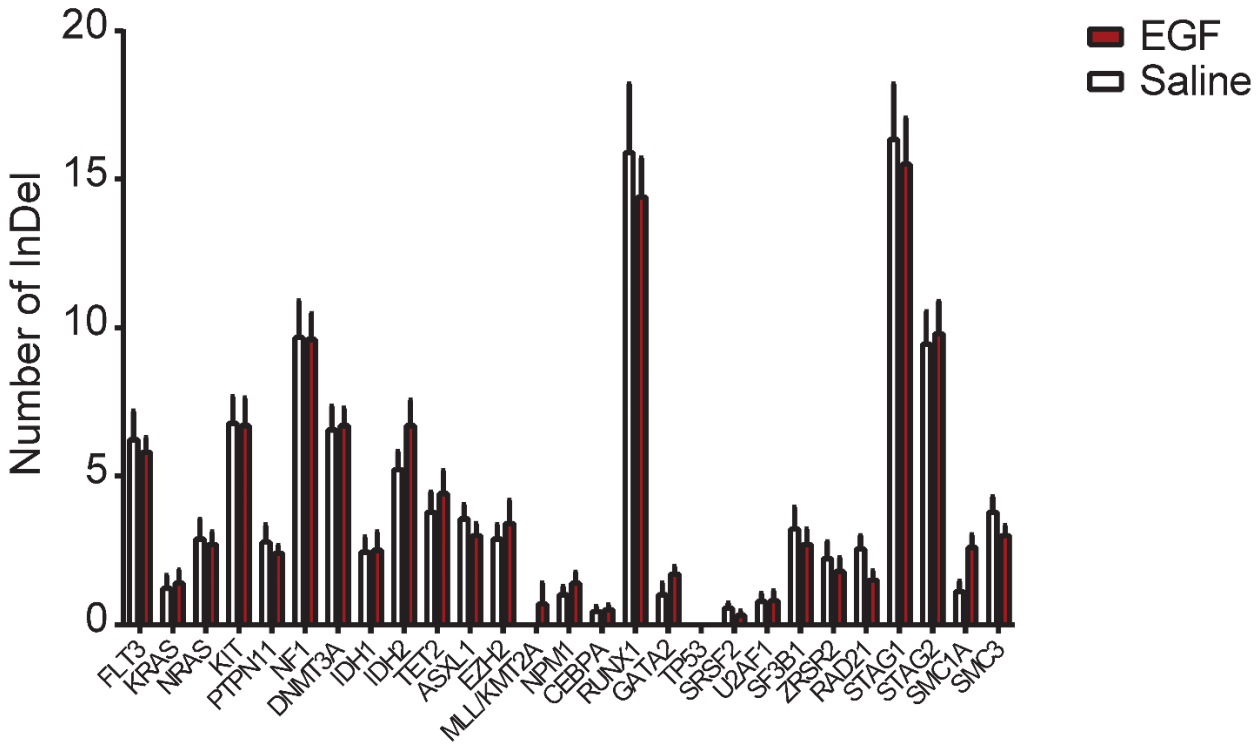

Figure 91. Mutation burdens in AML related genes from WGS. Mutations burdens in AML related genes in whole-genome sequencing data from KSL cells collected at 6 weeks post 500cGy TBI. (Top) SNPs of AML related genes (n=9-10, means ± SEM, Two-way ANOVA). (Bottom) InDels of AML related genes (n=9-10, means ± SEM, Two-way ANOVA). **FLT3**: Fms Like Tyrosine Kinase 3; **KRAS**: Kirsten Rat Sarcoma Viral Oncogene Homolog; **NRAS**: Neuroblastoma RAS Viral Oncogene Homolog; **KIT**: Proto-Oncogene C-KIT; **PTPN11**: Tyrosine-Protein Phosphatase Non-Receptor Type 11; **NF1**: Neurofibromatosis Type 1; **DNMT3A**: DNA (Cytosine-5)-Methyltransferase 3A; **IDH1**: Isocitrate Dehydrogenase 1; **IDH2**: Isocitrate Dehydrogenase 2; **TET2**: Tet Methylcytosine Dioxygenase 2; **ASXL1**: Additional Sex Combs Like 1; **EZH2**: Enhancer Of Zeste Homolog 2; **MLL/KMT2A**: Mixed Lineage Leukemia/Histone-Lysine N-Methyltransferase 2A Fusion Gene; **NPM1**: Nucleophosmin 1; **CEBPA**: CCAAT/Enhancer-Binding Protein Alpha; **RUNX1**: Runt-Related Transcription Factor 1; **GATA2**: GATA-Binding Factor 2; **TP53**: Tumor Protein P53; **SRSF2**: Serine And Arginine Rich Splicing Factor 2; **U2AF1**:

U2 Small Nuclear RNA Auxiliary Factor 1; **SF3B1**: Splicing Factor 3b Subunit 1; **ZRSR2**: Zinc Finger CCCH-Type, RNA Binding Motif And Serine/Arginine Rich 2; **RAD21**: Double-Strand-Break Repair Protein Rad21 Homolog; **STAG1**: Stromal Antigen 1; **STAG2**: Stromal Antigen 2; **SMC1A**: Structural Maintenance of Chromosomes protein 1A; **SMC3**: Structural Maintenance Of Chromosomes Protein 3 (SMC-3).

We found no increase in SNPs or InDels in AML oncogenes in BM KSL cells from EGF – treated mice compared to saline-treated controls. The WGS dataset has been deposited in the Sequence Read Archive (SRA) of NCBI under project ID PRJNA612325.

BM KSL cells from irradiated, EGF – treated mice demonstrated a distinct pattern of gene expression compared to irradiated, saline-treated mice (Figure 92).

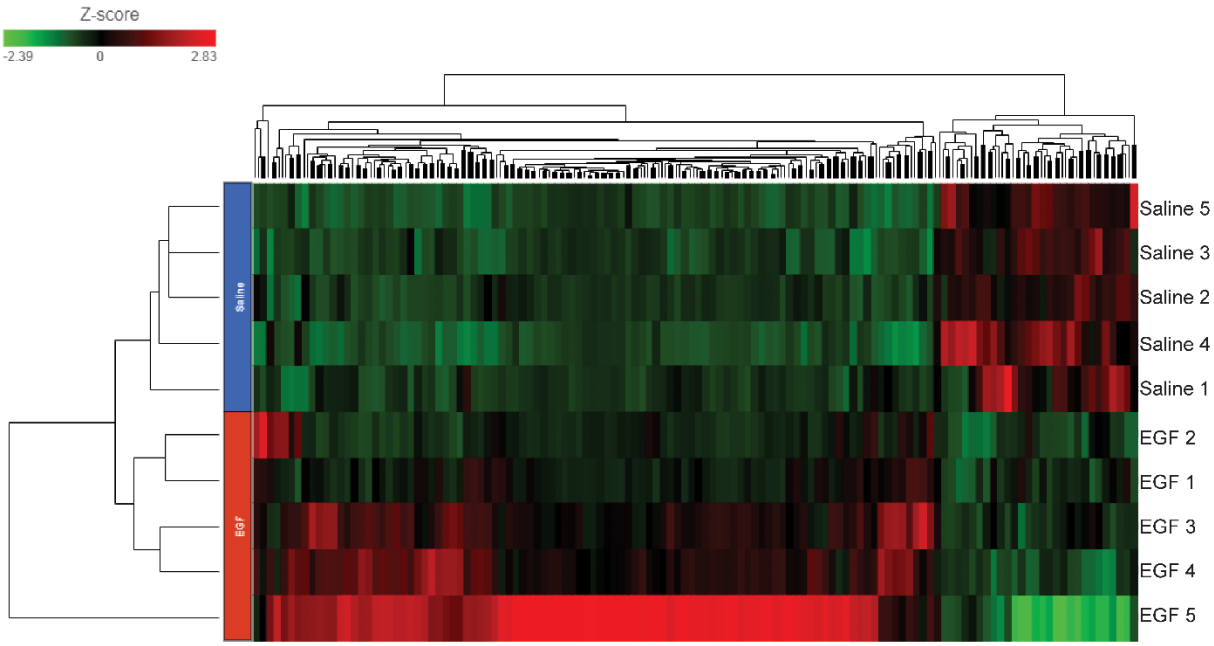

Figure 92. RNA sequencing of BM KSL cells from irradiated mice treated with saline or EGF. Heat map of differentially expressed genes. Mice were irradiated at 500cGy TBI and treated with EGF or saline. RNA was extracted from KSL cells collected at 6 weeks post-radiation (n=5/group).

BM KSL cells from irradiated, EGF – treated mice also displayed upregulation of inflammatory signaling pathways, including TH1, Interleukin-6, and dendritic cell – natural killer cell crosstalk pathways, compared to saline-treated mice (Figure 93).

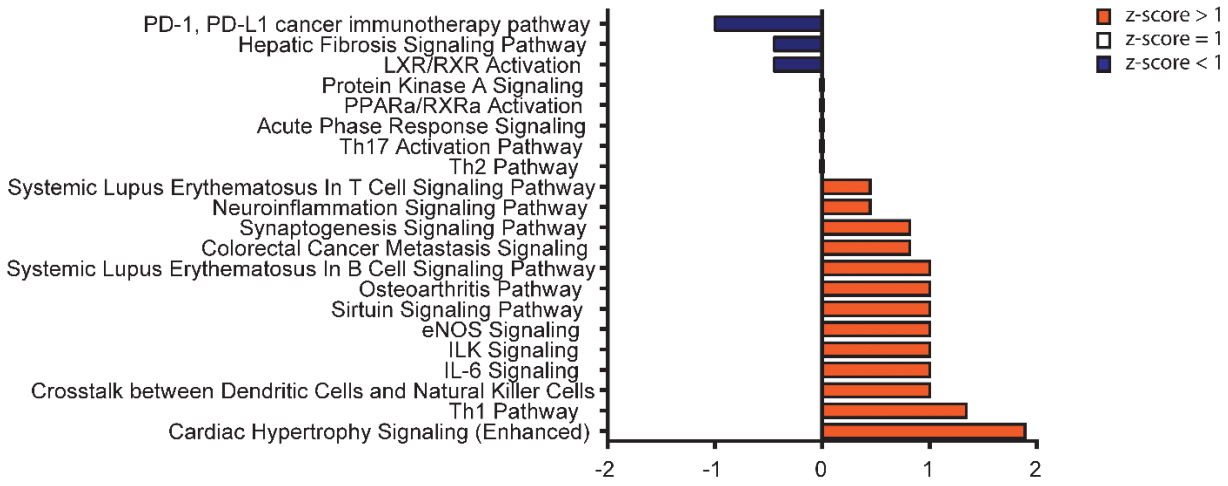

Figure 93. Signaling pathway analysis from RNA sequencing. Ingenuity pathway analysis of canonical pathways ranked by z-score (n=5/group). Z-score >1 indicates pathways with increased expression in EGF treated group. Z-score <1 indicates pathways with decreased expression in EGF treated group. Pathways with undetected z-score or z-score = 0 were filtered out.

The complete RNAseq analysis of KSL cells from EGF – treated mice and control mice has been deposited in the Gene Expression Omnibus (GEO) database under accession number GSE146371.

3. Conclusions and Future Studies

Chapter 3.3 discussion section is adapted from a publication based on the thesis project by Tiancheng Fang et al. [121].

3.1. Conclusions

Based on the results in Chapter 2, I conclude that EGFR signaling activated by EGF promotes HSC regeneration after radiation and chemotherapy. Mechanistically, EGFR signaling facilitates Non-homologous End Joining DNA repair through EGFR/Akt/DNA PKcs axis. Administration of EGF does not accelerate relapse of AML or impose higher mutation burdens on the genome of HSPCs. Therefore, EGF administration has the clinical potential to regenerate HSCs in patients who underwent radiation or chemotherapy whose disease does not involve EGFR mutation, or in patients with bone marrow failure.

3.2. Future studies

To explore the clinical potential of EGF as a stimulator of HSC regeneration, more studies are needed. First, further investigation is needed to examine whether EGF administration would render a higher risk of hematologic malignancy. Despite the data showing no increase in AML replase with EGF treatment in the murine model, transformation of hematologic malignancy in human usually requires more time. To study that, deeper sequencing of human HSCs and progenitors are required to assess clonal hematopoiesis. Since EGF is a natural growth factor and has a short half-life after administration, I would also consider chemically modifying it through PEGylation to extend its half-life. Dose escalation experiment is necessary to determine the therapeutic window of EGF administration. Thorough pharmacokinetic and pharmacodynamic experiments are also required to understand how the drug would act in vivo.

On the other hand, more studies are needed to better elucidate the mechanisms of how EGFR signaling regulates DNA repair in the HSCs. Data in Chapter 2 discovers EGFR/Akt/DNA-PKcs as an indispensable signaling pathway for DNA repair in HSCs. However, how EGFR signaling stimulates the transcription of *Xrcc6* gene in the murine and human HSPCs remains unknown. I propose to incorporate chromatin immunoprecipitation assay to unravel the transcription factors responsible for the transcription of *Xrcc6* after EGFR activation. I also need to investigate what is the mediator between EGFR and Akt in the HSCs. To answer this question, I would perform a proteomics experiment to reveal other molecules that are phosphorylated upon EGF activation in the HSCs. More importantly, even though we didn't detect upregulation of the transcription of some genes or increased activity of some proteins involved in homologous recombination, more careful examinations are needed to conclude whether the activity of homologous recombination was affected by the activation of EGFR signaling. One experiment could be site-specific genome sequencing. This could be achieved by site-specific induction of DNA double-strand break followed by sequencing of the region that covers the DNA breakage site after EGF stimulation. If the data obtained from this experiment shows more fidel DNA repair after EGF treatment, then homologous recombination might also be promoted by EGFR signaling in the HSCs.

3.3. Discussion

DNA damage response mechanisms are essential for HSCs to maintain genomic integrity over time in response to intrinsic stresses, such as cellular respiration, DNA replication, and aging [174], and extrinsic stresses, such as inflammation and irradiation [122,175]. DNA repair is also critical for the response of HSCs to medically-relevant stresses

such as chemotherapy and high dose irradiation utilized in the treatment of cancer [122,176,177]. In principle, therapies capable of augmenting DNA repair in HSCs could have therapeutic benefits following exposure to such genotoxic treatments by facilitating the recovery of functional HSCs and the hematopoietic system. Recently, it was shown that TPO administered just before radiation exposure protected HSCs from DNA damage by inducing DNA-PKcs activity [127,128].

Other HSC growth factors, stem cell factor (SCF) and Flt-3 ligand had no protective effect on HSC DNA damage at the time of irradiation, suggesting a specific activity for TPO in promoting DNA-PKcs activity in HSPCs [127]. Here, we show that EGF treatment delivered after TBI suppresses DNA damage in HSCs in vivo via augmentation of NHEJ, through activation of EGFR, Akt, Artemis, and DNA-PKcs, and increased expression of Xrcc6, which encodes Ku70 [163]. The Ku70-Ku80 heterodimer can increase the affinity of DNA PKcs for the Ku:DNA complex by up to 100-fold, thereby increasing DNA-PKcs function [162]. We hypothesize that EGF mitigates DNA damage in HSPCs after irradiation because it causes a broad activation of the NHEJ machinery, resulting in increased activation of DNA PKcs and augmented affinity of DNA-PKcs for sites of DNA damage in HSPCs. Of note, we found that short duration of EGF treatment was insufficient to promote hematopoietic regeneration in irradiated mice, likely due to the persistence of DNA damage that occurs in HSPCs following TBI, thereby requiring a longer duration of EGF treatment to be therapeutically effective.

In addition to the direct effects of EGF on HSPCs following irradiation or chemotherapy, BM ECs and LepR+ stromal cells express EGFR [170,171] and EGF may promote hematopoietic regeneration indirectly via niche effects. Our studies suggest that EGF

treatment decreased BM vascular area after TBI, which has been associated with restoration of the BM vasculature [172], implying that EGF may have a direct action on BM ECs. We did not detect substantial effects of EGF treatment on the recovery of LepR+ stromal cells after TBI. Going forward, to define the role of EGFR-expressing BM niche cells in regulating EGF effects on hematopoietic regeneration and HSC recovery after myelosuppression, we will utilize Cre;loxP technology to control EGFR expression in BM hematopoietic cells and BM niche cells in mice treated with EGF in homeostasis and following myelosuppression.

Our studies suggest that EGF treatment strongly accelerates the recovery of essential mature blood elements (e.g. neutrophils) and BM HSPCs in mice treated with chemotherapy. This suggests the therapeutic potential of EGF or EGF mimetics for patients receiving chemotherapy. One concern in treating such patients would be whether EGF treatment might promote the relapse or progression of residual tumor. Our studies of EGF treatment of mice bearing HOXA9/MEIS1+ AML demonstrated no significant effects of EGF treatment on AML growth or progression in vivo. A rational strategy for the clinical application of EGF or EGF mimetics might be to include only patients in complete remission and with EGFR – negative malignancy.

In addition to hematopoietic gain-of-function in response to EGF treatment, we have shown using EGFR-DN mice that EGFR signaling in HSPCs is necessary for normal NHEJ repair and HSC recovery in vivo following TBI. EGFR-WT mice activate the EGFR/Akt/DNA-PKcs pathway in HSPCs in response to endogenous EGF following TBI, whereas EGFR-DN mice fail to activate this DNA repair pathway in the absence of functional EGFR, leading to HSC depletion. Systemic administration of EGF further

increases activation of the EGFR/Akt/DNA PKcs pathway in HSPCs in irradiated wild type mice. We propose that the administration of EGF to irradiated mice for up to 10 days promotes HSC recovery and hematopoietic regeneration via the sustained activation of the EGFR/Akt/DNA- PKcs pathway and sustained NHEJ repair in HSPCs.

To further highlight the translational potential of EGF, we show that EGF abrogates radiation-induced DNA damage in human HSCs and promotes human hematopoietic regeneration via activation of DNA-PKcs. Importantly, short-duration treatment of irradiated human HSPCs with EGF caused a marked increase in the recovery of human HSCs capable of multilineage in vivo repopulation in immune-deficient mice. These results demonstrate the potential importance of EGF- EGFR signaling in regulating human hematopoietic regeneration and provide the basis for further preclinical studies to define the efficacy of EGF treatment for human hematopoietic cell engraftment and regeneration.

In light of the potency of EGF treatment in promoting hematopoietic recovery in mice following TBI or chemotherapy via augmented NHEJ, it is important to assess potential adverse effects on the HSC genome. Mohrin et al. showed that more than 30% of quiescent HSCs that underwent NHEJ repair following 2 Gy irradiation displayed major genomic mutations. Here, we observed that EGF did not increase the overall frequency of mutations at 6 weeks post-TBI in BM KSL cells. These results may be explained by the possibility that EGF treatment upregulated canonical NHEJ, which is dependent on DNA-PKcs and relatively accurate [178,179,180], rather than alternative NHEJ, which is DNA- PKcs – independent and associated with error-prone end-joining [178,181,182]. It is noteworthy, however, that BM KSL cells from irradiated, EGF – treated mice displayed increased

numbers of intergenic mutations, specifically CNVs, compared to control mice. Further analysis demonstrated that mutations were not increased in frequency in AML oncogenes, but the significance of intergenic CNVs will require long-term studies to determine the incidence of clonal hematopoiesis or myelodysplasia. The broader significance of mutations in non-coding, intergenic DNA remains poorly understood, but such mutations occur in many cancers and are the subject of intense ongoing research [183,184,185]. RNAseq analysis revealed that EGF treatment of irradiated mice was also associated with substantial changes in gene expression and activation of inflammatory and metabolic signaling pathways in BM HSPCs compared to irradiated controls. Determination of the impact of therapeutic growth factors such as EGF on long-term hematopoiesis following chemotherapy or TBI will be an important focus going forward.

4. Appendices

4.1. Appendix B: List of antibodies and reagents

4.1.1. Table 1. Detailed information regarding reagents

REAGENT	COMPANY	CATALOG	DILUTION / CONCENTRATION
EGFR [phospho Tyr1173] polyclonal antibody	Abcam	ab5652	1:100
Alexa Fluor® 488 H2A.X [phospho Ser139] monoclonal antibody (2F3)	Biolegend	613406	1:50
DNA-PKcs [phospho S2056] polyclonal antibody	Abcam	ab18192	1:100
Artemis [phospho Ser516] Polyclonal Antibody	ThermoFisher Scientific	PA5-38260	1:200
Akt [phospho Ser473] monoclonal antibody (D9E)	Cell Signaling Technology	4060S	1:100
DNA-PKcs [phospho Thr2609] polyclonal antibody	Novus biologicals	NBP1-02456	1:50

FITC Annexin V Apoptosis Detection Kit I	BD Biosciences	556547	Per the manufacturer's protocol
V450 Mouse Lineage Antibody Cocktail with Isotype Control	BD Biosciences	561301	20µl/10^6 cells
APC-Cy7 Sca-1 (Ly-6A/E) monoclonal antibody (D7)	BD Biosciences	560654	2µl/10^6 cells
PE c-kit (CD117) monoclonal antibody (2B8)	BD Biosciences	553355	2µl/10^6 cells
Alexa Fluor® 488 CD41 monoclonal antibody (MWReg30)	Biolegend	133908	2µl/10^6 cells
FITC CD48 monoclonal antibody (HM48-1)	BD Biosciences	557484	2µl/10^6 cells
Alexa Fluor® 647 CD150 monoclonal antibody (Q38-480)	BD Biosciences	562647	2µl/10^6 cells
PE Mac-1 (CD11b)monoclonal antibody (M1/70)	BD Biosciences	552094	2µl/10^6 cells
PE Gr-1 (Ly-6G and Ly-6C) monoclonal antibody (RB6-8C5)	BD Biosciences	561389	2µl/10^6 cells
APC-Cy7 B220 (CD45R) monoclonal antibody (RA3-6B2)	BD Biosciences	557909	2µl/10^6 cells
V450 CD3 Molecular Complex monoclonal antibody (17A2)	BD Biosciences	553772	2µl/10^6 cells
FITC CD45.2 monoclonal antibody (104)	ThermoFisher Scientific	PA5-38260	2µl/10^6 cells
Brilliant Violet 605 CD45.1 monoclonal antibody (A20)	Cell Signaling Technology	3033T	2µl/10^6 cells
Rad51 polyclonal antibody	Abcam	ab63801	1:100
V450 Mouse Anti-Human CD45 antibody	BD Biosciences	560367	2µl/10^6 cells
Brilliant Violet 605 anti-mouse CD45 antibody	Biolegend	103139	2µl/10^6 cells
APC/Cy7 anti-mouse/rat/human CD27 Antibody	Biolegend	124226	2µl/10^6 cells
Brilliant Violet 605™ anti-mouse/human CD11b Antibody	Biolegend	101237	2µl/10^6 cells
Alexa Fluor® 700 anti-mouse CD23 Antibody	Biolegend	101632	2µl/10^6 cells
PE anti-human CD13 antibody	Biolegend	301704	2µl/10^6 cells
PE anti-human CD33 antibody	Biolegend	366608	2µl/10^6 cells
APC/Cy7 anti-human CD19 antibody	Biolegend	302218	2µl/10^6 cells
APC anti-human CD3 antibody	Biolegend	300312	2µl/10^6 cells
FITC anti-human CD34 antibody	Biolegend	343604	2µl/10^6 cells

APC Mouse anti-Human CD38 antibody	BD Biosciences	555462	2µl/10^6 cells
Alexa Fluor® 488Goat anti-mouse IgM heavy chain secondary antibody	ThermoFisher Scientific	A-21042	1:200
Alexa Fluor 647 Goat anti-Rabbit IgG (H+L) Secondary Antibody	ThermoFisher Scientific	A-21244	1:200
Alexa Fluor 647 Donkey anti-Rabbit IgG (H+L) Highly Cross-Adsorbed Secondary Antibody	ThermoFisher Scientific	A31573	1:200
FITC Mouse Anti-Ki-67 Set, with FITC Mouse IgG1, κ Isotype Control	BD Biosciences	556026	Per the manufacturer's protocol
Mouse IgG, κ Isotype Ctrl (ICFC) Antibody (Clone MOPC-21)	Biolegend	400134	1:50
Rabbit IgG, polyclonal - Isotype Control (ChIP Grade)	Abcam	ab171870	1:100
FITC Rat IgG2a, κ Isotype Control (R35-95)	BD Biosciences	554688	2µl/10^6 cells
APC-Cy7 Rat IgG2a, κ Isotype Control (R35-95)	BD Biosciences	552770	2µl/10^6 cells
PE Rat IgG2a, κ Isotype Control (R35-95)	BD Biosciences	553930	2µl/10^6 cells
FITC Rat IgG2b, κ Isotype Control (A95-1)	BD Biosciences	553988	2µl/10^6 cells
V450 Rat IgG2b, κ Isotype Control (A95-1)	BD Biosciences	560457	2µl/10^6 cells
APC Rat IgG2b, κ Isotype Control (A95-1)	BD Biosciences	556924	2µl/10^6 cells
Alexa Fluor 647 Rat IgG2a, κ Isotype Control	BD Biosciences	557690	2µl/10^6 cells
BV605Rat IgG2b, κ Isotype Control (R35-38)	BD Biosciences	563145	2µl/10^6 cells

4.1.2. Table 2. List of oligonucleotides

Oligonucleotide	**SOURCE**	**IDENTIFIER**
Mouse Rpa1 Taqman gene expression assay	ThermoFisher	Mm01253368_m1
Mouse Atrip Taqman gene expression assay	ThermoFisher	Mm00555350_m1
Mouse EGFR extracellular domain Taqman gene expression assay	ThermoFisher	Mm01187861_m1

Mouse EGFR intracellular domain Taqman gene expression assay	ThermoFisher	Mm01187868_m1
Mouse Xrcc6(Ku70) Taqman gene expression assay	ThermoFisher	Mm00487458_m1
Mouse GAPDH Taqman gene expression assay	ThermoFisher	Mm99999915_g1
Human Xrcc6 Taqman PCR primer	ThermoFisher	Hs01922652_g1
Human GAPDH PCR primer	ThermoFisher	Hs02786624_g1

Bibliography

1. Orkin, S. H. & Zon, L. I. Hematopoiesis: an evolving paradigm for stem cell biology. Cell **132**, 631–44 (2008).

2. Wolber, F. M. et al. Roles of spleen and liver in development of the murine hematopoietic system. Exp. Hematol. **30**, 1010–1019 (2002).

3. Golden-Mason, L. & O'Farrelly, C. Having it all? Stem cells, haematopoiesis and lymphopoiesis in adult human liver. Immunol. Cell Biol. **80**, 45–51 (2002).

4. Zhou, X. et al. The Genetic Landscape of Hematopoietic Stem Cell Frequency in Mice. Stem Cell Reports **5**, 125–138 (2015).

5. Pang, W. W. et al. Isolation of a candidate human hematopoietic stem-cell population. Proc. Natl. Acad. Sci. **108**, 20012–20017 (2011).

6. Cheshier, S. H., Morrison, S. J., Liao, X. & Weissman, I. L. In vivo proliferation and cell cycle kinetics of long-term self-renewing hematopoietic stem cells. Proc. Natl. Acad. Sci. **96**, 3120–3125 (1999).

7. TILL, J. E. & McCULLOCH, E. A. A direct measurement of the radiation sensitivity of normal mouse bone marrow cells. Radiat. Res. **14**, 213–222 (1961).

8. Becker, A. J., McCulloch, E. A. & Till, J. E. Cytological demonstration of the clonal nature of spleen colonies derived from transplanted mouse marrow cells. Nature **197**, 452–454 (1963).

9. Traver, D. & Zon, L. I. Walking the Walk: Migration and Other Common Themes in Blood and Vascular Development. Cell **108**, 731–734 (2002).

10. Murray, P. D. F. The Development in vitro of the Blood of the Early Chick Embryo. Proc. R. Soc. B Biol. Sci. **111**, 497–521 (1932).

11. Palis, J., McGrath, K. E. & Kingsley, P. D. Initiation of hematopoiesis and vasculogenesis in murine yolk sac explants. Blood **85**, 156–163 (1995).

12. Müller, A. M., Medvinsky, A., Strouboulis, J., Grosveld, F. & Dzierzakt, E. Development of hematopoietic stem cell activity in the mouse embryo. Immunity **1**, 291–301 (1994).

13. Ema, H. & Nakauchi, H. Expansion of hematopietic stem cells in the developing liver of a mouse embryo. Blood **95**, 2284–2288 (2000).

14. Lee, L. K., Ueno, M., Van Handel, B. & Mikkola, H. K. A. Placenta as a newly identified source of hematopoietic stem cells. Current Opinion in Hematology **17**, 313–318 (2010).

15. Moore, M. A. & Owen, J. J.. STEM-CELL MIGRATION IN DEVELOPING MYELOID AND LYMPHOID SYSTEMS. Lancet **290**, 658–659 (1967).

16. Kumaravelu, P. et al. Quantitative developmental anatomy of definitive haematopoietic stem cells/long-term repopulating units (HSC/RUs): role of the aorta-gonad-mesonephros (AGM) region and the yolk sac in colonisation of the mouse embryonic liver. Development **129**, 4891–9 (2002).

17. Dieterlen-Lièvre, F. & Le Douarin, N. M. Developmental rules in the hematopoietic and immune systems of birds: how general are they? Semin. Dev. Biol. **4**, 325–332 (1993).

18. Yang, L. et al. Identification of Lin(-)Sca1(+)kit(+)CD34(+)Flt3- short-term hematopoietic stem cells capable of rapidly reconstituting and rescuing myeloablated transplant recipients. Blood **105**, 2717–23 (2005).

19. Curtis, D. J. et al. SCL is required for normal function of short-term repopulating hematopoietic stem cells. Blood **103**, 3342–8 (2004).

20. Morrison, S. J., Wandycz, A. M., Hemmati, H. D., Wright, D. E. & Weissman, I. L. Identification of a lineage of multipotent hematopoietic progenitors. Development **124**, 1929–1939 (1997).

21. Reya, T., Morrison, S. J., Clarke, M. F. & Weissman, I. L. Stem cells, cancer, and cancer stem cells. Nature **414**, 105–111 (2001).

22. Liu, L. et al. Homing and Long-Term Engraftment of Long- and Short-Term Renewal Hematopoietic Stem Cells. PLoS One **7**, e31300 (2012).

23. Iwasaki, H. & Akashi, K. Myeloid Lineage Commitment from the Hematopoietic Stem Cell. Immunity **26**, 726–740 (2007).

24. Macaulay, I. C. et al. Single-Cell RNA-Sequencing Reveals a Continuous Spectrum of Differentiation in Hematopoietic Cells. Cell Rep. **14**, 966–977 (2016).

25. Velten, L. et al. Human haematopoietic stem cell lineage commitment is a continuous process. Nat. Cell Biol. **19**, 271–281 (2017).

26. Yamamoto, R. et al. Clonal analysis unveils self-renewing lineage-restricted progenitors generated directly from hematopoietic stem cells. Cell **154**, 1112–1126 (2013).

27. Weissman, I. L. & Shizuru, J. A. The origins of the identification and isolation of hematopoietic stem cells, and their capability to induce donor-specific transplantation tolerance and treat autoimmune diseases. Blood **112**, 3543–53 (2008).

28. Rusten, L. S. et al. Functional differences between CD38- and DR- subfractions of CD34+ bone marrow cells. Blood **84**, 1473–1481 (1994).

29. Hao, Q. L., Shah, A. J., Thiemann, F. T., Smogorzewska, E. M. & Crooks, G. M. A functional comparison of CD34 + CD38- cells in cord blood and bone marrow. Blood

86, 3745–3753 (1995).

30. Majeti, R., Park, C. Y. & Weissman, I. L. Identification of a hierarchy of multipotent hematopoietic progenitors in human cord blood. Cell Stem Cell **1**, 635–45 (2007).

31. Okada, S. et al. In vivo and in vitro stem cell function of c-kit- and Sca-1-positive murine hematopoietic cells. Blood **80**, 3044–3050 (1992).

32. Kiel, M. J. et al. SLAM Family Receptors Distinguish Hematopoietic Stem and Progenitor Cells and Reveal Endothelial Niches for Stem Cells. Cell **121**, 1109–1121 (2005).

33. Osawa, M., Hanada, K., Hamada, H. & Nakauchi, H. Long-term lymphohematopoietic reconstitution by a single CD34-low/negative hematopoietic stem cell. Science **273**, 242–5 (1996).

34. Matsuoka, S. et al. CD34 expression on long-term repopulating hematopoietic stem cells changes during developmental stages. Blood **97**, 419–25 (2001).

35. Pereira, C., Clarke, E. & Damen, J. Hematopoietic Colony-Forming Cell Assays. Methods Mol Biol **407**, 177–208 (2007).

36. Bock, T. A. Assay systems for hematopoietic stem and progenitor cells. Stem Cells **15**, 185–195 (1997).

37. Petzer, A. L., Hogge, D. E., Landsdorp, P. M., Reid, D. S. & Eaves, C. J. Self-renewal of primitive human hematopoietic cells (long-term-culture-initiating cells) in vitro and their expansion in defined medium. Proc. Natl. Acad. Sci. U. S. A. **93**, 1470–1474 (1996).

38. Harrison, D. Competitive repopulation: a new assay for long-term stem cell functional capacity. Blood **55**, 77–81 (1980).

39. Jordan, C. T. & Lemischka, I. R. Clonal and systemic analysis of long-term hematopoiesis in the mouse. Genes Dev. **4**, 220–32 (1990).

40. Harrison, D. E. & Zhong, R. K. The same exhaustible multilineage precursor produces both myeloid and lymphoid cells as early as 3-4 weeks after marrow transplantation. Proc. Natl. Acad. Sci. U. S. A. **89**, 10134–8 (1992).

41. Zhong, R. K., Astle, C. M. & Harrison, D. E. Distinct developmental patterns of short-term and long-term functioning lymphoid and myeloid precursors defined by competitive limiting dilution analysis in vivo. J. Immunol. **157**, 138–45 (1996).

42. Morrison, S. J. & Weissman, I. L. The long-term repopulating subset of hematopoietic stem cells is deterministic and isolatable by phenotype. Immunity **1**, 661–673 (1994).

43. Doan, P. L. et al. Epidermal growth factor regulates hematopoietic regeneration after radiation injury. Nat. Med. **19**, 295–304 (2013).

44. Himburg, H. A. et al. Pleiotrophin regulates the expansion and regeneration of hematopoietic stem cells. Nat. Med. **16**, 475–82 (2010).

45. Gao, X., Xu, C., Asada, N. & Frenette, P. S. The hematopoietic stem cell niche: From embryo to adult. Dev. **145**, (2018).

46. Butler, J. M. et al. Endothelial Cells Are Essential for the Self-Renewal and Repopulation of Notch-Dependent Hematopoietic Stem Cells. Cell Stem Cell **6**, 251–264 (2010).

47. Kumano, K. et al. Notch1 but not Notch2 is essential for generating hematopoietic stem cells from endothelial cells. Immunity **18**, 699–711 (2003).

48. Doan, P. L. et al. Tie2 + Bone Marrow Endothelial Cells Regulate Hematopoietic Stem Cell Regeneration Following Radiation Injury. Stem Cells **31**, 327–337 (2013).

49. Kobayashi, H. et al. Angiocrine factors from Akt-activated endothelial cells balance self-renewal and differentiation of haematopoietic stem cells. Nat. Cell Biol. **12**, 1046–1056 (2010).

50. Salter, A. B. et al. Endothelial progenitor cell infusion induces hematopoietic stem cell reconstitution in vivo. Blood **113**, 2104–2107 (2009).

51. Kubota, Y., Takubo, K. & Suda, T. Bone marrow long label-retaining cells reside in the sinusoidal hypoxic niche. Biochem. Biophys. Res. Commun. **366**, 335–339 (2008).

52. Hooper, A. T. et al. Engraftment and Reconstitution of Hematopoiesis Is Dependent on VEGFR2-Mediated Regeneration of Sinusoidal Endothelial Cells. Cell Stem Cell **4**, 263–274 (2009).

53. Xu, C. et al. Stem cell factor is selectively secreted by arterial endothelial cells in bone marrow. Nat. Commun. **9**, (2018).

54. Futrega, K., Atkinson, K., Lott, W. B. & Doran, M. R. Spheroid Coculture of Hematopoietic Stem/Progenitor Cells and Monolayer Expanded Mesenchymal Stem/Stromal Cells in Polydimethylsiloxane Microwells Modestly Improves in Vitro Hematopoietic Stem/Progenitor Cell Expansion. Tissue Eng. - Part C Methods **23**, 200–218 (2017).

55. Acar, M. et al. Deep imaging of bone marrow shows non-dividing stem cells are mainly perisinusoidal. Nature **526**, 126–130 (2015).

56. Van Overstraeten-Schlogel, N., Beguin, Y. & Gothot, A. Role of stromal-derived factor-1 in the hematopoietic-supporting activity of human mesenchymal stem cells. Eur. J. Haematol. **76**, 488–493 (2006).

57. Sugiyama, T., Kohara, H., Noda, M. & Nagasawa, T. Maintenance of the Hematopoietic Stem Cell Pool by CXCL12-CXCR4 Chemokine Signaling in Bone

Marrow Stromal Cell Niches. Immunity **25**, 977–988 (2006).

58. Kim, J.-A. et al. Identification of a Stroma-Mediated Wnt/β-Catenin Signal Promoting Self-Renewal of Hematopoietic Stem Cells in the Stem Cell Niche. Stem Cells **27**, 1318–1329 (2009).

59. Asada, N. et al. Differential cytokine contributions of perivascular haematopoietic stem cell niches. Nat. Cell Biol. **19**, 214–223 (2017).

60. Morrison, S. J. & Scadden, D. T. The bone marrow niche for haematopoietic stem cells. Nature **505**, 327–334 (2014).

61. Bruns, I. et al. Megakaryocytes regulate hematopoietic stem cell quiescence through CXCL4 secretion. Nat. Med. **20**, 1315–1320 (2014).

62. Zhao, M. et al. Megakaryocytes maintain homeostatic quiescence and promote post-injury regeneration of hematopoietic stem cells. Nat. Med. **20**, 1321–1326 (2014).

63. Calvi, L. M. et al. Osteoblastic cells regulate the haematopoietic stem cell niche. Nature **425**, 841–846 (2003).

64. CALVI, L. M. Osteoblastic Activation in the Hematopoietic Stem Cell Niche. Ann. N. Y. Acad. Sci. **1068**, 477–488 (2006).

65. Yoshihara, H. et al. Thrombopoietin/MPL Signaling Regulates Hematopoietic Stem Cell Quiescence and Interaction with the Osteoblastic Niche. Cell Stem Cell **1**, 685–697 (2007).

66. Fitch, S. R. et al. Signaling from the sympathetic nervous system regulates hematopoietic stem cell emergence during embryogenesis. Cell Stem Cell **11**, 554–566 (2012).

67. Katayama, Y. et al. Signals from the sympathetic nervous system regulate hematopoietic stem cell egress from bone marrow. Cell **124**, 407–421 (2006).

68. García-García, A. et al. Dual cholinergic signals regulate daily migration of hematopoietic stem cells and leukocytes. Blood **133**, 224–236 (2019).

69. Lucas, D. et al. Chemotherapy-induced bone marrow nerve injury impairs hematopoietic regeneration. Nat. Med. **19**, 695–703 (2013).

70. Maryanovich, M. et al. Adrenergic nerve degeneration in bone marrow drives aging of the hematopoietic stem cell niche. Nat. Med. **24**, 782–791 (2018).

71. Yamazaki, S. et al. Nonmyelinating Schwann cells maintain hematopoietic stem cell hibernation in the bone marrow niche. Cell **147**, 1146–1158 (2011).

72. Ferguson, K. M. Structure-Based View of Epidermal Growth Factor Receptor Regulation. Annu. Rev. Biophys. **37**, 353–373 (2008).

73. Wang, Z., Zhang, L., Yeung, T. K. & Chen, X. Endocytosis deficiency of epidermal growth factor (EGF) receptor-ErbB2 heterodimers in response to EGF stimulation. Mol. Biol. Cell **10**, 1621–1636 (1999).

74. Littlefield, P. et al. Structural analysis of the EGFR/HER3 heterodimer reveals the molecular basis for activating HER3 mutations. Sci. Signal. **7**, ra114 (2014).

75. Lu, C. et al. Mechanisms for Kinase-mediated Dimerization of the Epidermal Growth Factor Receptor. J. Biol. Chem. **287**, 38244-38253 (2012).

76. Downward, J., Parker, P. & Waterfield, M. D. Autophosphorylation sites on the epidermal growth factor receptor. Nature **311**, 483–485 (1984).

77. Bublil, E. M. et al. Kinase-mediated quasi-dimers of EGFR. FASEB J. **24**, 4744–4755 (2010).

78. Pines, G., Huang, P. H., Zwang, Y., White, F. M. & Yarden, Y. EGFRvIV: A previously uncharacterized oncogenic mutant reveals a kinase autoinhibitory mechanism. Oncogene **29**, 5850–5860 (2010).

79. Gajiwala, K. S. EGFR: Tale of the C-terminal tail. Protein Sci. **22**, 995–999 (2013).

80. Singh, B., Carpenter, G. & Coffey, R. J. EGF receptor ligands: Recent advances [version 1; referees: 3 approved]. F1000Research **5**, (2016).

81. Herbst, R. S. Review of epidermal growth factor receptor biology. Int. J. Radiat. Oncol. Biol. Phys. **59**, S21–S26 (2004).

82. Parmar, S. et al. Pharmacogenetic predictors for EGFR inhibitor-associated skin toxicity. Pharmacogenomics J. **13**, 181–188 (2013).

83. Li, T. & Perez-Soler, R. Skin toxicities associated with epidermal growth factor receptor inhibitors. Targeted Oncology **4**, 107–119 (2009).

84. Wiesen, J. F., Young, P., Werb Z., Cunha, G. R. Signaling through the stromal epidermal growth factor receptor is necessary for mammary ductal development. Development **126**, 335–344 (1999).

85. Nicholson, R. I., Gee, J. M. W. & Harper, M. E. EGFR and cancer prognosis. Eur. J. Cancer **37**, 9 (2001).

86. Miettinen, P. J. et al. Epithelial immaturity and multiorgan failure in mice lacking epidermal growth factor receptor. Nature **376**, 337–341 (1995).

87. Kornblum, H. I. et al. Abnormal astrocyte development and neuronal death in mice lacking the epidermal growth factor receptor. J. Neurosci. Res. **53**, 697–717 (1998).

88. Sibilia M.; Steinbach J P.; Stingl L.; Aguzzi A and Wagner E F. A strain-independent postnatal neurodegeneration in mice lacking the EGF receptor. EMBO J. **17**, 719–731 (1998).

89. Luetteke, N. C. et al. The mouse waved-2 phenotype results from a point mutation in the EGF receptor tyrosine kinase. Genes Dev. **8**, 399–413 (1994).

90. Avraham, R. & Yarden, Y. Feedback regulation of EGFR signalling: Decision making by early and delayed loops. Nature Reviews Molecular Cell Biology **12**, 104–117 (2011).

91. Oda, K., Matsuoka, Y., Funahashi, A. & Kitano, H. A comprehensive pathway map of epidermal growth factor receptor signaling. Mol. Syst. Biol. **1**, 2005.0010 (2005).

92. Harris, R. S. et al. DNA deamination mediates innate immunity to retroviral infection. Cell **113**, 803–809 (2003).

93. Tanaka, K. & Okamoto, A. Degradation of DNA by bisulfite treatment. Bioorganic Med. Chem. Lett. **17**, 1912–1915 (2007).

94. Esteller, M. et al. Inactivation of the DNA-Repair Gene MGMT and the Clinical Response of Gliomas to Alkylating Agents. N. Engl. J. Med. **343**, 1350–1354 (2000).

95. Fu, D., Calvo, J. A. & Samson, L. D. Balancing repair and tolerance of DNA damage caused by alkylating agents. Nature Reviews Cancer **12**, 104–120 (2012).

96. Lindahl, T. Instability and decay of the primary structure of DNA. Nature **362**, 709–715 (1993).

97. Burrows, C. J. & Muller, J. G. Oxidative Nucleobase Modifications Leading to Strand Scission. Chem. Rev. **98**, 1109–1151 (1998).

98. Schroeder, G. K., Lad, C., Wyman, P., Williams, N. H. & Wolfenden, R. The time required for water attack at the phosphorus atom of simple phosphodiesters and of DNA. Proc. Natl. Acad. Sci. U. S. A. **103**, 4052–4055 (2006).

99. Chandra, M., Sachdeva, A. & Silverman, S. K. DNA-catalyzed sequence-specific hydrolysis of DNA. Nat. Chem. Biol. **5**, 718–720 (2009).

100. Rowe, L. A., Degtyareva, N. & Doetsch, P. W. DNA damage-induced reactive oxygen species (ROS) stress response in Saccharomyces cerevisiae. Free Radic. Biol. Med. **45**, 1167–1177 (2008).

101. Vignard, J., Mirey, G. & Salles, B. Ionizing-radiation induced DNA double-strand breaks: A direct and indirect lighting up. Radiother. Oncol. **108**, 362–369 (2013).

102. Jekimovs, C. et al. Chemotherapeutic compounds targeting the DNA double-strand break repair pathways: The good, the bad, and the promising. Frontiers in Oncology **4**, (2014).

103. Krokan, H. E., Nilsen, H., Skorpen, F., Otterlei, M. & Slupphaug, G. Base excision repair of DNA in mammalian cells. FEBS Letters **476**, 73–77 (2000).

104. Krokan, H. E. & Bjørås, M. Base excision repair. Cold Spring Harb. Perspect. Biol.

5, 1–22 (2013).

105. Schärer, O. D. Nucleotide excision repair in Eukaryotes. Cold Spring Harbor Perspectives in Biology **5**, a012609 (2013).

106. de Laat, W. L. ., Jaspers, N. G. J. . & Hoeijmakers, J. H. J. Molecular mechanism of nucleotide excision repair. Genes Dev **13**, 768–785 (1999).

107. Van Gent, D. C., Hoeijmakers, J. H. J. & Kanaar, R. Chromosomal stability and the DNA double-stranded break connection. Nature Reviews Genetics **2**, 196–206 (2001).

108. Kunkel, T. A. & Erie, D. A. DNA MISMATCH REPAIR. Annu. Rev. Biochem. **74**, 681–710 (2005).

109. Daniels, D. S. et al. DNA binding and nucleotide flipping by the human DNA repair protein AGT. Nat. Struct. Mol. Biol. **11**, 714–720 (2004).

110. Boer, J. de, & Hoeijmakers, J. H. J. Nucleotide excision repair and human syndromes. Carcinogenesis **21**, 453–460 (2000).

111. Franco, S. et al. DNA-PKcs and Artemis function in the end-joining phase of immunoglobulin heavy chain class switch recombination. J. Exp. Med. **205**, 557–564 (2008).

112. Brandsma, I. & Gent, D. C. Pathway choice in DNA double strand break repair: Observations of a balancing act. Genome Integrity **3**, 9 (2012).

113. Shao, Z. et al. DNA-PKcs has KU-dependent function in rRNA processing and haematopoiesis. Nature **579**, 291–296 (2020).

114. Lord, C. J. & Ashworth, A. BRCAness revisited. Nat. Rev. Cancer **16**, 110–120 (2016).

115. Sleeth, K. M. et al. RPA Mediates Recombination Repair During Replication Stress and Is Displaced from DNA by Checkpoint Signalling in Human Cells. J. Mol. Biol. **373**, 38–47 (2007).

116. Kolodner, R. D. & Marsischky, G. T. Eukaryotic DNA mismatch repair. Curr. Opin. Genet. Dev. **9**, 89–96 (1999).

117. Jiricny, J. The multifaceted mismatch-repair system. Nature Reviews Molecular Cell Biology **7**, 335–346 (2006).

118. Sedgwick, B., Bates, P. A., Paik, J., Jacobs, S. C. & Lindahl, T. Repair of alkylated DNA: Recent advances. DNA Repair (Amst). **6**, 429–442 (2007).

119. Yi, C. & He, C. DNA repair by reversal of DNA damage. Cold Spring Harbor Perspectives in Biology **5**, a012575 (2013).

120. Mishina, Y., Duguid, E. M. & He, C. Direct reversal of DNA alkylation damage. Chem. Rev. **106**, 215–232 (2006).

121. Fang, T. et al. Epidermal growth factor receptor-dependent DNA repair promotes murine and human hematopoietic regeneration. Blood **136**, 441–454 (2020).

122. Mohrin, M. et al. Hematopoietic stem cell quiescence promotes error-prone DNA repair and mutagenesis. Cell Stem Cell **7**, 174–185 (2010).

123. Sancar, A., Lindsey-Boltz, L. A., Ünsal-Kaçmaz, K. & Linn, S. Molecular Mechanisms of Mammalian DNA Repair and the DNA Damage Checkpoints. Annu. Rev. Biochem. **73**, 39–85 (2004).

124. Weinstock, D. M., Richardson, C. A., Elliott, B. & Jasin, M. Modeling oncogenic translocations: Distinct roles for double-strand break repair pathways in translocation formation in mammalian cells. DNA Repair (Amst). **5**, 1065–1074 (2006).

125. Hanahan, D. & Weinberg, R. A. The Hallmarks of Cancer Review evolve progressively from normalcy via a series of pre. Cell **100**, (2000).

126. Park, Y. & Gerson, S. L. DNA Repair Defects in Stem Cell Function and Aging. Annu. Rev. Med. **56**, 495–508 (2005).

127. De Laval, B. et al. Thrombopoietin-increased DNA-PK-dependent DNA repair limits hematopoietic stem and progenitor cell mutagenesis in response to DNA damage. Cell Stem Cell **12**, 37–48 (2013).

128. De Laval, B. et al. Thrombopoietin promotes NHEJ DNA repair in hematopoietic stem cells through specific activation of Erk and NF-kB pathways and their target, IEX-1. Blood **123**, 509–519 (2014).

129. Bandyopadhyay, D., Mandal, M., Adam, L., Mendelsohn, J. & Kumar, R. Physical interaction between epidermal growth factor receptor and DNA- dependent protein kinase in mammalian cells. J. Biol. Chem. **273**, 1568–1573 (1998).

130. Dittmann, K., Mayer, C. & Rodemann, H.-P. Inhibition of radiation-induced EGFR nuclear import by C225 (Cetuximab) suppresses DNA-PK activity. Radiother. Oncol. **76**, 157–161 (2005).

131. Toulany, M. et al. Akt1 and Akt3 but not Akt2 through interaction with DNA-PKcs stimulate proliferation and post-irradiation cell survival of K-RAS-mutated cancer cells. Cell Death Discov. **3**, 1–10 (2017).

132. Himburg, H. A. et al. Pleiotrophin Regulates the Retention and Self-Renewal of Hematopoietic Stem Cells in the Bone Marrow Vascular Niche. Cell Rep. **2**, 964–975 (2012).

133. Wilson, A. et al. Hematopoietic Stem Cells Reversibly Switch from Dormancy to

Self-Renewal during Homeostasis and Repair. Cell **135**, 1118–1129 (2008).

134. Koschmieder, S. et al. Inducible chronic phase of myeloid leukemia with expansion of hematopoietic stem cells in a transgenic model of BCR-ABL leukemogenesis. Blood **105**, 324–334 (2005).

135. Roh, M., Paterson, A. J., Asa, S. L., Chin, E. & Kudlow, J. E. Stage-Sensitive Blockade of Pituitary Somatomammotrope Development by Targeted Expression of a Dominant Negative Epidermal Growth Factor Receptor in Transgenic Mice. Mol. Endocrinol. **15**, 600–613 (2001).

136. Himburg, H. A. et al. Dickkopf-1 promotes hematopoietic regeneration via direct and niche-mediated mechanisms. Nat. Med. **23**, 91–99 (2017).

137. Narayan, R. S. et al. The allosteric AKT inhibitor MK2206 shows a synergistic interaction with chemotherapy and radiotherapy in glioblastoma spheroid cultures. BMC Cancer **17**, 204 (2017).

138. Li, H. & Durbin, R. Fast and accurate short read alignment with Burrows-Wheeler transform. **25**, 1754–1760 (2009).

139. Wilhelm, B. T. et al. RNA-seq analysis of 2 closely related leukemia clones that differ in their self-renewal capacity. Blood **117**, e27–e38 (2011).

140. Callicott, R. J. & Womack, J. E. Real-time PCR Assay for Measurement of Mouse Telomeres. Comp. Med. **56**, 17–22 (2006).

141. Stavropoulou, V. et al. MLL-AF9 Expression in Hematopoietic Stem Cells Drives a Highly Invasive AML Expressing EMT-Related Genes Linked to Poor Outcome. Cancer Cell **30**, 43–58 (2016).

142. Li, H. Aligning sequence reads, clone sequences and assembly contigs with BWA-MEM. (2013).

143. Li, H. et al. The Sequence Alignment/Map format and SAMtools. Bioinforma. Appl. NOTE **25**, 2078–2079 (2009).

144. McKenna, A. et al. The genome analysis toolkit: A MapReduce framework for analyzing next-generation DNA sequencing data. Genome Res. **20**, 1297–1303 (2010).

145. Abyzov, A., Urban, A. E., Snyder, M. & Gerstein, M. CNVnator: An approach to discover, genotype, and characterize typical and atypical CNVs from family and population genome sequencing. Genome Res. **21**, 974–984 (2011).

146. Fan, X., Abbott, T. E., Larson, D. & Chen, K. BreakDancer: Identification of genomic structural variation from paired-end read mapping. Curr. Protoc. Bioinforma. **45**, (2014).

147. Cingolani, P. et al. A program for annotating and predicting the effects of single

nucleotide polymorphisms, SnpEff: SNPs in the genome of Drosophila melanogaster strain w1118; iso-2; iso-3. Fly (Austin). **6**, 80–92 (2012).

148. Dobin, A. et al. STAR: Ultrafast universal RNA-seq aligner. Bioinformatics **29**, 15–21 (2013).

149. Krämer, A., Green, J., Pollard, J. & Tugendreich, S. Causal analysis approaches in ingenuity pathway analysis. Bioinformatics **30**, 523–530 (2014).

150. Lips, J; Kaina, B. DNA double-strand breaks trigger apoptosis in p53-deficient fibroblasts. Carcinogenesis **22**, 579–585 (2001).

151. Milyavsky, M. et al. A Distinctive DNA damage response in human hematopoietic stem cells reveals an apoptosis-independent role for p53 in self-renewal. Cell Stem Cell **7**, 186–197 (2010).

152. Yu, H. et al. Deletion of Puma protects hematopoietic stem cells and confers long-term survival in response to high-dose γ-irradiation. Blood **115**, 3472–3480 (2010).

153. Durdik, M. et al. Hematopoietic stem/progenitor cells are less prone to undergo apoptosis than lymphocytes despite similar DNA damage response. Oncotarget **8**, 48846–48853 (2017).

154. Ivashkevich, A., Redon, C. E., Nakamura, A. J., Martin, R. F. & Martin, O. A. Use of the γ-H2AX assay to monitor DNA damage and repair in translational cancer research. Cancer Letters **327**, 123–133 (2012).

155. Klaude, M., Eriksson, S., Nygren, J. & Ahnström, G. The comet assay: Mechanisms and technical considerations. Mutat. Res. - DNA Repair **363**, 89–96 (1996).

156. Nijnik, A. et al. DNA repair is limiting for haematopoietic stem cells during ageing. Nature **447**, 686–690 (2007).

157. Rossi, D. J. et al. Deficiencies in DNA damage repair limit the function of haematopoietic stem cells with age. Nature **447**, 725–729 (2007).

158. Ferguson, D. O. et al. The nonhomologous end-joining pathway of DNA repair is required for genomic stability and the suppression of translocations. Proc. Natl. Acad. Sci. U. S. A. **97**, 6630–6633 (2000).

159. Iliakis, G. et al. Mechanisms of DNA double strand break repair and chromosome aberration formation. Cytogenetic and Genome Research **104**, 14–20 (2004).

160. Weinstock, D. M., Brunet, E. & Jasin, M. Formation of NHEJ-derived reciprocal chromosomal translocations does not require Ku70. Nat. Cell Biol. **9**, 978–981 (2007).

161. Meyn, R. E., Munshi, A., Haymach, J. V., Milas, L. & Ang, K. K. Receptor signaling as a regulatory mechanism of DNA repair. Radiotherapy and Oncology **92**, 316–322 (2009).

162. West, R. B., Yaneva, M. & Lieber, M. R. Productive and Nonproductive Complexes of Ku and DNA-Dependent Protein Kinase at DNA Termini. Mol. Cell. Biol. **18**, 5908–5920 (1998).

163. Chang, H. H. Y., et al. Different DNA end configurations dictate which NHEJ components are most important for joining efficiency. J. Biol. Chem. **291**, 24377–24389 (2016).

164. Burdova, K., Mihaljevic, B., Sturzenegger, A., Chappidi, N. & Janscak, P. The Mismatch-Binding Factor MutSβ Can Mediate ATR Activation in Response to DNA Double-Strand Breaks. Mol. Cell **59**, 603–614 (2015).

165. Godin, S. K., Sullivan, M. R. & Bernstein, K. A. Novel insights into RAD51 activity and regulation during homologous recombination and DNA replication1. Biochemistry and Cell Biology **94**, 407–418 (2016).

166. Zhao, Y. et al. Preclinical evaluation of a potent novel DNA-dependent protein kinase inhibitor NU7441. Cancer Res. **66**, 5354–5362 (2006).

167. Minjgee, M., Toulany, M., Kehlbach, R., Giehl, K. & Rodemann, H. P. K-RAS(V12) induces autocrine production of EGFR ligands and mediates radioresistance through EGFR-dependent Akt signaling and activation of DNA-PKcs. Int. J. Radiat. Oncol. Biol. Phys. **81**, 1506–1514 (2011).

168. Kiel, M. J. et al. SLAM family receptors distinguish hematopoietic stem and progenitor cells and reveal endothelial niches for stem cells. Cell **121**, 1109–1121 (2005).

169. Xiao, Y., Deng, T., Su, C. & Shang, Z. MicroRNA 217 inhibits cell proliferation and enhances chemosensitivity to doxorubicin in acute myeloid leukemia by targeting KRAS. Oncol. Lett. **13**, 4986–4994 (2017).

170. Himburg, H. A. et al. A Molecular Profile of the Endothelial Cell Response to Ionizing Radiation. Radiat. Res. **186**, 152 (2016).

171. Tikhonova, A. N. et al. The bone marrow microenvironment at single-cell resolution. Nature **569**, 222–228 (2019).

172. Chen, Q. et al. Apelin+ Endothelial Niche Cells Control Hematopoiesis and Mediate Vascular Regeneration after Myeloablative Injury. Cell Stem Cell **25**, 768–783 (2019).

173. Wunderlich, M. et al. Improved multilineage human hematopoietic reconstitution and function in NSGS mice. PLoS One **13**, e0209034 (2018).

174. Orford, K. W. & Scadden, D. T. Deconstructing stem cell self-renewal: Genetic insights into cell-cycle regulation. Nat. Rev. Genet. **9**, 115–128 (2008).

175. Allan, J. M. & Travis, L. B. Mechanisms of therapy-related carcinogenesis. Nat. Rev.

Cancer **5**, 943–955 (2005).

176. Biechonski, S., Yassin, M. & Milyavsky, M. DNA-damage response in hematopoietic stem cells: an evolutionary trade-off between blood regeneration and leukemia suppression. Carcinogenesis **38**, 367–377 (2017).

177. Maze, R. et al. Increasing DNA repair methyltransferase levels via bone marrow stem cell transduction rescues mice from the toxic effects of 1,3-bis(2-chloroethyl)-1-nitrosourea, a chemotherapeutic alkylating agent. Proc. Natl. Acad. Sci. U. S. A. **93**, 206–210 (1996).

178. Bétermier, M., Bertrand, P. & Lopez, B. S. Is Non-Homologous End-Joining Really an Inherently Error-Prone Process? PLoS Genet. **10**, e1004086 (2014).

179. Feldmann, E., Schmiemann, V., Goedecke, W., Reichenberger, S. & Pfeiffer, P. DNA double-strand break repair in cell-free extracts from Ku80-deficient cells: implications for Ku serving as an alignment factor in non-homologous DNA end joining. Nucleic Acids Res. **28**, 2585–2596 (2000).

180. Kabotyanski, E. B., Gomelsky, L., Han, J.-O., Stamato, T. D. & Roth, D. B. Double-strand break repair in Ku86-and XRCC4-deficient cells. Nucleic Acids Res. **26**, 5333–5342 (1998).

181. Smith, J., Baldeyron, C., De Oliveira, I., Sala-Trepat, M. & Papadopoulo, D. The influence of DNA double-strand break structure on end-joining in human cells. Nucleic Acids Res. **29**, 4783–4792 (2001).

182. Smith, J. et al. Impact of DNA ligase IV on the ®delity of end joining in human cells. Nucleic Acids Res. **31**, 2157–2167 (2003).

183. Lehoczky, J. A. et al. A Novel Intergenic ETnII-β Insertion Mutation Causes Multiple Malformations in Polypodia Mice. PLoS Genet. **9**, e1003967 (2013).

184. Whitelaw, E. & Martin, D. I. K. Retrotransposons as epigenetic mediators of phenotypic variation in mammals. Nat. Genet. **27**, 361–365 (2001).

185. Herz, H. M. Enhancer deregulation in cancer and other diseases. BioEssays **38**, 1003–1015 (2016).